Adaptive Backstepping Control of Quanser 2DOF Helicopter

Theory and Experiments

SIRI MARTE SCHLANBUSCH

SUPERVISOR

Jing Zhou

University of Agder, 2019
Faculty of Engineering and Science
Department of Engineering Sciences

Acknowledgements

This thesis is submitted as partial fulfillment of the requirements for the degree of Master of Science in Mechatronics by the University of Agder, and has been carried out at the Department of Engineering Sciences, Faculty of Engineering and Science.

I would like to thank my supervisor, professor Jing Zhou for guidance and advice during the course and for giving an interesting problem to solve. I would also like to thank Morten Ebbesen for his inputs to the modeling of the system. Lastly, I would like to thank my husband Rune Schlanbusch for his inputs to my work and for interesting discussions throughout this master thesis.

Grimstad, May 24, 2019

Siri M. Schlanbusch

Abstract

In this thesis, an adaptive backstepping controller is proposed for tracking of a desired trajectory for the attitude of a laboratory helicopter from Quanser called Aero. The Aero has two degrees of freedom (DOF), and can rotate around two axes, and is a multiple-inputs-multiple-outputs (MIMO) system. A mathematical model of the system is first derived based on Newton's law and Eulers rotational dynamics and parameters for the model are estimated. A theoretical proof of stability with adaptive backstepping is given with the use of constructed Lyapunov functions, where tracking is achieved and also boundedness of all signals in the closed loop system. Also, the transient performance for the tracking errors in terms of $\mathcal{L}_2$ norm is derived, where the tracking error performance can be improved by adjusting the design parameters. Simulations and experiments are carried out where the performance of the adaptive backstepping controller is compared with the performance of a linear quadratic regulator (LQR). Different disturbances have been added to see the behavior of the controllers. For all the tests, the adaptive controller is able to estimate the parameters and track the desired reference signal. For different step inputs to the angles at different time instances, the two controllers show a similar behavior. Planning the path and using a smoother transition between the steps, a better performance is observed for both controllers both in terms of lower total error and less voltage use. The adaptive backstepping controller shows a better performance relative to error than the LQR under smoother steps.

Contents

List of Abbreviations

CCW	Counter-clockwise
DC	Direct current
DOF	Degrees of freedom
FBD	Free-body diagram
GUAS	Globally uniformly asymptotically stable
I/O	Input/output
IMU	Inertial measurement unit
KD	Kinetic diagram
LFC	Lyapunov function candidate
LQR	Linear quadratic regulator
MIMO	Multiple-inputs-multiple-outputs
MPC	Model predictive control
MRAC	Model reference adaptive control
ODE	Ordinary differential equation
PD	Proportional-derivative
PID	proportional–integral–derivative
PV	Proportional-velocity
PWM	Pulse width modulation
SE(3)	Special Euclidean Group of dimension 3
SISO	Single-input-single-output
SO(3)	Special Orthogonal Group of dimension 3
SPI	Serial Peripheral Interface Bus
USB	Universal Serial Bus

List of Symbols

$(\boldsymbol{\omega}_{ib}^{b})^{\mathrm{x}}$	Skew symmetric matrix of the angular velocities
$\alpha_i, i = 1, 2$	Virtual controls, adaptive backstepping control
$\dot{\boldsymbol{\omega}}_{ib}^{b}$	Angular acceleration vector of body frame relative to inertial frame when looking from body frame
$\boldsymbol{\lambda}$	Euler angles
$\boldsymbol{\omega}_{ib}^{b}$	Angular velocity vector of body frame relative to inertial frame, looking from body frame
γ	Adaption gain, adaptive backstepping control
$\Gamma_i, i = 1, 2$	Positive definite adaption gain matrices, adaptive backstepping control
$\hat{\Theta}_i, i = 1, 2$	Estimated parameters, adaptive backstepping control
$\ddot{\mathbf{r}}_i$	Acceleration for the Aero body in inertial frame
$\dot{\mathbf{r}}_i$	Velocity for the Aero body in inertial frame
$\sum \mathbf{F_i}$	Sum of forces in inertial frame
$\sum \mathbf{M_b}$	Sum of moments in body frame
$\mathbf{A}$	State matrix
$\mathbf{B}$	Input matrix
$\mathbf{C}$	Output matrix
$\mathbf{D}$	Direct transmission matrix
$\mathbf{E}_b(\lambda)$	Rotation matrix from Euler angular velocities to body frame angular velocities
$\mathbf{I}_{b/o}$	Mass moment of inertia about the pivot point in body frame
$\mathbf{K}$	State feedback gain, LQR control
$\mathbf{P}$	Square, symmetric matrix, LQR control
$\mathbf{Q}$	Weight matrix for the state variables, LQR control
$\mathbf{R}$	Weight matrix for the control values, LQR control
$\mathbf{R}_b^i$	Direction cosine matrix
$\mathbf{r}_i$	Position of the Aero body in inertial frame
$\mathbf{R}_y(\theta)$	Rotation matrix about y-axis
$\mathbf{R}_z(\psi)$	Rotation matrix about z-axis
$\mathbf{r}_{cm1}$	Center of mass for 1 DOF setup
$\mathbf{r}_{cm}$	Center of mass for the Aero body
$\mathbf{R}_x(\phi)$	Rotation matrix about x-axis

$\mathbf{s}$	Tracking vector, LQR control
$\mathbf{u}$	Control vaiables
$\mathbf{x}$	State space variables
$\mathbf{y}$	Output variables
$\mathbf{z}$	Error state
$\mathcal{B}$	Body frame
$\mathcal{I}$	Inertial frame
ϕ	Roll angle
Φ_1	Known nonlinear function for pitch, adaptive backstepping control
Φ_2	Known nonlinear function for yaw, adaptive backstepping control
ψ	Yaw angle
τ_Δ	Disturbance torque
θ	Pitch angle
Θ_1	Unknown vector constants for pitch, adaptive backstepping control
Θ_2	Unknown vector constants for yaw, adaptive backstepping control
$\tilde{\Theta}_i, i = 1, 2$	Error of vector constants, adaptive backstepping control
$c_i, i = 1, 2, 3, 4$	Positive constants, adaptive backstepping control
D_{Vp}	Viscous damping about the pitch axis
D_{Vy}	Viscous damping about the yaw axis
$f_1(V_p)$	Main torque about pitch axis
$f_2(V_y)$	Cross torque about pitch axis
$f_3(V_y)$	Main torque about yaw axis
$f_4(V_p)$	Cross torque about yaw axis
F_g	Gravity force
F_n	Normal force at pivot point
F_t	Tangential force at pivot point
F_{My}	Force from main motor in y_b-direction
F_{Mz}	Force from main motor in z_b-direction
F_{Ty}	Force from tail motor in y_b-direction
F_{Tz}	Force from tail motor in z_b-direction
g	Constant of acceleration due to gravity
I_p	Inertia about the pitch axis

I_y	Inertia about the yaw axis
J	Cost function, LQR control
K_d	Derivative gain, PID control
K_i	Integration gain, PID control
K_p	Proportional gain, PID control
$K_{d(\psi)}$	Derivative gain for yaw, PV control
$K_{d(\theta)}$	Derivative gain for pitch, PV control
$K_{p(\psi)}$	Proportional gain for yaw, PV control
$K_{p(\theta)}$	Proportional gain for pitch, PV control
K_{pp}	Torque trust gain from the main motor acting on pitch
K_{py}	Cross-torque thrust gain acting on pitch from tail motor
K_{sp}	Spring constant
K_{yp}	Cross-torque thrust gain acting on yaw from main motor
K_{yy}	Torque trust gain from the tail motor acting on yaw
l_1	Distance from x_b-axis to mass center of motors
l_{cm}	Distance to center of mass in y_b- and z_b-direction
l_{tube}	Length of the horizontal metal tube in the Aero body
m_b	Mass of the Aero body
m_p	Mass of thruster with propeller and motor
m_{tube}	Mass of the horizontal metal tube in the Aero body
r_m	Distance to center of mass in z_b-direction for 1 DOF setup
r_p	Distance from pivot point to the motors
u_p	Control input for pitch, adaptive backstepping control
u_y	Control input for yaw, adaptive backstepping control
$V_i, i = 1, 2$	Control Lyapunov functions, adaptive backstepping control
V_p	Input voltage to the main motor
V_y	Input voltage to the tail motor
x_i, y_i, z_i	Axes in inertial frame
$x_{r1}(t)$	Reference signal for pitch
$x_{r2}(t)$	Reference signal for yaw
$e(t)$	Error, difference between desired and measured output, PID control
x_b,y_b,z_b	Axes in body frame

List of Figures

List of Tables

Chapter 1

Introduction

The history of helicopters goes back over 2000 years when the Chinese made a toy called Chinese Top [1]. This toy had a propeller on a stick that would fly when the stick was spun. Over the years, several design of a helicopter was constructed, and the modern helicopter was invented in the 1930's by the Russian Igor Sikorsky, and the first helicopter was build in 1939. The helicopter had one main and one tail rotor. The main rotor was mounted horizontally and gave a lifting force, but at the same time it would generate aerodynamic forces, drag, that makes the helicopter rotate about yaw. The invention of using a tail rotor to account for the torque produced by the main rotor made the helicopter practical to fly. The tail rotor was mounted vertically and gave an opposite torque to the main rotor so that the helicopter did not spin around.

One of the greatest advantage with a helicopter is its ability to have vertical take-off and landing and have practical use where there is not need for a runway. This makes helicopters useful for rescue of people in mountains and at sea, to transport people to hospitals and to platforms at sea and use in military actions among other things. When the helicopter is in the air, it will encounter disturbances from weather conditions, and wind is one of the challenges. Also if a helicopter is to land on a platform at sea, it will have disturbance from waves and so a helicopter needs to adapt to different flight conditions fast.

In this project a laboratory equipment from Quanser called Aero is used to experiment with different control structures, with focus on adaptive backstepping control. The Aero has two degrees of freedom, pitch and yaw, and resembles the behavior of a helicopter. There is a cross-coupling between the two rotors, making it challenging to control. For the laboratory helicopter rotor blades are fixed, while on a helicopter the airfoils can change angles. For the Aero, control is achieved by changing speed of the rotors while control is achieved by changing angles of the airfoils for a helicopter. The Aero also has the center of mass below the pivot point, so that it resembles a pendulum, which is one of the things making control of pitch angle nonlinear. This is a multiple-inputs-multiple-outputs (MIMO) nonlinear dynamic system, and because of the complexity it is difficult to both model and to design a good control structure.

1.1 Project Description

In this thesis the following have had main focus

- Perform a literature review of previous work related to 2 degrees of freedom (DOF) helicopter models similar to the one in this thesis.
- Derive a mathematical model of the Aero dynamics with actuation of rotation of the system.
- Design of four different controllers for the Aero including two PID based controllers, one linear controller, LQR, and one nonlinear controller. The main focus has been to the nonlinear controller using adaptive backstepping.

- Perform a theoretical analysis of stability of the Aero with adaptive backstepping control.
- Simulation of the system with the different controllers in Matlab/Simulink. Simulation results will be presented.
- Testing of the different controllers for control of the Aero. Results from testing will also be presented.

1.2 Previous Work

Air vehicles such as helicopters and unmanned aerial vehicles have received an increased interest the past years. This has also resulted in more research later years for control of such systems. Helicopter models like the one from Quanser gives a good opportunity to test different controllers and there have been proposed many different control structures/design for tracking and stabilizing helicopters based on such models. Here is a presentation of some of the works that have been published relating to control of a helicopter.

Conventional controllers like proportional – integral – derivative (PID) controller and linear quadratic regulator (LQR) have been tested for twin rotor MIMO systems. Pandey and Laxmi (2014) [2] presented a linearized model of a twin rotor MIMO system. First a conventional PID controller to control pitch and yaw separately was tested and this was compared with an optimal state feedback controller using LQR technique where both state and control input were in the cost function. This was evaluated with step input and the conclusion was that the optimal controller gave better performance both in terms of transient and steady state response compared to the PID controller. In Ramalakshmi and Manoharan (2012)[3], two different type of PID controllers were evaluated for a twin rotor MIMO system. First vertical and horizontal movements were controlled separately with PID controllers, then a cross coupling of four PID controllers were tested. Three different inputs were given to the system, step, sine and a square wave. It is difficult to say if the cross coupled PID controller had a better performance than the separate PID controllers based on the presented results.

More advanced controllers have also been tested where a nonlinear model often is used. Predictive or adaptive controllers have been tested and the performance is often compared with performance of a conventional controller. In 2018, Gabrielsen and Frasik [4] wrote a master thesis for the same system as for this thesis. In their work, several controllers were tested for the Aero to control the pitch and yaw angular position. This included cascade P-PI, LQR and the more advanced controllers like model predictive control (MPC) and model reference adaptive control (MRAC). MPC is an approach that first make a prediction of the system output and then chooses future control signals over a control horizon that minimizes future error of what is desired and what is predicted. This is repeated for every time step. MRAC is a controller that continuously change the control parameters based on a reference model of the controlled system. A combined step response sequence for pitch and yaw was simulated and tested on the system. Also a test with emulated actuator damage was performed, where the tail propeller was changed with a propeller with higher efficiency.
In Dutka et al.(2003) [8] a nonlinear predictive control was applied to a 2DOF helicopter model. The nonlinear algorithm was based on state-space generalized predictive control. Here the future control was predicted, and then future states for the model and time-varying parameters were predicted based on the control. A desired setpoint for the angles was given, and the proposed algorithm was able of stabilizing the system. In Ramalakshmi et al.(2016) [7] a MPC for a 2DOF helicopter was developed. Based on a model of the system, performance of a PID controller was compared with performance from the MPC controller when disturbances of step and sine were applied to the model. Both had the same settling time but PID has a higher overshoot than MPC. MPC had a smoother control compared to PID in this test and maintained system stability and reduced the effect of disturbances and noise. Ahmed et al (2010) tested a 2-Sliding mode based robust controller for a 2DOF helicopter in [9]. Variations in mass distribution were tested, where a wanted constant pitch angle was tracked under disturbance from changing center of gravity during the experiment. This gave unwanted moments that the controller had to deal with, and the results showed a good

performance under these uncertainties. In Lopéz-Martinéz (2005)[12] a nonlinear $\mathcal{H}_\infty$ controller for a twin rotor laboratory helicopter was designed and tested. This controller had a structure as a nonlinear PID controller with gains that varied over time. The controller was tested with different series of step references and showed a good performance given the references.
Chalupa et.al. (2015) presented modelling of a twin rotor MIMO system and an adaptive controller for the system in [5] and [6]. A significant cross-coupling between the two rotors was observed and also a nonlinear behaviour of the system. A model based on first-principle was derived for the helicopter model. The adaptive controller tested was a self-tuning controller based on online identification of controlled process, and where the linearized model of the plant was used. In Patel et al. (2017) [10] an adaptive integral backstepping control scheme for tracking control for a Quanser 2DOF Helicopter was proposed. The advantage of such a controller is that it is robust to uncertainties and unmodeled dynamics. Performance of this controller was compared with a LQR controller. A mass in form of a marker pen was placed onto the front propeller after 30 s, trying to hold a given pitch angle and so there is an uncertainty to the mass. Simulations and testing on the Quanser helicopter with this showed a better performance for the integral backstepping controller when such uncertainties were present. In Zou and Huo (2015)[11] an adaptive tracking control for a model helicopter in presence of external disturbances was presented. The design was based on backstepping and a proof that the tracking errors are bounded was also given. Simulation of position tracking and tracking of the yaw showed that the control design was robust to disturbances.

1.3 Outline

The outline of this M.Sc thesis is:

Chapter 2 provide a description of the Aero that is used in this thesis before a short description about state space approach is given and then modeling of the kinematics and dynamics of the system is described. The parameters for the model are then estimated.

In Chapter 3 a short description of multivariable system is given before different control designs that will be simulated and tested for control of the Aero is given. This include two PID based controllers, one linear and one nonlinear controller. The focus is on a linear controller, LQR, and a nonlinear controller using adaptive backstepping. A stability proof of the Aero with the adaptive controller is also given.

The next chapter, Chapter 4, provides simulation and testing of the different controllers with control of the Aero. First the models are verified to see that they have a behavior as expected before the different controllers are simulated and tested for different control inputs such as a sine-wave and step-input at different time instances. To compare the controllers, the total error and also the total voltage is measured. Then different disturbances is added to the model to compare the behavior of the LQR and the adaptive backstepping controller.

A conclusion and suggested future work is given in Chapter 5.

Chapter 2

Description and Modeling of the Aero

2.1 Description of the System

The main equipment used in this project is a Quanser Aero which is shown in Figure 2.1. This is a two-rotor laboratory equipment with 2DOF used for flight control based experiments, designed for education and research purposes.

The Aero can be configured with either control by a computer via USB connection or by the use of a microcontroller device. The components of the Aero are:

1. *Aero base.* Here the system input/output (I/O) is connected, such as power, USB or SPI Data connector. The Aero base is stationary and have zero DOF.

2. *Aero frame.* A support yoke is connected to the Aero base. To this, a horizontal metal tube with two thrusters including the motors are connected, defining these components as the *Aero body*. The support yoke and the Aero body can rotate along the vertical axis of the support yoke and a slip ring allows for unlimited rotation. The Aero body can also be tilted about a pivot point. This gives the Aero body 2DOF. The tilting angle for the Aero body is constrained to ± 62 degrees from a horizontal position due to physical limits on the equipment. An inertial measurement unit (IMU) with accelerometers and gyros is mounted in the Aero body, making it possible to have real time measurements of angular positions and velocities along the primary axis. Two DC-motors powered by a PWM amplifier are used to drive the system, and rotary encoders are used to measure position for the motors and tachometer to measure the speed of the motors. There are also two optical encoders mounted in the Aero frame as illustrated in Figure 2.1 to measure the angles.

It is possible to lock the support yoke so that it does not rotate and it is also possible to lock the Aero body so that it does not tilt. Locking one of them separately reduces DOF so that only 1DOF remains. This will be used when finding different estimates for the parameters in the mathematical model.

The propellers used in this thesis is shown in Figure 2.2a and are low efficiency eight-vane 3D-printed propellers. It is possible to change propellers to another set of high efficiency propellers shown in Figure 2.2b. When testing for disturbances on the system, one or two of the propellers will be exchanged with these.

The thruster angles can be adjusted to a horizontal or vertical position. The setup used in this thesis is a horizontal position of the main thruster and a vertical position of the tail thruster as Figure 2.1 shows, and this resembles a helicopter.

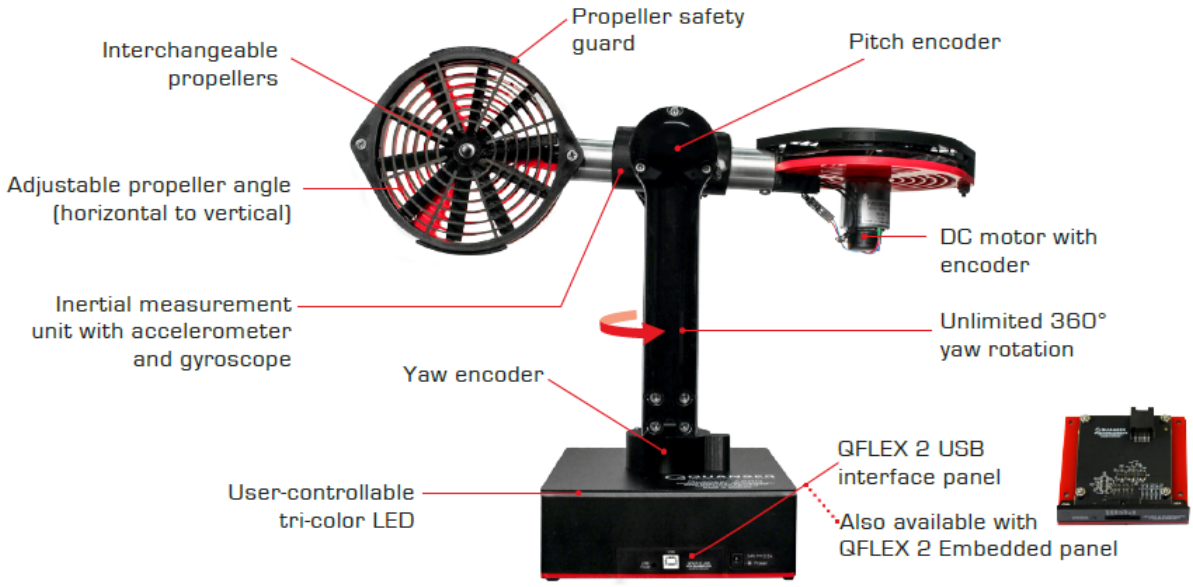

Figure 2.1: Quanser Aero, equipment used in project

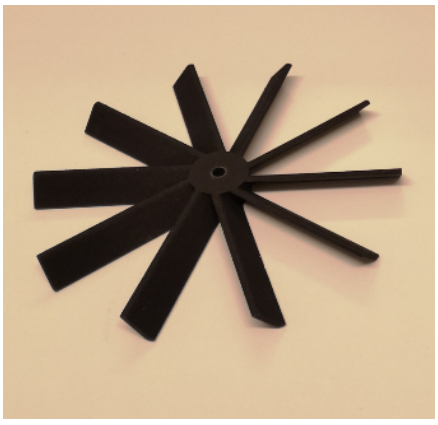

(a) Low efficiency propellers used on Aero

(b) High efficiency propellers

Figure 2.2: Propellers

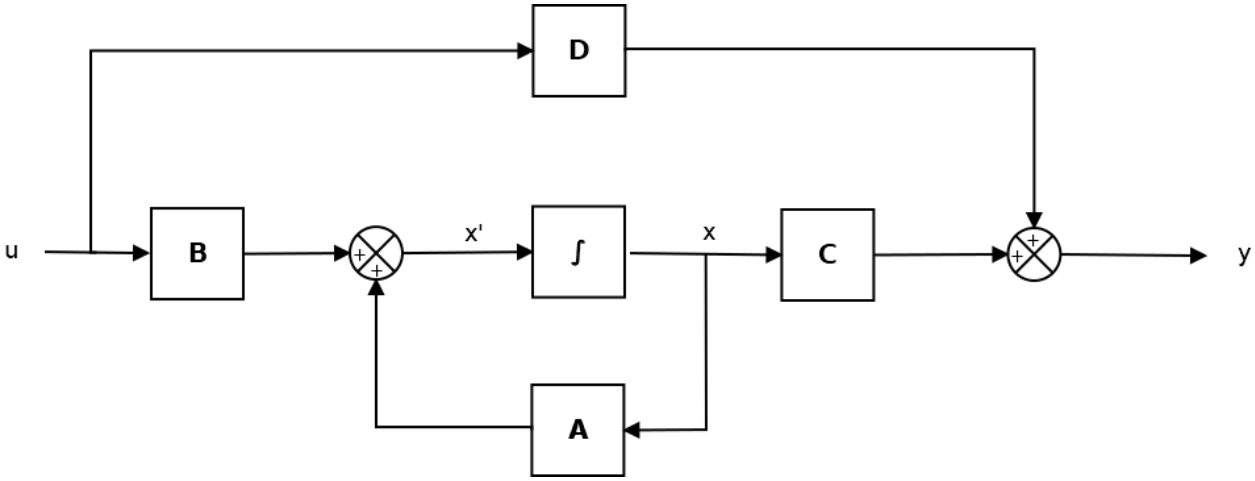

Figure 2.3: Block diagram of a system in state space

2.2 State Space Approach

The state space form is one way of describing the behavior of a dynamical system. The system is then formulated as a set of first order differential equations with state variables $x_1, x_2, ..., x_n = \mathbf{x}$, and input variables $u_1, u_2, ..., u_m = \mathbf{u}$, that in general form looks like

$$\dot{\mathbf{x}} = f(\mathbf{x}, \mathbf{u}) \tag{2.1}$$
$$\mathbf{y} = h(\mathbf{x}), \tag{2.2}$$

and will describe a nonlinear system. If the system can be describes in the form

$$\begin{aligned}
\dot{x}_1 &= a_{11}x_1 + a_{12}x_2 + ... + a_{1n}x_n + b_{11}u_1 + b_{12}u_2 + ... + b_{1m}u_m, \\
\dot{x}_2 &= a_{21}x_1 + a_{22}x_2 + ... + a_{2n}x_n + b_{21}u_1 + b_{22}u_2 + ... + b_{2m}u_m, \\
&\vdots \\
\dot{x}_n &= a_{n1}x_1 + a_{n2}x_2 + ... + a_{nn}x_n + b_{n1}u_1 + b_{n2}u_2 + ... + b_{nm}u_m,
\end{aligned} \tag{2.3}$$

and the output variables $(y_1, y_2, ..., y_k)$ also can be formulated with the state- and input variables where

$$\begin{aligned}
y_1 &= c_{11}x_1 + c_{12}x_2 + ... + c_{1n}x_n + d_{11}u_1 + d_{12}u_2 + ... + d_{1m}u_m, \\
y_2 &= c_{21}x_1 + c_{22}x_2 + ... + c_{2n}x_n + d_{21}u_1 + d_{22}u_2 + ... + d_{2m}u_m, \\
&\vdots \\
y_k &= c_{k1}x_1 + c_{k2}x_2 + ... + c_{kn}x_n + d_{k1}u_1 + d_{k2}u_2 + ... + d_{km}u_m,
\end{aligned} \tag{2.4}$$

Then both the equations for the system and for the output can be presented in matrix form as

$$\dot{\mathbf{x}} = \mathbf{A}\mathbf{x} + \mathbf{B}\mathbf{u} \tag{2.5}$$
$$\mathbf{y} = \mathbf{C}\mathbf{x} + \mathbf{D}\mathbf{u} \tag{2.6}$$

where matrix $\mathbf{A}$ is the state matrix, $\mathbf{B}$ is the input matrix, $\mathbf{C}$ is the output matrix and $\mathbf{D}$ is the direct transmission matrix. This is the linear state space form, and a block diagram of the linearized system in state space is shown in Figure 2.3. One advantage of using state space form is that it applies for MIMO- and nonlinear- systems as well as for single-input-single-output (SISO)- and linear- systems [13].

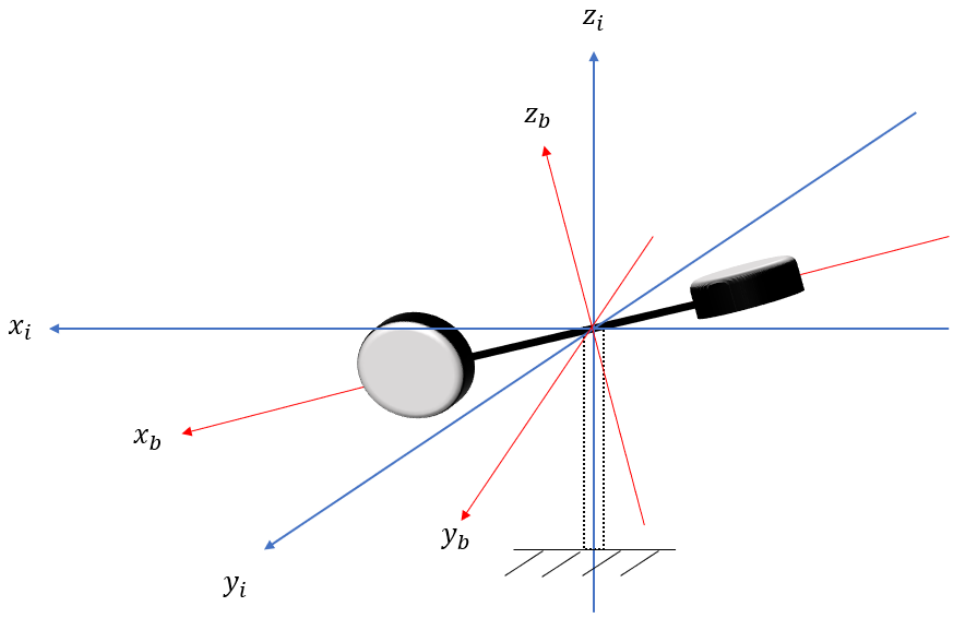

Figure 2.4: Coordinate system of Aero body and inertial frame

2.3 Modeling of the Aero

The first step in control design is to have a mathematical model of the system where this model is an approximate representation of the real system. In this section a model for the Aero is developed. The system for the Aero is a MIMO system with two system inputs, V_p and V_y, that is the voltages applied to the main and tail motors and four state variables, that is the tilting angle of the Aero body, the angle from rotation of the support yoke and Aero body along the vertical axis, and then the angular velocities for these. All state variables can be measured. The system has 2DOF, and thus there will be two equations describing the dynamic of Aero. The rotor blades are airfoils, that can have different characteristics giving different aerodynamic forces for a helicopter, mostly affecting the lifting force. The design of these and how this effect the model are outside the scope of this thesis.

The Aero is considered as a rigid body, and with the use of Newton's law and Euler's rotational dynamics, the Newton-Euler equations of motion are [14]

$$\begin{bmatrix} m_b & 0 \\ 0 & \mathbf{I}_{b/o} \end{bmatrix} \begin{bmatrix} \ddot{\mathbf{r}}_i \\ \dot{\boldsymbol{\omega}}^b_{ib} \end{bmatrix} = \begin{bmatrix} \sum \mathbf{F}_i \\ \sum \mathbf{M}_b - (\boldsymbol{\omega}^b_{ib})^{\times} \mathbf{I}_{b/o} \boldsymbol{\omega}^b_{ib} + \tau_{\Delta} \end{bmatrix} \tag{2.7}$$

where a subscript or superscript, b, denotes the body frame, i denotes the inertial frame and o denotes the pivot point. The scalar m_b is the mass of the Aero body, matrix $\mathbf{I}_{b/o}$ is the mass moment of inertia about the pivot point, the vector $\ddot{\mathbf{r}}_i$ is the acceleration for the mass, $\boldsymbol{\omega}_{ib}$ is the angular velocity vector of body frame relative to inertial frame, and with superscript b for this, $\boldsymbol{\omega}^b_{ib}$, means this is the angular velocity when looking from the body frame. This is the angular velocity that can be measured from the IMU's rate gyroscopes. Vector $\dot{\boldsymbol{\omega}}^b_{ib}$ is the angular acceleration vector, vector $\sum \mathbf{F_i}$ is the sum of forces, and the vector $\sum \mathbf{M_b}$ is the sum of moments. The matrix $(\boldsymbol{\omega}^b_{ib})^{\times}$ is the skew symmetric matrix of the angular velocities. Vector τ_{Δ} is the disturbance torque. When finding these equations, the translational forces is considered in the inertial frame, and the rotational is considered in the body frame. Equations in this section is from [14] and [15].

To find these equations and make a mathematical model, a coordinate system is first selected. The inertial frame, $\mathcal{I}$, for the model is shown in Figure 2.4, where origin is chosen in the pivot point for the Aero body and the axes are denoted (x_i, y_i, z_i). This is considered fixed relative to ground. The helicopter have a body frame, $\mathcal{B}$, also with origin in the pivot point and with axes denoted (x_b,y_b,z_b).

The orientation of the body frame relative to the inertial frame is described by a direction cosine matrix $\mathbf{R}_b^i$ expressed with Cardan angles, better known as Euler angles. This is a rotation matrix from the inertial frame to the body frame, and is rotation about x-, y- and z-axis with Euler angles $\boldsymbol{\lambda} = [\phi, \theta, \psi]^T$ called roll-pitch-yaw angles. There are twelve possible combinations of Euler angles based on which order of rotation is chosen. A rotation first about z-axis, then y-axis and then x-axis is typical for aircraft and spacecraft attitude angles and is therefore chosen for this system. The direction cosine matrix for this system is then [15]

$$\mathbf{R}_b^i = \mathbf{R}_x(\phi)\mathbf{R}_y(\theta)\mathbf{R}_z(\psi) = \begin{bmatrix} \mathrm{c}\theta\mathrm{c}\psi & \mathrm{c}\theta\mathrm{s}\psi & -\mathrm{s}\theta \\ -\mathrm{c}\phi\mathrm{s}\psi + \mathrm{s}\phi\mathrm{s}\theta\mathrm{c}\psi & \mathrm{c}\phi\mathrm{c}\psi + \mathrm{s}\phi\mathrm{s}\theta\mathrm{s}\psi & \mathrm{s}\phi\mathrm{c}\theta \\ \mathrm{s}\phi\mathrm{s}\psi + \mathrm{c}\phi\mathrm{s}\theta\mathrm{c}\psi & -\mathrm{s}\phi\mathrm{c}\psi + \mathrm{c}\phi\mathrm{s}\theta\mathrm{s}\psi & \mathrm{c}\phi\mathrm{c}\theta \end{bmatrix}, \tag{2.8}$$

where $\mathbf{R}_z$, $\mathbf{R}_y$ and $\mathbf{R}_x$ are the rotation matrices about z-, y-, and x-axis, and $\mathrm{c}(\cdot)$ and $\mathrm{s}(\cdot)$ is abbreviation for $\cos(\cdot)$ and $\sin(\cdot)$. The rotation matrix about x-axis can be reduced to an identity matrix since there is no rotation about x for the Aero, and so Equation (2.8) can be simplified to

$$\mathbf{R}_b^i = \mathbf{R}_x(\phi)\mathbf{R}_y(\theta)\mathbf{R}_z(\psi) = \begin{bmatrix} \mathrm{c}\theta\mathrm{c}\psi & \mathrm{c}\theta\mathrm{s}\psi & -\mathrm{s}\theta \\ -\mathrm{s}\psi & \mathrm{c}\psi & 0 \\ \mathrm{s}\theta\mathrm{c}\psi & \mathrm{s}\theta\mathrm{s}\psi & \mathrm{c}\theta \end{bmatrix}. \tag{2.9}$$

The pitch angle is zero when the helicopter is horizontal relative to ground, and has a positive pitch angle for a counter-clockwise (CCW) rotation about y-axis. The yaw angle is zero at start, and has a positive yaw angle for CCW rotation about z-axis. When the angles are zero, the two reference frames are coincident.

The rotation matrix is orthogonal and we have

$$\mathbf{R}_b^i \mathbf{R}_b^{i,\top} = \mathbf{I}. \tag{2.10}$$

When differentiating this with time, this gives

$$\frac{d}{dt}[\mathbf{R}_b^i \mathbf{R}_b^{i,\top}] = \dot{\mathbf{R}}_b^i \mathbf{R}_b^{i,\top} + \mathbf{R}_b^i \dot{\mathbf{R}}_b^{i,\top} = 0, \tag{2.11}$$

and so the matrix $\dot{\mathbf{R}}_b^i \mathbf{R}_b^{i,\top}$ is skew symmetric. Defining this skew symmetric matrix as

$$\dot{\mathbf{R}}_b^i \mathbf{R}_b^{i,\top} = (\boldsymbol{\omega}_{ib}^i)^{\mathrm{x}}, \tag{2.12}$$

the kinematic differential equation of the rotation matrix can be formulated as

$$\dot{\mathbf{R}}_b^i = (\boldsymbol{\omega}_{ib}^i)^{\mathrm{x}} \mathbf{R}_b^i = \mathbf{R}_b^i (\boldsymbol{\omega}_{ib}^b)^{\mathrm{x}}. \tag{2.13}$$

The skew symmetric matrix for the angular velocities is

$$(\boldsymbol{\omega}_{ib}^b)^{\mathrm{x}} = \begin{bmatrix} 0 & -\omega_{bz} & \omega_{by} \\ \omega_{bz} & 0 & -\omega_{bx} \\ -\omega_{by} & \omega_{bx} & 0 \end{bmatrix}, \tag{2.14}$$

where ω_{bx}, ω_{by} and ω_{bz} are the angular velocities in x_b-, y_b- and z_b-directions in body frame.

The angular velocities of the Euler angles is $\dot{\boldsymbol{\lambda}} = [\dot{\phi}, \dot{\theta}, \dot{\psi}]^T$. The angular velocity in body frame relative to this will be [14]

$$\boldsymbol{\omega}_{ib}^b = \begin{bmatrix} \omega_{bx} \\ \omega_{by} \\ \omega_{bz} \end{bmatrix} = \mathbf{E}_b(\lambda)\dot{\lambda} = \begin{bmatrix} 1 & 0 & -\mathrm{s}\theta \\ 0 & \mathrm{c}\phi & \mathrm{c}\theta\mathrm{s}\phi \\ 0 & -\mathrm{s}\phi & \mathrm{c}\theta\mathrm{c}\phi \end{bmatrix} \begin{bmatrix} \dot{\phi} \\ \dot{\theta} \\ \dot{\psi} \end{bmatrix}. \tag{2.15}$$

The determinant of matrix $\mathbf{E}_b(\lambda)$ is equal to $\cos\theta$, and when this is zero there is a singularity to the matrix. This is the Euler-angle singularity for this choice of rotation matrix, meaning it is not possible to describe the angular velocity for all components when $\theta = \pm$ 90 degrees. Since the pitch angle for this system is constrained to $\pm$ 62 degrees, this will not be an issue for the Aero. For small angles, the angular velocities in body frame, $\boldsymbol{\omega}_{ib}^b$, can be approximated to the angular velocities, $\dot{\boldsymbol{\lambda}}$, and this will be used when linearizing the dynamic equations for the Aero in the next section.

Inverting the matrix $\mathbf{E}_b(\lambda)$ gives the angular velocities of the Euler angles relative to angular velocities in body frame

$$\begin{bmatrix} \dot{\phi} \\ \dot{\theta} \\ \dot{\psi} \end{bmatrix} = \frac{1}{\mathrm{c}\theta} \begin{bmatrix} \mathrm{c}\theta & \mathrm{s}\phi\mathrm{s}\theta & \mathrm{c}\phi\mathrm{s}\theta \\ 0 & \mathrm{c}\phi\mathrm{c}\theta & -\mathrm{s}\phi\mathrm{c}\theta \\ 0 & \mathrm{s}\phi & \mathrm{c}\phi \end{bmatrix} \begin{bmatrix} \omega_{bx} \\ \omega_{by} \\ \omega_{bz} \end{bmatrix}. \tag{2.16}$$

Now the position, velocity and acceleration of the center of mass relative to the inertial frame can be found. The center of mass, $\mathbf{r}_{cm}$, for the Aero body is located in position $[0, -l_{cm}, -l_{cm}]^\top$ relative to the body frame. The position and velocity of the center of mass in the inertial frame will be

$$\mathbf{r}_i = \mathbf{R}_b^i \mathbf{r}_b, \tag{2.17}$$

$$\dot{\mathbf{r}}_i = \dot{\mathbf{R}}_b^i \mathbf{r}_b + \mathbf{R}_b^i \dot{\mathbf{r}}_b. \tag{2.18}$$

Since the position of the center of mass is constant in the body frame, the time derivative of this will be zero, reducing the Equation (2.18) to

$$\begin{aligned} \dot{\mathbf{r}}_i &= \dot{\mathbf{R}}_b^i \mathbf{r}_b \\ &= \mathbf{R}_b^i (\boldsymbol{\omega}_{ib}^b)^{\mathrm{x}} \mathbf{r}_b. \end{aligned} \tag{2.19}$$

The acceleration is then

$$\begin{aligned} \ddot{\mathbf{r}}_i &= \ddot{\mathbf{R}}_b^i \mathbf{r}_b, \\ &= \dot{\mathbf{R}}_b^i (\boldsymbol{\omega}_{ib}^b)^{\mathrm{x}} \mathbf{r}_b + \mathbf{R}_b^i (\dot{\boldsymbol{\omega}}_{ib}^b)^{\mathrm{x}} \mathbf{r}_b \\ &= \mathbf{R}_b^i (\boldsymbol{\omega}_{ib}^b)^{\mathrm{x}} (\boldsymbol{\omega}_{ib}^b)^{\mathrm{x}} \mathbf{r}_b + \mathbf{R}_b^i (\dot{\boldsymbol{\omega}}_{ib}^b)^{\mathrm{x}} \mathbf{r}_b, \end{aligned} \tag{2.20}$$

where the first term of Equation (2.20) is the centripetal acceleration and the second term is the transversal acceleration.

The forces on the Aero body is visualized in Figure 2.5 showing both a free body diagram (FBD) and a kinetic diagram (KD). The main motor is producing two forces, one main force, F_{Mz}, in the z_b-direction that will give a positive pitch angle and also a force, F_{My}, in the y_b-direction, meaning this will give a yaw angle. This last force is due to the aerodynamic forces. The tail motor is also producing two forces, F_{Tz} and F_{Ty}. This motor is basically here to counteract the yaw from the main motor and thus control the yaw while the main motor is controlling the pitch. These forces are functions of the two system inputs V_p and V_y. Viscous damping, proportional to the velocity of the Aero body, is also present. An angular velocity ω_{bz}, gained with a damping constant D_{Vy}, is damping for a rotation about yaw axis, z_b, and an angular velocity ω_{by}, gained with a damping constant D_{Vp}, is damping for a rotation about pitch axis, y_b.
The Aero body is pivoted in origo with the support yoke, and there is one tangential force, F_t and one normal force, F_n in this point. The tangential force will have one component in x_b direction, while the normal force will have one component in y_b- and z_b- direction. There is also a gravity force, F_g caused by the total mass of the Aero body, m_b, and the constant of acceleration due to gravity, g. Since the center of mass is below the pivot point, the Aero body behaves as a pendulum. Now that the acceleration is found and all forces identified, the first equation for the motion of Aero body can be found.

To find the inertia and moments for the Equation (2.3), the system is considered in the body

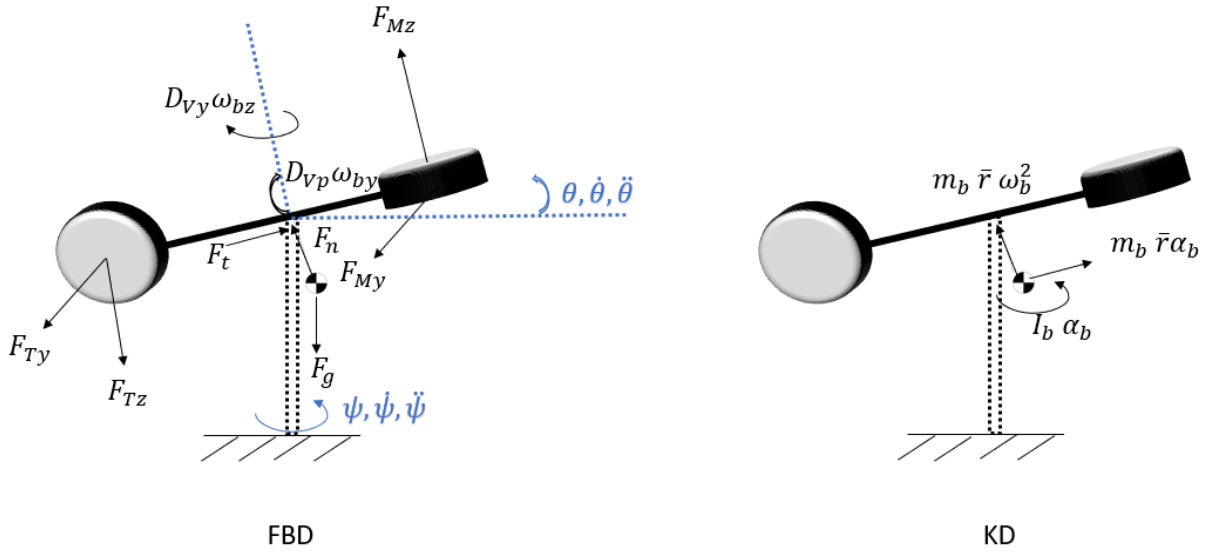

Figure 2.5: Free body diagram and kinetic diagram of the Aero body

frame. By taking the sum of moments about the pivot point, the tangential and normal force will not give any moments. The sum of moments for the Aero body is then

$$\sum \mathbf{M}_b = \begin{bmatrix} 0 \\ F_{Mz} r_p + F_{Tz} r_p - F_g l_{cm} \mathrm{s}\theta - D_{Vp}\omega_{by} \\ F_{Ty} r_p - F_{My} r_p - D_{Vy}\omega_{bz} \end{bmatrix} \tag{2.21}$$

$$= \begin{bmatrix} 0 \\ f_1(V_p) + f_2(V_y) - F_g l_{cm} \mathrm{s}\theta - D_{Vp}\omega_{by} \\ f_3(V_y) + f_4(V_p) - D_{Vy}\omega_{bz} \end{bmatrix}, \tag{2.22}$$

where r_p is distance from the pivot point to the motors, the functions $f_1(V_p)$ and $f_2(V_y)$ are the main- and cross torque about pitch axis, y_b, produced by input voltages, and functions $f_3(V_y)$ and $f_4(V_p)$ are the main- and cross torque about the yaw axis, z_b, produced by input voltages.

The inertia tensor is

$$\mathbf{I_{b/o}} = \begin{bmatrix} I_{xx} & I_{xy} & I_{xz} \\ I_{yx} & I_{yy} & I_{yz} \\ I_{zx} & I_{zy} & I_{zz} \end{bmatrix}, \tag{2.23}$$

which is the inertia about the three axis x_b, y_b and z_b. For the Aero body, the elements in this matrix will be constant and invariant with time since this is relative to the body frame. The masses for the Aero body is divided into three components as illustrated in Figure 2.6. That is the mass of the horizontal metal tube and one mass for each of the thrusters with propeller and motor. The metal tube is considered as a rod rotating about its center with mass m_{tube} and length l_{tube}, where the center of mass is in the pivot point, $[0, 0, 0]^\top$. The two thrusters are considered as point masses, m_p, rotating at distance r_p from the pivot point. The main thruster has its center of mass in $[-r_p, 0, -l_1]^\top$ while the tail thruster has its center of mass in $[r_p, -l_1, 0]^\top$. The distances l_1 in Figure 2.6 is exaggerated for illustration purpose only.

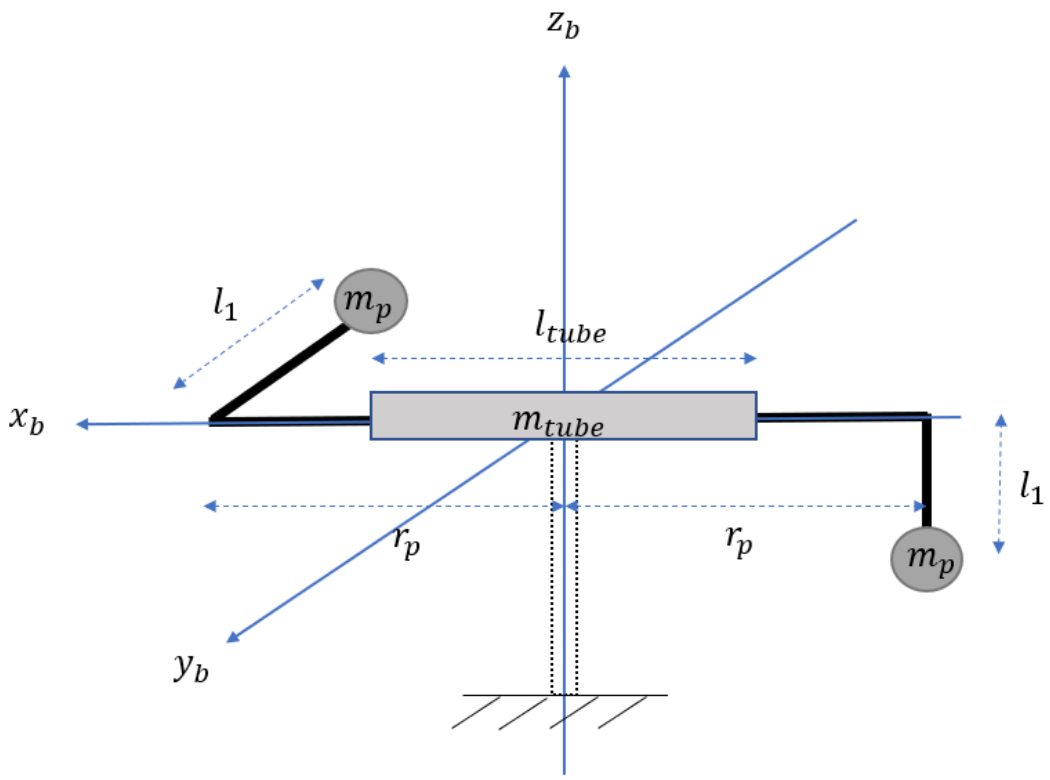

Figure 2.6: Mass components for the Aero body

This gives the following inertia for the Aero body :

$$\begin{aligned} I_{pb(xx)} &= 2m_p l_1^2 \\ I_{pb(xy)} &= I_{pb(yx)} = m_p l_1 r_p, \\ I_{pb(xz)} &= I_{pb(zx)} = -m_p l_1 r_p, \\ I_{pb(yz)} &= I_{pb(zy)} = 0, \\ I_{pb(yy)} &= \frac{1}{12} m_{tube} l_{tube}^2 + 2m_p r_p^2 + m_p l_1^2, \\ I_{pb(zz)} &= I_{pb(yy)}. \end{aligned} \tag{2.24}$$

There are also signals that will affect the system but that are not chosen as input to the system. These are disturbance signals [16]. For this model, there are still unmodeled dynamics like Coulomb friction not included in the model that will be a disturbance to the plant. The support yoke will also rotate with a rotation $\mathbf{R}_z(\psi)$, changing inertia of the system. To simplify the system some, the support yoke has been disregarded, and so this will give a disturbance to the system in form of unmodeled dynamic. The mass of the two thrusters that are considered as point masses give a disturbance to the model since the inertia for these are simplified. There can be load variations that affect the system that can not be controlled like wind and turbulence for air vehicles and also measurement disturbances in gyros and accelerometers like electronic noise, drifts and misalignment. There can also be changes in the plant caused by for instance wear. All these disturbances are included in the model as τ_Δ.

Now all components for the second equation of motion is found and we have

$$\mathbf{I}_{b/o}\dot{\omega}_{ib}^b = \sum \mathbf{M}_b - (\omega_{ib}^b)^{\times}\mathbf{I}_{b/o}\omega_{ib}^b + \tau_\Delta. \tag{2.25}$$

The pitch angle is as mentioned before constrained for the Aero to the range of $\pm$ 62 deg and also the input voltages V_p and V_y are constrained with limits of $\pm$ 24 V, and both constraints have a

nonlinear behavior, i.e. saturation. The Aero is not able to roll, and so the angular velocity in roll, $\dot{\phi}$, is set to zero.

2.3.1 Nonlinear model of the Aero

The objective is to control the attitude of the Aero with control of pitch and yaw angles. The state space variables are then defined as

$$\mathbf{x}^T = [\theta, \psi, \omega_{by}, \omega_{bz}], \tag{2.26}$$

with output variables

$$\mathbf{y}^T = [\theta, \psi, \omega_{by}, \omega_{bz}], \tag{2.27}$$

and control variables

$$\mathbf{u}^T = [V_p, V_y]. \tag{2.28}$$

The model can be expressed as

$$\begin{bmatrix} \dot{\theta} \\ \dot{\psi} \\ \dot{\omega}_{by} \\ \dot{\omega}_{bz} \end{bmatrix} = \begin{bmatrix} \omega_{by} \\ \frac{1}{\cos\theta}\omega_{bz} \\ \mathbf{I}_{2b}^{-1}[\sum \mathbf{M}_b - (\omega_2)^{\mathrm{x}}\mathbf{I}_{2b}\omega_{ib}^b + \tau_{\Delta,y}] \\ \mathbf{I}_{3b}^{-1}[\sum \mathbf{M}_b - (\omega_3)^{\mathrm{x}}\mathbf{I}_{3b}\omega_{ib}^b + \tau_{\Delta,z}] \end{bmatrix}, \tag{2.29}$$

where matrix $\mathbf{I}_{2b}^{-1}$ and $\mathbf{I}_{3b}^{-1}$ is the second and third row of matrix $\mathbf{I}_{b/o}^{-1}$, matrix $(\boldsymbol{\omega}_2)^{\mathrm{x}}$ and $(\boldsymbol{\omega}_3)^{\mathrm{x}}$ is the second and third row of the skew symmetric matrix $(\boldsymbol{\omega}_{ib}^b)^{\mathrm{x}}$ and $\mathbf{I}_{2b}$ and $\mathbf{I}_{3b}$ is the second and third row of the inertia matrix $\mathbf{I}_{b/o}$ and $\tau_{\Delta,y}$ and $\tau_{\Delta,z}$ are disturbances.

A simplified version of this is

$$\begin{bmatrix} \dot{\theta} \\ \dot{\psi} \\ \dot{\omega}_{by} \\ \dot{\omega}_{bz} \end{bmatrix} = \begin{bmatrix} \omega_{by} \\ \frac{1}{\cos\theta}\omega_{bz} \\ I_p^{-1}\sum \mathbf{M}_{by} \\ I_y^{-1}\sum \mathbf{M}_{bz} \end{bmatrix} \tag{2.30}$$

$$= \begin{bmatrix} \omega_{by} \\ \frac{1}{\cos\theta}\omega_{bz} \\ I_p^{-1}(f_1(V_p) + f_2(V_y) - F_g l_{cm}\mathrm{s}\theta - D_{Vp}\omega_{by}) \\ I_y^{-1}(f_3(V_y) + f_4(V_p) - D_{Vy}\omega_{bz}) \end{bmatrix}, \tag{2.31}$$

where the cross terms of the angular velocities are disregarded and only the diagonal elements from the inertia tensor is included and I_p is the same as inertia I_{yy} and I_y is the same as I_{zz} and where the disturbances are not included. Another simplification is considering the functions of the input variables, $f_1(V_p)$, $f_2(V_y)$, $f_3(V_y)$ and $f_4(V_p)$ as linear. Then the model can be expressed as

$$\begin{bmatrix} \dot{\theta} \\ \dot{\psi} \\ \dot{\omega}_{by} \\ \dot{\omega}_{bz} \end{bmatrix} = \begin{bmatrix} \omega_{by} \\ \frac{1}{\cos\theta}\omega_{bz} \\ I_p^{-1}(K_{pp}V_p + K_{py}V_y - F_g l_{cm}\mathrm{s}\theta - D_{Vp}\omega_{by}) \\ I_y^{-1}(K_{yy}V_y + K_{yp}V_p - D_{Vy}\omega_{bz}) \end{bmatrix}, \tag{2.32}$$

where K_{pp} and K_{yy} are torque thrust gains from main and tail motors, K_{py} is cross-torque thrust gain acting on pitch from tail motor, and K_{yp} is cross-torque thrust gain acting on yaw from main motor. Rewriting Equation (2.32) into state space form gives

$$\dot{\mathbf{x}} = \begin{bmatrix} x_3 \\ \frac{1}{\cos x_1}x_4 \\ I_p^{-1}(K_{pp}u_1 + K_{py}u_2 - F_g l_{cm}\sin x_1 - D_{Vp}x_3) \\ I_y^{-1}(K_{yy}u_2 + K_{yp}u_1 - D_{Vy}x_4) \end{bmatrix}, \tag{2.33}$$

and this is the model that will be used for the nonlinear controller.

2.3.2 Linearized model of Quanser Aero

The model for the Aero has also been linearized. If assuming small changes in the angles, the model can be linearized with $\sin\theta \approx \theta$ and $\cos\theta \approx 1$, $\omega_{by} \approx \dot{\theta}$ and $\omega_{bz} \approx \dot{\psi}$. Then the state space variables from Equation (2.26) can be linearized to

$$\mathbf{x}^\top = [\theta, \psi, \dot{\theta}, \dot{\psi}], \tag{2.34}$$

and the output and control variables are the same as for the nonlinear model as given in Equations (2.27) and (2.28). The nonlinear state space model from Equation (2.33) can now be expressed as

$$\dot{\mathbf{x}} = \begin{bmatrix} x_3 \\ x_4 \\ I_p^{-1}(K_{pp}u_1 + K_{py}u_2 - F_g l_{cm} x_1 - D_{Vp}x_3) \\ I_y^{-1}(K_{yy}u_2 + K_{yp}u_1 - D_{Vy}x_4) \end{bmatrix}. \tag{2.35}$$

This gives the linear state space model

$$\begin{aligned} \dot{\mathbf{x}} &= \mathbf{A}\mathbf{x} + \mathbf{B}\mathbf{u} \\ &= \begin{bmatrix} 0 & 0 & 1 & 0 \\ 0 & 0 & 0 & 1 \\ -\frac{F_g l_{cm}}{I_p} & 0 & -\frac{D_{Vp}}{I_p} & 0 \\ 0 & 0 & 0 & -\frac{D_{Vy}}{I_y} \end{bmatrix} \mathbf{x} + \begin{bmatrix} 0 & 0 \\ 0 & 0 \\ \frac{K_{pp}}{I_p} & \frac{K_{py}}{I_p} \\ \frac{K_{yp}}{I_y} & \frac{K_{yy}}{I_y} \end{bmatrix} \mathbf{u}, \end{aligned} \tag{2.36}$$

$$\begin{aligned} \mathbf{y} &= \mathbf{C}\mathbf{x} + \mathbf{D}\mathbf{u} \\ &= \begin{bmatrix} 1 & 0 & 0 & 0 \\ 0 & 1 & 0 & 0 \\ 0 & 0 & 1 & 0 \\ 0 & 0 & 0 & 1 \end{bmatrix} \mathbf{x} + \begin{bmatrix} 0 & 0 \\ 0 & 0 \\ 0 & 0 \\ 0 & 0 \end{bmatrix} \mathbf{u}. \end{aligned} \tag{2.37}$$

This is the model that will be used for the linear controller, LQR. In the next section the parameters for the model are estimated.

2.4 Estimation of Variables

All the parameters for the equation of motion need to be estimated, and for this model this mean finding values for all mass components of the Aero, the distance between the pivot point and thrusters, r_p, length of metal tube l_{tube}, the center of mass, $\mathbf{r}_{cm}$, the viscous damping coefficients D_{Vp} and D_{Vy}, and finding the main and cross torque gains for the four functions $f_1(V_p)$, $f_2(V_y)$, $f_3(V_y)$ and $f_4(V_p)$. The mass components are the Aero body, $m_b = 1.075$ kg, mass of thruster including motor $m_p = 0.43$ kg and mass of metal tube $m_{tube} = 0.094$ kg, and are supplied in a MATLAB file from Quanser. There are uncertainties to these value since they have not been measured. Also the lengths $r_p = 0.158$ m and $l_{tube} = 0.1651$ m are given in documents from Quanser and are also easily measured to verify the values. All inertia components can be estimated based on these values for mass and lengths. The other values will now be estimated.

2.4.1 Estimating Center of Mass

The distance to center of mass for a 1DOF configuration as shown in Figure 2.7 is given in documents from Quanser. This is used to find the center of mass for the 2DOF configuration. The center of

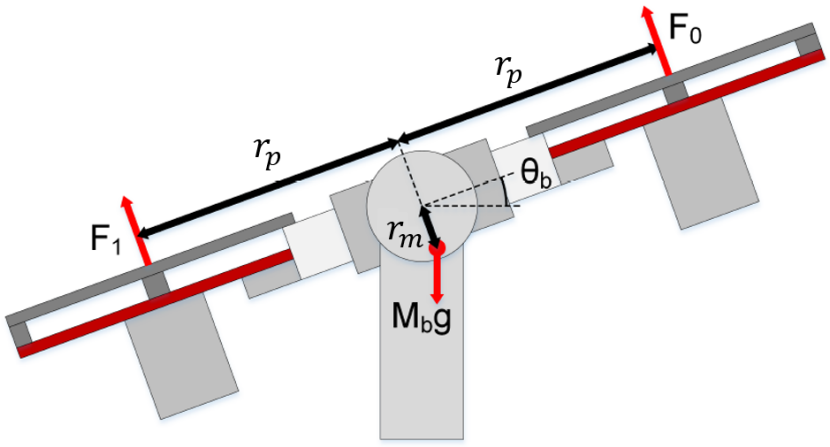

Figure 2.7: 1DOF configuration of Quanser Aero

mass for the 1DOF configuration is located at

$$\mathbf{r}_{cm1} = \frac{\sum_1^n m_i \mathbf{r}_i}{m_b} \tag{2.38}$$

$$= \frac{m_p[-r_p, 0, -l_1]^\top + m_p[r_p, 0, -l_1]^\top + m_{tube}[0, 0, 0]^\top}{m_b} \tag{2.39}$$

$$= \frac{2m_p}{m_b}[0, 0, -l_1]^\top \tag{2.40}$$

$$= [0, 0, -r_m]^\top, \tag{2.41}$$

where r_m is distance to center of mass in z_b-direction. From this the value of l_1, that is the distance from the x_b-axis to the mass center of the motors can be estimated and is equal $r_m m_b/2m_p$. Now the center of mass for the 2DOF configuration can be found.

$$\mathbf{r}_{cm} = \frac{\sum_1^n m_i \mathbf{r}_i}{m_b} \tag{2.42}$$

$$= \frac{m_p[-r_p, 0, -l_1]^\top + m_p[r_p, -l_1, 0]^\top + m_{tube}[0, 0, 0]^\top}{m_b} \tag{2.43}$$

$$= [0, -l_{cm}, -l_{cm}]^\top, \tag{2.44}$$

and l_{cm} is estimated equal $l_1 m_p/m_b$. The center of mass, $\mathbf{r}_{cm}$, for the pitch body is then located below the pivot point in negative z_b direction and also in negative y_b direction.
The distance to center of mass have also been estimated by testing on the Aero [4]. Then a mass, M, in the form of small washers was applied at a distance r_p from the pivot point and the pitch angle was measured for different masses. Solving for the equilibrium torque

$$m_b g l_{cm} \sin\theta = M g r_p \cos\theta, \tag{2.45}$$

the center of mass could be estimated. This was calculated for different masses as Figure 2.8 shows, and the average was then calculated to be the center of mass, giving $l_{cm} = 2.6$ mm. From the first method the value for l_{cm} was found to be 3.8 mm and so there is uncertainty related to this value.

2.4.2 Estimating Viscous Damping about Pitch Axis

The method to estimate viscous damping was similar to the method described in Quansers Lab Guide [17] and theory for this is from [18]. To estimate the viscous damping for the pitch axis, the yaw axis was first locked to make the system 1DOF. Then an initial disturbance in form of a short impulse of -20 V was applied to the main motor. Since the pivot point is not equal to the center

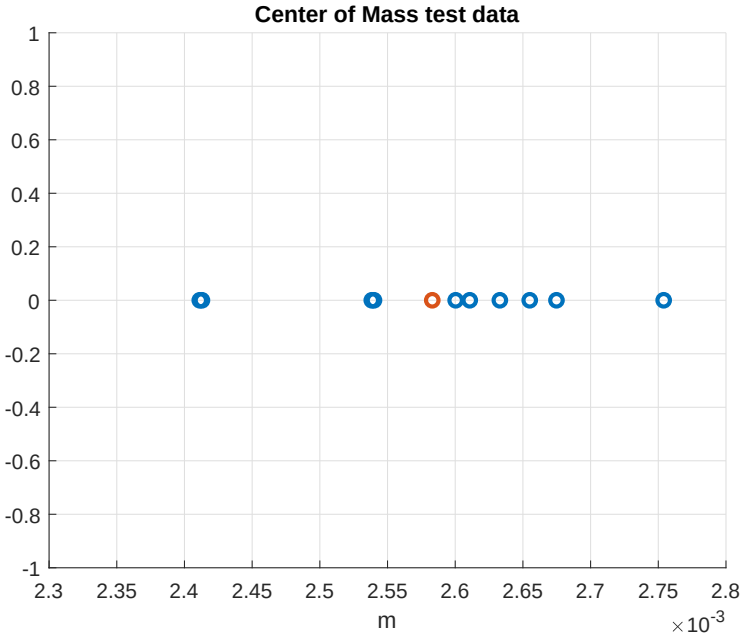

Figure 2.8: Test data for center of mass of pitch body

of mass of the pitch body, the gravitational force makes the system oscillate about the pivot point, and so the free vibration of the pitch body was looked at. Figure 2.9 shows the pitch angle and velocity as the system oscillates. The 1DOF equation of motion is now

$$I_p\ddot{\theta} = -D_{Vp}\dot{\theta} - m_b g l_{cm} \sin\theta, \tag{2.46}$$

and because this is a second order nonlinear differential equation an approximate solution is considered when finding the damping and assuming small angular displacements, $\sin\theta \approx \theta$. The second order differential equation is then:

$$I_p\ddot{\theta} + D_{Vp}\dot{\theta} + K_{sp}\theta = 0, \tag{2.47}$$

where K_{sp} is equal $m_b g l_{cm}$. Assuming a solution in the form $\theta(t) = Ce^{rt}$, the characteristic equation is

$$I_p r^2 + D_{Vp} r + K_{sp} = 0, \tag{2.48}$$

where the roots are

$$r_{1,2} = -\frac{D_{Vp}}{2I_p} \pm \sqrt{\left(\frac{D_{Vp}}{2I_p}\right)^2 - \frac{K_{sp}}{I_p}} \tag{2.49}$$

and the solution to this can be written as

$$\theta(t) = C_1 e^{(-\zeta+\sqrt{\zeta^2-1})\omega_n t} + C_2 e^{(-\zeta+\sqrt{\zeta^2-1})\omega_n t}, \tag{2.50}$$

where ζ is the damping ratio, ω_n is the undamped natural frequency and C_1 and C_2 are constants determined from the initial conditions of $\theta(0)$ and $\dot{\theta}(0)$. For this system the initial velocity is assumed to be $\dot{\theta}(0) = 0$. From Figure 2.9 the system can be seen to have an underdamped solution. From this, the frequency of the damped vibration can be calculated as

$$\omega_d = \frac{2\pi}{t_{osc}}, \tag{2.51}$$

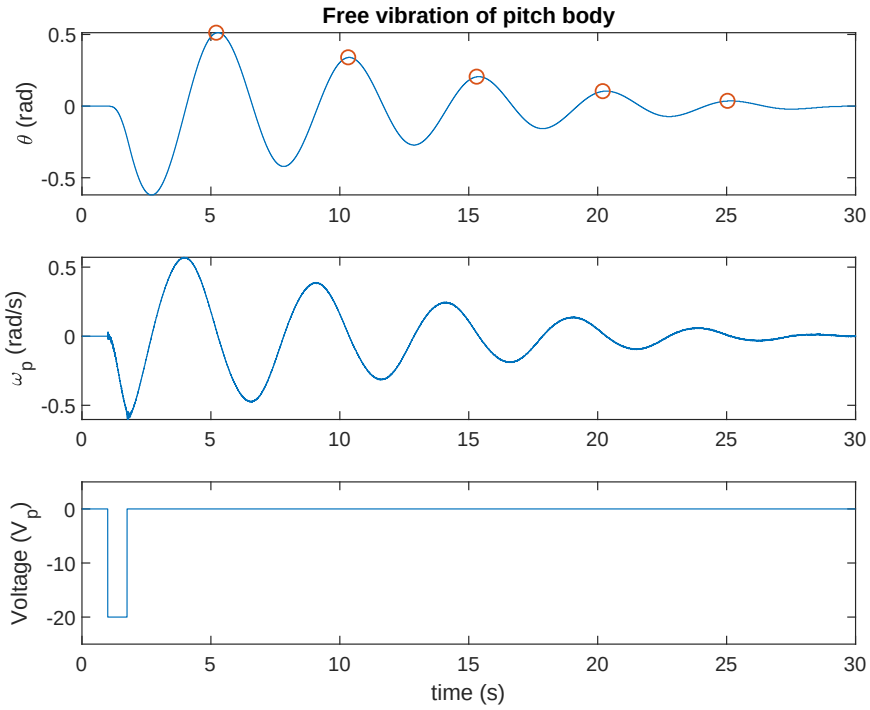

Figure 2.9: Free vibration of pitch body

where t_{osc} is the time between each amplitude. The amplitude of the first and the nth overshoot was measured and the logarithmic decrement computed as

$$\delta = \frac{1}{n-1} \ln \frac{\theta_1}{\theta_n}. \tag{2.52}$$

The viscous damping ratio was then found as

$$\zeta = \frac{\delta}{\sqrt{(2\pi)^2 + \delta^2}}, \tag{2.53}$$

and so the undamped natural frequency could be found as

$$\omega_n = \frac{\omega_d}{\sqrt{1-\zeta^2}}. \tag{2.54}$$

The logarithmic decrement is equal to

$$\delta = \frac{2\pi}{\omega_d} \frac{D_{Vp}}{2I_p}, \tag{2.55}$$

and so the damping was estimated to be

$$D_{Vp} = \frac{I_p \delta \omega_d}{\pi}. \tag{2.56}$$

The same test was performed five times giving five estimates of the damping, and an average of this was calculated. The value of D_{Vp} was found to be 0.0052.

2.4.3 Estimating Viscous Damping about Yaw Axis

To estimate the viscous damping for yaw axis, the same method as described in Quansers Lab guide [17] was used. First, the pitch axis was locked, so the system only has 1DOF. Then a short impulse

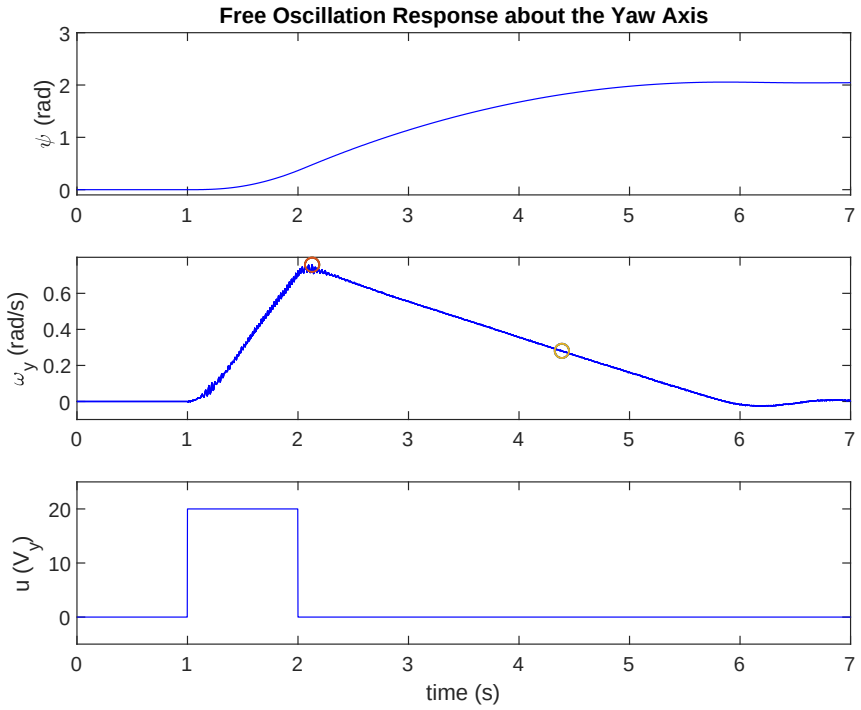

Figure 2.10: Estimation of viscous damping for yaw axis

of -20V was applied to the tail motor, V_y, and the free oscillation response was looked at. The equation of motion was then

$$I_y\ddot{\psi} = -D_{Vy}\dot{\psi}, \tag{2.57}$$

and in terms of angular rate this is

$$I_y\dot{\omega}_{by} + D_{Vy}\omega_{by} = 0. \tag{2.58}$$

Laplace transforming this one gets

$$\omega_{by}(s) = \frac{I_y/D_{Vy}}{I_y/D_{Vy}s + 1}\omega_{by}(0), \tag{2.59}$$

and this is similar to a first order response with a time constant, τ, equal I_y/D_{Vy}. To find the time constant, the time to reach 63% of the final value is looked at, defined as $\tau = t_1 - t_0$. Here t_0 is the start time and t_1 is the time when 63% of the final value is reached. The final value will be zero and so we are looking to find t_1 when

$$\omega_{by}(t_1) = (1 - e^{-1})(\omega_{by,ss} - \omega_{by}(t_0)) = e^{-1}\omega_{by}(0). \tag{2.60}$$

A plot of this test is shown in Figure 2.10, where $\omega_{by}(t_1)$ and $\omega_{by}(t_0)$ is marked in the second subplot. Now the time constant was estimated $\tau = t_1 - t_0$ and so the damping was found as

$$D_{Vy} = \frac{I_y}{\tau}. \tag{2.61}$$

The same test was performed five times giving five estimates of the damping, and an average of this was calculated. The value of D_{Vy} was estimated to be 0.0095.

2.4.4 Estimating Main Torque for Pitch Axis

To estimate the parameters for the main torque $f_1(V_p)$ from Equation (2.22) for the pitch axis, the yaw axis was first locked. The system can then not rotate about the yaw axis and has only 1DOF.

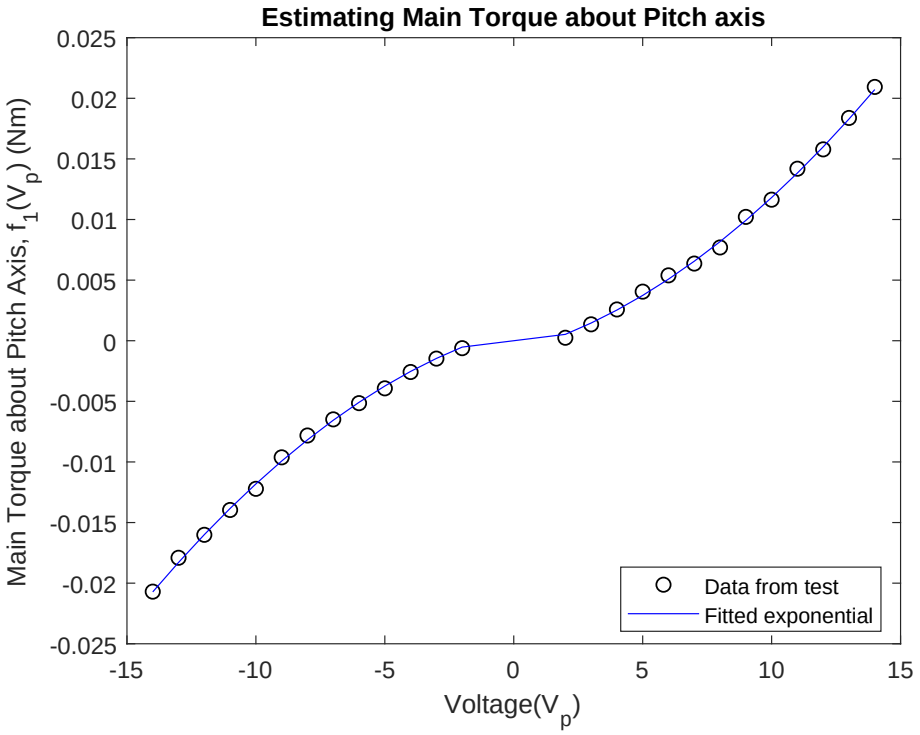

Figure 2.11: Estimating parameters for the main torque from applying different voltages to the main motor.

Then a voltage was applied to the main motor, V_p, and the resulting pitch angle when the system was at rest was measured. Since $\ddot{\theta} = \dot{\theta} = V_y = 0$, the equilibrium for this is

$$0 = f_1(V_p) - m_b g l_{cm} \sin\theta, \tag{2.62}$$

and so the main torque can be estimated based on torque from the gravity that will change for different angles. A plot of the test data is shown in Figure 2.11. A least square curve fit was used to get the parameters for the curve on the form

$$f_1(V_p) = \text{sign}(V_p) K_{p1} V_p^2 + K_{p2} V_p - K_{p3}\text{sign}(V_p), \tag{2.63}$$

giving satisfying results with a correlation of 99.98% between data and estimated curve. An applied voltage between -1.8V and $+1.8$V did not change the pitch angle.
The resulted parameters were: $K_{p1} = 6.80e^{-5}$, $K_{p2} = 5.95e^{-4}$ and $K_{p3} = 9.37e^{-4}$.

A linearized estimate was also found from the same data giving the linear function

$$f_1(V_p) = K_{pp} V_p, \tag{2.64}$$

where K_{pp} is estimated to 0.0012.

2.4.5 Estimating Main Torque for Yaw Axis

To find the parameters for the main torque about the yaw axis, $f_3(V_y)$, from Equation (2.22), the pitch axis was first locked, thus the system can only rotate about the yaw axis and has 1DOF. A voltage was applied to the tail motor, V_y over a period of 4 seconds, and the angular velocity was recorded. The equation of motion was then

$$I_y \ddot{\psi} = f_3(V_y) - D_{Vy}\dot{\psi}, \tag{2.65}$$

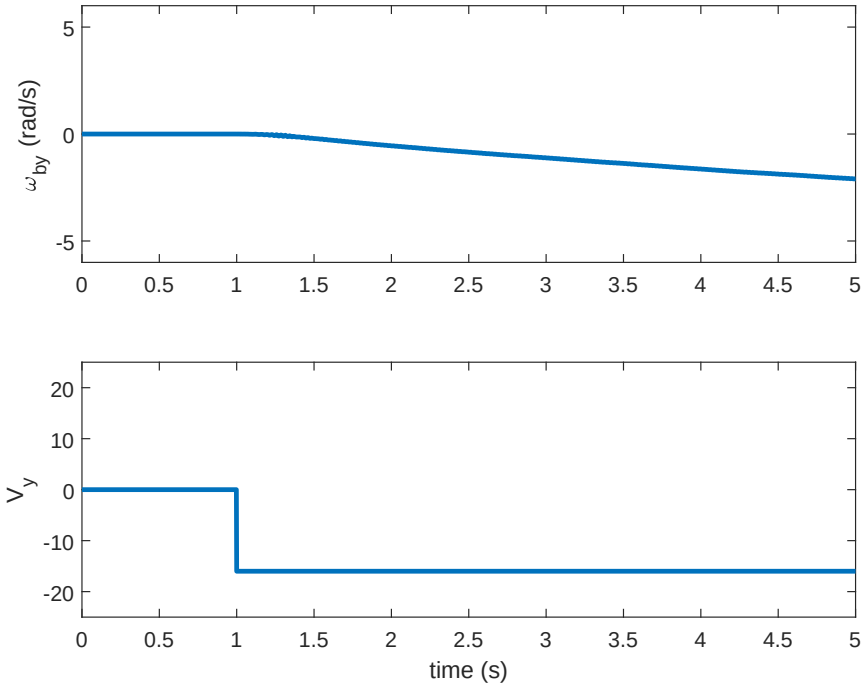

Figure 2.12: Test to estimate parameters for the main torque about yaw.

and so the function $f_3(V_y)$ was estimated from

$$\begin{aligned} f_3(V_y) &= I_y\dot{\omega}_{by} + D_{Vy}\omega_{by} \\ &= I_y\frac{\Delta\omega_{by}}{\Delta t} + D_{Vy}\Delta\omega_{by}, \end{aligned} \tag{2.66}$$

where Δt is the time from the voltage was applied to the test was stopped, and $\Delta\omega_{by}$ is the change of angular rate over this time. Figure 2.12 shows one of the tests where a voltage of -16 V was applied to the tail motor. This was tested for different values of V_y and used for solving Equation (2.66). The results was plotted as Figure 2.13 shows. A least square curve fit was used to get the parameters for the curve on the same form as for the main torque about pitch, where

$$f_3(V_y) = \text{sign}(V_y)K_{y1}V_y^2 + K_{y2}V_y - K_{y3}\text{sign}(V_y), \tag{2.67}$$

and the resulted parameters were: $K_{y1} = 4.00e^{-5}$, $K_{y2} = 1.65e^{-3}$ and $K_{y3} = 1.09e^{-2}$.

A linearized estimate was also found from the same data giving the linear function

$$f_3(V_3) = K_{yy}V_y, \tag{2.68}$$

where K_{yy} was estimated to 0.00176.

2.4.6 Estimating Cross Torque for Pitch and Yaw axis

To estimate the parameters for the cross torque $f_2(V_y)$ from Equation (2.22), the same method as described in Quansers lab guide [17] was followed. The equation was first linearized. Next, a voltage V_y was applied to the Aero while $V_p = 0$ and the response for pitch axis was recorded. The equation is then

$$I_p\ddot{\theta} = f_2(V_y) - D_{Vp}\dot{\theta} - m_b g l_{cm}\theta, \tag{2.69}$$

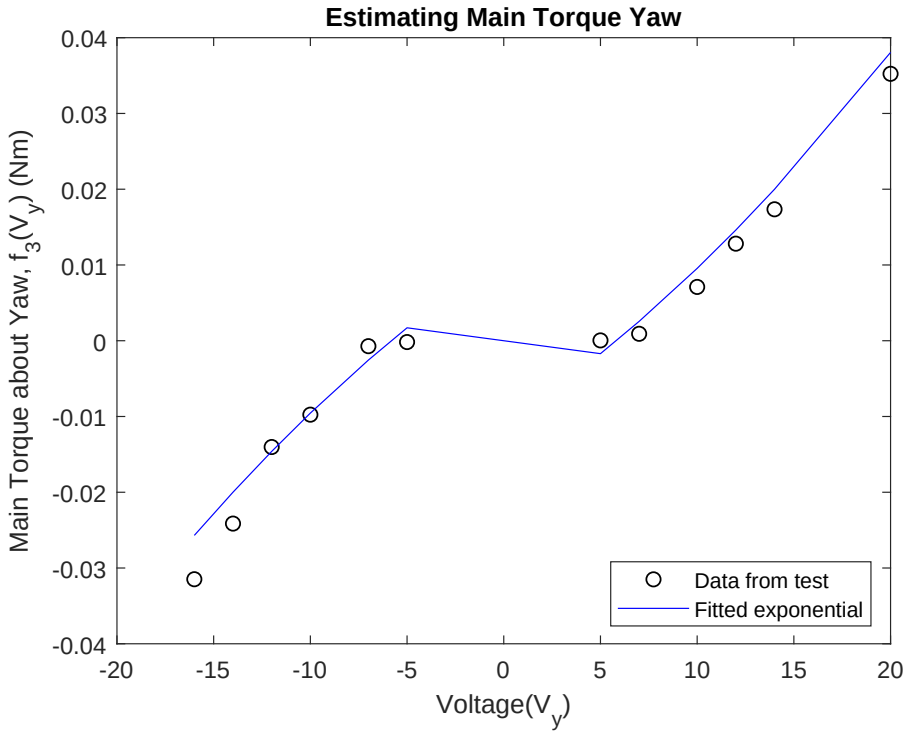

Figure 2.13: Estimating parameters for the main torque from applying different voltages to the tail motor.

that in terms of angular velocity gives

$$\begin{aligned} f_2(V_y) &= I_p\dot{\omega}_{by} + D_{Vp}\omega_{by} \\ &= I_p\frac{\Delta\omega_{by}}{\Delta t} + D_{Vp}\Delta\omega_{by}, \end{aligned} \tag{2.70}$$

where Δt is the time from applied voltage to angular velocity is maximum and $\Delta\omega_{by}$ is the change of angular rate that is equal to the maximum angular velocity. The test was performed for different voltages as Figure 2.14 shows, and a linear function for this was found to be

$$f_2(V_y) = K_{py}V_y, \tag{2.71}$$

with the value for K_{py} to be 0.0012.

The same method was used when finding the cross torque about the yaw axis. The equilibrium equation was then

$$I_y\ddot{\psi} = f_4(V_p) - D_{Vy}\dot{\psi}, \tag{2.72}$$

that in terms of angular velocity gives

$$\begin{aligned} f_4(V_p) &= I_y\dot{\omega}_{bz} + D_{Vy}\omega_{bz} \\ &= I_y\frac{\Delta\omega_{bz}}{\Delta t} + D_{Vy}\Delta\omega_{bz}, \end{aligned} \tag{2.73}$$

and a linear function was estimated to be

$$f_4(V_p) = K_{yp}V_p, \tag{2.74}$$

with the value of K_{yp} to be -0.0014.

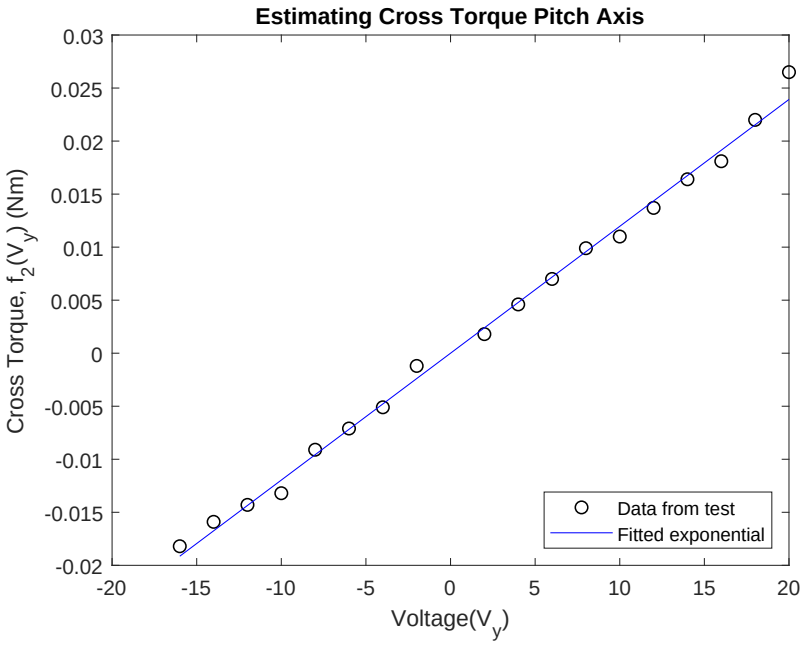

Figure 2.14: Test data for cross torque for pitch axis

Chapter 3

Control Design

3.1 Control of Multivariable systems (MIMO)

A MIMO system has more than one input and output to its system [16]. One input can affect more than one output, and it is the cross coupling between inputs and outputs that makes a MIMO system difficult to control. For a MIMO system, one can connect each input to an output and then control every pair as a SISO system. The problem with this approach is that even though every SISO system in the MIMO system is stable, the MIMO system can still be unstable. And all partial SISO systems can be minimum-phase and the MIMO system can be non-minimum phase. If there is a strong cross coupling between input and outputs, the system is better treated as one unit.

Modeling of a single variable system leads to a differential equation that contains input and output. For a multivariable system one get a vector-differential equation. The easiest way of representing such a system is in state space.

Stability of a linear MIMO system is just as for a linear SISO system. The system is stable if all poles are in the left half plane. The poles are the eigenvalues counted with multiplicity of the system matrix $\mathbf{A}$ when the system is represented in state space form. The number of poles gives the order of the system as well.[16, Theorem 3.10]

An important feature in the design of control systems is whether or not the system is controllable and observable. Definitions of these are therefor given.

Definition 1 (Controllability) *[16] The state x^* is said to be **controllable** if there is an input that in finite time gives the state x^* from the initial state $x(0) = 0$. The system is said to be **controllable** if all states are controllable.*

Definition 2 (Observability) *[16] The state $x^* \neq 0$ is said to be **unobservable** if, when $u(t) = 0$, $t \geq 0$ and $x(0) = x^*$, the output is $y(t) \equiv 0, t \geq 0$. The system is said to be **observable** if it lacks unobservable states.*

Considering a system

$$\dot{\mathbf{x}} = \mathbf{A}\mathbf{x} + \mathbf{B}\mathbf{u}, \tag{3.1}$$

$$\mathbf{y} = \mathbf{C}\mathbf{x}, \tag{3.2}$$

where $\mathbf{A}$ is an $n \times n$ matrix, $\mathbf{u}$ is an m-vector and $\mathbf{C}$ is a $p \times n$ matrix, the condition for complete state controllability requires that the rank of the $n \times nm$ matrix

$$[\mathbf{B} \;\; \mathbf{AB} \;\; \cdots \;\; \mathbf{A}^{n-1}\mathbf{B}], \tag{3.3}$$

is n. The condition for complete state observability is that the rank of the $np \times n$ matrix

$$\begin{bmatrix} \mathbf{C} \\ \mathbf{CA} \\ \vdots \\ \mathbf{CA}^{n-1} \end{bmatrix} \tag{3.4}$$

is n. A controllable system can always be stabilized and an observable system is always detectable. For a linear system like Equation (3.1), one important feature is that the eigenvalues in the **A**-matrix can be modified with state feedback if the system is controllable. If the system is not completely controllable, only the controllable eigenvalues can be modified.

3.1.1 Linear vs nonlinear model

There are different methods for control of a MIMO system. Linear controllers are widely used because there is a well developed mathematical theory for linear systems. But a real control system contain some form of nonlinearity, and with linear controllers approximations are used. The more advanced controllers can use a nonlinear model of the system for control and then use a more accurate model. When a linear model is used, the principle of superposition is valid, and this is not the case for nonlinear models since then the outputs are not proportional to the inputs. Another option is to linearize the model piecewise, defining different state space models for each instance [16].

There are two basic limitations with linearization. Linear approximations will only be valid over a limited range, when the system is outside the range, the linear controller will not be effective and the error will increase. Also, the dynamics of a linear system will not be as rich as the dynamics of a nonlinear system. [19].

Some non-linear properties are saturation, where a variable have limits to the amplitude, sine, cosine and exponential functions.

In this thesis, two PID based controllers will be simulated and tested, treating the system as two SISO system for controlling pitch and yaw separately. These controllers are not model-based. A linear controller, LQR, will be simulated and tested with the linear model of Aero and a nonlinear controller using adaptive backstepping will be simulated and tested using the nonlinear model of the Aero.

3.2 PID

A PID controller has a proportional-, derivative and an integrating term added together and is a well known feedback controller. With a control input *u(t)* and an error *e(t)* defined as the difference between the desired setpoint and the measured output, this can be expressed as

$$u(t) = K_p e(t) + K_i \int_0^t e(\varphi) d\varphi + K_d \dot{e}(t), \tag{3.5}$$

where K_p is the proportional gain, K_i is the integration gain and K_d is the derivative gain.

In this thesis, two different PID controllers will be simulated and tested. The PID controllers are not model-based.

3.2.1 Decoupled PID Control of the Aero

The system for Aero has two inputs that affect both control of pitch angle and of yaw angle. Now a decoupled controller is considered where one PID controller will be designed for control of pitch and one PID controller for yaw for the main torques, and where the cross coupling is considered as a disturbance to the system.

The two equations describing the dynamics of the system from Equation (2.35) is then rewritten into

$$I_p\ddot{\theta} = K_{pp}V_p - D_{Vp}\dot{\theta} - m_b g l_{cm}\theta, \tag{3.6}$$
$$I_y\ddot{\psi} = K_{yy}V_y - D_{Vy}\dot{\psi}, \tag{3.7}$$

just neglecting the cross torques. Now the system can be described by two transfer functions and so by taking the Laplace transform of Equations (3.6) and (3.7), and assuming the initial conditions for the angles and velocities are zero, $\theta(0) = \dot{\theta}(0) = \psi(0) = \dot{\psi}(0) = 0$, gives

$$I_p s^2\theta(s) = K_{pp}V_p(s) - D_{Vp}s\theta(s) - m_b g l_{cm}\theta(s), \tag{3.8}$$
$$\frac{\theta(s)}{V_p(s)} = \frac{K_{pp}}{I_p s^2 + D_{Vp}s + m_b g l_{cm}}, \tag{3.9}$$

for pitch and

$$I_y s^2\psi = K_{yy}V_y(s) - D_{Vy}s\psi, \tag{3.10}$$
$$\frac{\psi(s)}{V_y(s)} = \frac{K_{yy}}{I_y s^2 + D_{Vy}s} \tag{3.11}$$

for yaw.

Laplace transforming the PID controller gives

$$C(s) = K_p + \frac{K_i}{s} + K_d s, \tag{3.12}$$

and the open loop for pitch, compensated with a PID gives

$$P_o(s) = C_1(s)\frac{\theta(s)}{V_p(s)} \tag{3.13}$$
$$= \frac{\frac{K_{pp}}{I_p}(K_p s + k_i + k_d s^2)}{s(s^2 + \frac{D_{Vp}}{I_p}s + \frac{m_b g l_{cm}}{I_p})}. \tag{3.14}$$

Closing the loop with unity feedback gives

$$P_c(s) = \frac{\frac{K_{pp}}{I_p}(K_p s + k_i + k_d s^2)}{s^3 + (\frac{D_{Vp}}{I_p} + \frac{K_{pp}}{I_p}k_d)s^2 + (\frac{m_b g l_{cm}}{I_p} + \frac{K_{pp}}{I_p}k_p)s + \frac{K_{pp}}{I_p}k_i}, \tag{3.15}$$

where the characteristic equation can be looked at as a third-order equation on the form

$$T(s) = (s + p_0)(s^2 + 2\zeta\omega_n s + \omega_n^2), \tag{3.16}$$

where p_0 is positon of a zero and ζ is damping and ω_n is frequency of the desired response. The gains are chosen by setting the characteristic equation from Equation (3.15) equal Equation (3.16) and choosing values for p_0, ζ and ω_n.
The same method is used for the compensator for yaw. A block diagram of the system is shown in Figure 3.1.

3.2.2 Decoupled PV Control of the Aero

Another PID-based controller is a proportional-velocity (PV) controller that is presented in Quansers lab guide [17]. This is almost like a PD controller except only the negative velocity is fed back unlike the PD controller where the velocity of the error is fed back. This is a decoupled controller just as the PID controller in Section 3.2.1. One PV controller is designed for control of pitch and one for control of yaw for the main torques, and the Equations (3.6) and (3.7) are used to describe the

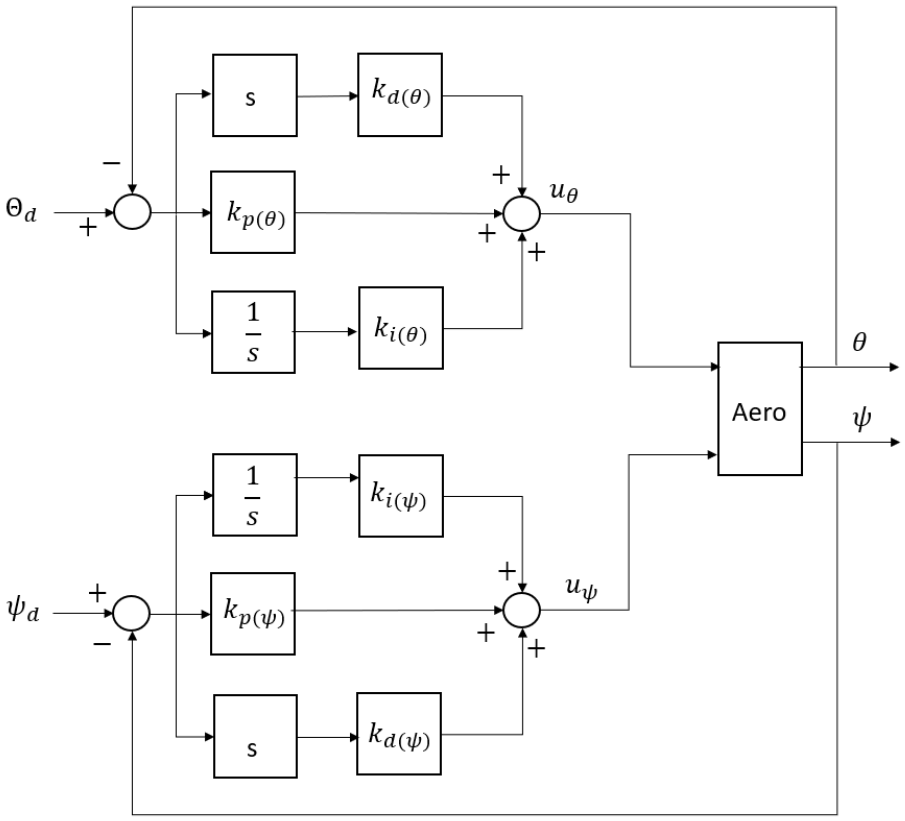

Figure 3.1: Block diagram of decoupled PID control of the Aero

system for Aero.
The two controllers can be expressed by

$$u_1(t) = K_{p(\theta)}e_1(t) - K_{d(\theta)}\dot{\theta}(t), \tag{3.17}$$

$$u_2(t) = K_{p(\psi)}e_2(t) - K_{d(\psi)}\dot{\psi}(t), \tag{3.18}$$

where $u_\theta(t) = V_p(t)$ is the control input for pitch angle, $u_\psi(t) = V_y(t)$ is control input for yaw angle, $e_1(t) = \theta_d(t) - \theta(t)$ is the error in pitch angle from desired to actual angle, $e_2(t) = \psi_d(t) - \psi(t)$ is the error in yaw angle, the constants $K_{p(\theta)}$ and $K_{p(\psi)}$ are proportional gains for pitch and yaw, and the constants $K_{d(\theta)}$ and $K_{d(\psi)}$ are the derivative gains for pitch and yaw.

All initial conditions are assumed to be zero. A block diagram of the control structure is shown in Figure 3.2. Laplace transforming of Equations (3.17) and (3.18) give

$$V_p(s) = K_{p(\theta)}(\theta_d(s) - \theta(s)) - K_{d(\theta)}s\theta(s), \tag{3.19}$$

$$V_y(s) = K_{p(\psi)}(\psi_d(s) - \psi(s)) - K_{d(\psi)}s\psi(s), \tag{3.20}$$

and using the Laplace transformation from Equations (3.9) and (3.11) for the system, the closed loop transfer functions for pitch and yaw can be found.

3.3 Linear Quadratic Regulator (LQR)

An optimal controller [13] seeks to maximize return from a system

$$\dot{\mathbf{x}} = f(\mathbf{x}(t), \mathbf{u}(t), t) \tag{3.21}$$

by finding a control $\mathbf{u}(t)$ that minimizes a cost function

$$J = \int_{t_0}^{t_1} h(\mathbf{x}(t), \mathbf{u}(t), t)dt. \tag{3.22}$$

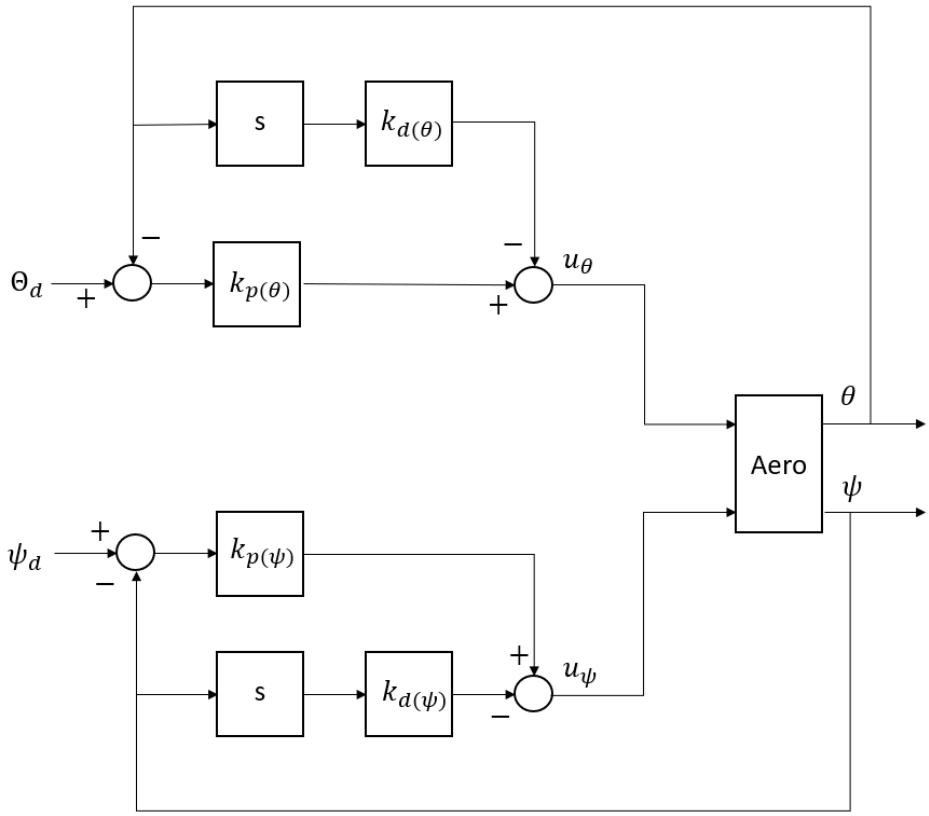

Figure 3.2: Block diagram of decoupled PV control of the Aero

How the cost function will look like depends on what kind of control problem to solve. For instance, the aim can be to minimize the control energy when transferring a state from an initial to a final state. This is used for satellite control. Another example is a regulator control problem, that is if a system has a displacement from its equilibrium point, the regulator will seek to return to equilibrium while minimizing the cost function. Generalizing this regulator problem for time-varying desired states, this is called tracking.

If the state and control variables in the cost function are squared, the cost function becomes quadratic, and this gives the advantage for a linear system of a solution with a linear control law

$$\mathbf{u}(t) = -\mathbf{K}\mathbf{x}(t), \tag{3.23}$$

where matrix $\mathbf{K}$ is the state feedback gain. An LQR is an optimized regulator for the linear system

$$\dot{\mathbf{x}} = \mathbf{A}\mathbf{x} + \mathbf{B}\mathbf{u}, \tag{3.24}$$

seeking to find the matrix $\mathbf{K}$ of the control law from Equation (3.23) with the aim of minimizing the cost function

$$J = \int_0^\infty (\mathbf{x}^\top \mathbf{Q}\mathbf{x} + \mathbf{u}^\top \mathbf{R}\mathbf{u})dt, \tag{3.25}$$

where $\mathbf{Q}$ is a weight matrix for the state variables and $\mathbf{R}$ is a weight matrix for the control values, both square and symmetric [20]. Solving this optimization problem gives

$$\begin{aligned} \dot{\mathbf{x}} &= \mathbf{A}\mathbf{x} - \mathbf{B}\mathbf{K}\mathbf{x}, \\ &= (\mathbf{A} - \mathbf{B}\mathbf{K})\mathbf{x}, \end{aligned} \tag{3.26}$$

and the matrix $(\mathbf{A} - \mathbf{BK})$ needs to be stable. By substituting Equation (3.23) into (3.25) yields

$$J = \int_0^\infty \mathbf{x}^\top (\mathbf{Q} + \mathbf{K}^\top \mathbf{R}\mathbf{K})\mathbf{x} dt, \tag{3.27}$$

and by setting

$$\mathbf{x}^\top (\mathbf{Q} + \mathbf{K}^\top \mathbf{R}\mathbf{K})\mathbf{x} = -\frac{d}{dt}(\mathbf{x}^\top \mathbf{P}\mathbf{x}), \tag{3.28}$$

where $\mathbf{P}$ is a square, symmetric matrix we get

$$\begin{aligned} \mathbf{x}^\top (\mathbf{Q} + \mathbf{K}^\top \mathbf{R}\mathbf{K})\mathbf{x} &= -\dot{\mathbf{x}}^\top \mathbf{P}\mathbf{x} - \mathbf{x}^\top \mathbf{P}\dot{\mathbf{x}}, \\ &= -\mathbf{x}^\top [(\mathbf{A} - \mathbf{BK})^\top \mathbf{P} + \mathbf{P}(\mathbf{A} - \mathbf{BK})]\mathbf{x}, \end{aligned} \tag{3.29}$$

and then

$$(\mathbf{Q} + \mathbf{K}^\top \mathbf{R}\mathbf{K}) = -[(\mathbf{A} - \mathbf{BK})^\top \mathbf{P} + \mathbf{P}(\mathbf{A} - \mathbf{BK})], \tag{3.30}$$

must hold true for any $\mathbf{x}$. Now the matrix $\mathbf{R}$ is set equal to $\mathbf{T}^\top \mathbf{T}$ and Equation (3.30) can be written as

$$\mathbf{Q} + \mathbf{K}^\top \mathbf{T}^\top \mathbf{T}\mathbf{K} + (\mathbf{A} - \mathbf{BK})^\top \mathbf{P} + \mathbf{P}(\mathbf{A} - \mathbf{BK}) = 0, \tag{3.31}$$

$$\mathbf{Q} + \mathbf{A}^\top \mathbf{P} + \mathbf{P}\mathbf{A} + [\mathbf{TK} - (\mathbf{T}^\top)^{-1}\mathbf{B}^\top \mathbf{P}]^\top [\mathbf{TK} - (\mathbf{T}^\top)^{-1}\mathbf{B}^\top \mathbf{P}] - \mathbf{P}\mathbf{B}\mathbf{R}^{-1}\mathbf{B}^\top \mathbf{P} = 0, \tag{3.32}$$

and the minimum occurs when

$$\mathbf{TK} = (\mathbf{T}^\top)^{-1}\mathbf{B}^\top \mathbf{P}. \tag{3.33}$$

This gives the optimal matrix $\mathbf{K}$ to be

$$\mathbf{K} = \mathbf{R}^{-1}\mathbf{B}^\top \mathbf{P}, \tag{3.34}$$

and so the optimal control law is

$$\mathbf{u}(t) = -\mathbf{K}\mathbf{x}(t), \tag{3.35}$$

$$= -\mathbf{R}^{-1}\mathbf{B}^\top \mathbf{P}\mathbf{x}(t). \tag{3.36}$$

Equation (3.30) can be reduced to

$$\mathbf{P}\mathbf{A} + \mathbf{A}^\top \mathbf{P} - \mathbf{P}\mathbf{B}\mathbf{R}^{-1}\mathbf{B}^\top \mathbf{P} + \mathbf{Q} = 0. \tag{3.37}$$

This is called the reduced matrix Riccati equation, and the matrix $\mathbf{P}$ must satisfy this equation. An LQR needs the matrices $\mathbf{A}$ and $\mathbf{B}$ to be able to calculate $\mathbf{K}$, and so a limitation of the LQR is that all the parameters in the linear model need to be estimated or known.

For a tracking problem where the state vector $\mathbf{x}(t)$ should follow a desired trajectory $\mathbf{x_r}(t)$, solution of minimizing the cost function yields the Riccatti equation (3.37) obtained for the LQR with an additional set [13]

$$\dot{\mathbf{s}} = (\mathbf{A} - \mathbf{B}\mathbf{R}^{-1}\mathbf{B}^\top \mathbf{P})^\top \mathbf{s} - \mathbf{Q}\mathbf{x_r}, \tag{3.38}$$

where $\mathbf{s}$ is a tracking vector with boundary conditions

$$\mathbf{s}(t_1) = 0. \tag{3.39}$$

3.3.1 Design Procedure of LQR

The design procedure for a LQR is to first check controllability of the system. If not all the state variables are available for feedback a state observer is needed to estimate the state variables that can not be measured, so a check of observability is needed. Then the matrices $\mathbf{Q}$ and $\mathbf{R}$ need to be found, where higher elements in the $\mathbf{Q}$ matrix will give faster system dynamics, requiring higher control values also, and a higher value of elements in $\mathbf{R}$ reduces the value of the control gains and so this says something to how aggressive the controller is. Now the solution for matrix $\mathbf{P}$ from the Riccati equation must be found. With matlab, if matrices $\mathbf{A}$, $\mathbf{B}$, $\mathbf{Q}$ and $\mathbf{R}$ are defined, the function $[\mathbf{K}, \mathbf{P}, \mathbf{E}] = \text{lqr}(\mathbf{A}, \mathbf{B}, \mathbf{Q}, \mathbf{R})$ gives the solution matrices, where vector $\mathbf{E}$ is the eigenvalues of $(\mathbf{A} - \mathbf{BK})$.

3.3.2 LQR of the Aero

The linear state space model

$$\begin{aligned}\dot{\mathbf{x}}(\mathbf{t}) &= \mathbf{A}\mathbf{x}(t) + \mathbf{B}\mathbf{u}(t) \\ &= \begin{bmatrix} 0 & 0 & 1 & 0 \\ 0 & 0 & 0 & 1 \\ -\frac{F_g l_{cm}}{I_p} & 0 & -\frac{D_{Vp}}{I_p} & 0 \\ 0 & 0 & 0 & -\frac{D_{Vy}}{I_y} \end{bmatrix} \mathbf{x}(t) + \begin{bmatrix} 0 & 0 \\ 0 & 0 \\ \frac{K_{pp}}{I_p} & \frac{K_{py}}{I_p} \\ \frac{K_{yp}}{I_y} & \frac{K_{yy}}{I_y} \end{bmatrix} \mathbf{u}(t), \end{aligned} \tag{3.40}$$

$$\begin{aligned}\mathbf{y}(t) &= \mathbf{C}\mathbf{x}(t) + \mathbf{D}\mathbf{u}(t) \\ &= \begin{bmatrix} 1 & 0 & 0 & 0 \\ 0 & 1 & 0 & 0 \\ 0 & 0 & 1 & 0 \\ 0 & 0 & 0 & 1 \end{bmatrix} \mathbf{x}(t) + \begin{bmatrix} 0 & 0 \\ 0 & 0 \\ 0 & 0 \\ 0 & 0 \end{bmatrix} \mathbf{u}(t) \end{aligned} \tag{3.41}$$

will be used for the LQR where $\mathbf{x}(t)$ are the state variables from the linearized model, repeated here as

$$\mathbf{x}(t)^\top = [\theta(t), \psi(t), \dot{\theta}(t), \dot{\psi}(t)] \tag{3.42}$$

and the control variables are

$$\mathbf{u}(\mathbf{t})^T = [V_p(t), V_y(t)]. \tag{3.43}$$

The objective for the Aero is to follow a desired state trajectory, and so an optimized control $\mathbf{u}(t)$ with the aim of minimizing the cost function

$$J = \int_0^\infty \Big((\mathbf{x_r}(t) - \mathbf{x}(t))^\top \mathbf{Q} (\mathbf{x_r}(t) - \mathbf{x}(t)) + \mathbf{u}(\mathbf{t})^\top \mathbf{R} \mathbf{u}(\mathbf{t}) \Big)\, dt, \tag{3.44}$$

needs to be found where $\mathbf{x_r}(t)$ are the desired state variables. The LQR is thus a regulator that in this case will be used as a tracking controller and so the design of this controller is probably not optimal as a tracking controller. The matrix $\mathbf{Q} \in \mathbb{R}^{4\times4}$ since there are four states, and the matrix $\mathbf{R} \in \mathbb{R}^{2\times2}$ since there are two control variables. The block diagram for this is shown in Figure 3.3, with the controller for this to be

$$\mathbf{u}(t) = \mathbf{K}(\mathbf{x}_r(t) - \mathbf{x}(t)), \tag{3.45}$$

where matrix $\mathbf{K} \in \mathbb{R}^{2\times4}$. The solution for the matrix $\mathbf{P} \in \mathbb{R}^{4\times4}$ for the Riccati equation is found in MATLAB with the function $[\mathbf{K}, \mathbf{P}, \mathbf{E}] = \text{lqr}(\mathbf{A}, \mathbf{B}, \mathbf{Q}, \mathbf{R})$, where there are four eigenvalues in the vector $\mathbf{E}$.

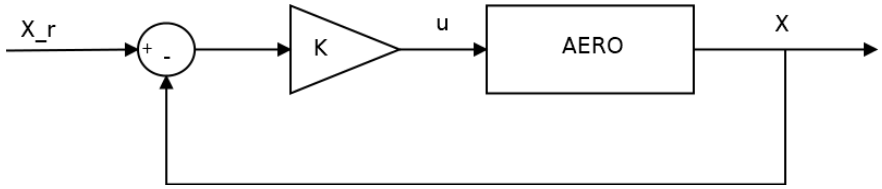

Figure 3.3: Block diagram for LQR of the Aero

3.4 Adaptive Control

Adaptive control systems have a history going back to the 1950's, when the idea of a controller that could adjust itself and adapt its parameters in a feedback system emerged. The goal for an adaptive controller is to control plants with unknown parameters and change behavior as a response to dynamic in a system and also change behavior if there are disturbances to the system. This controller can be used both for linear and nonlinear systems, and has been most successful for parameters appearing linearly. An adaptive controller is designed with a combination of a control law together with estimates of the unknown parameters that are adjusted when the system is operating [21].

There have been proposed several different adaptive control designs, such as MRAC, adaptive pole placement control and adaptive backstepping. The adaptive control technique can be classified into Lyapunov-based and estimation-based techniques. The difference between these two is that they have different update laws for the unknown parameters and different ways of proving stability and convergence.

Lyapunov-based design uses a Lyapunov function to prove stability and to choose the control so that stability of the equilibrium is achieved. Stability is the main requirement for all controllers and stability of equilibrium points is Lyapunov stability and will be the focus in the next section.

3.4.1 Lyapunov Stability

Since the system of the Aero considered in this thesis is a non-autonomous system where the solution to the differential equation depends on both t and t_0, the stability of the equilibrium point for such a system is looked into. The objective is then to stabilize a system

$$\dot{\mathbf{x}} = f(t, \mathbf{x}), \quad \mathbf{x}(t_0) = \mathbf{x}_0, \tag{3.46}$$

where $\mathbf{x} \in \mathbb{R}^n$, and $f(t, \mathbf{x}) : \mathbb{R}_+ \times \mathbb{R}^n \to \mathbb{R}^n$ is piecewise continuous in t and locally Lipschitz in $\mathbf{x}$, and the origin is an equilibrium point of (3.46). If a system does not have the equilibrium point at the origin, a change of variables is used so that the system is transformed to have its equilibrium at the origin. If assuming this change of variables is done for (3.46), then the origin is an an equilibrium point at $t = 0$ if

$$f(t, \mathbf{0}) = \mathbf{0}, \quad \forall t \geq 0. \tag{3.47}$$

Definition 3 *[21] A continuous function $\gamma : [0, a) \to \mathbb{R}_+$ is said to belong to klass $\mathcal{K}$ if it is strictly increasing and $\gamma(0) = 0$. It is said to belong to class $\mathcal{K}_\infty$ if $a = \infty$ and $\gamma(r) \to \infty$ as $r \to \infty$.*

To see if an equilibrium point is stable or not, a definition of the systems stability of the origin with respect to initial time is now given.

Definition 4 *[19] The equilibrium point $\mathbf{x} = \mathbf{0}$ of (3.46) is*

- *stable if, for each $\epsilon > 0$, there is $\delta = \delta(\epsilon, t_0) > 0$ such that*

$$\|\mathbf{x}(t_0)\| < \delta \Rightarrow \|\mathbf{x}(t)\| < \epsilon, \ \forall t \geq t_0 \geq 0; \tag{3.48}$$

- *uniformly stable if, for each* $\epsilon > 0$, *there is* $\delta = \delta(\epsilon) > 0$, *independent of* t_0, *such that* (3.48) *is satisfied;*
- *unstable if not stable;*
- *asymptotically stable if it is stable and there is a positive constant* $c = c(t_0)$ *such that* $x(t) \to 0$ *as* $t \to \infty$, *for all* $\|\mathbf{x}(t_0)\| < c$;
- *uniformly asymptotically stable if it is uniformly stable and there is a positive constant* c, *independent of* t_0, *such that for all* $\|\mathbf{x}(t_0)\| < c$, $\mathbf{x}(t) \to 0$ *as* $t \to \infty$, *uniformly in* t_0, *that is, for each* $\eta > 0$, *there is* $T = T(\eta) > 0$ *such that*

$$\|\mathbf{x}(t)\| < \eta, \ \forall t \geq t_0 + T(\eta), \ \forall \|\mathbf{x}(t_0)\| < c; \tag{3.49}$$

- *globally uniformly asymptotically stable if it is uniformly stable,* $\delta(\epsilon)$ *can be chosen to satisfy* $\lim_{\epsilon \to \infty} \delta(\epsilon) = \infty$, *and, for each pair of positive numbers* η *and* c, *there is* $T = T(\eta, c) > 0$ *such that*

$$\|\mathbf{x}(t)\| < \eta, \ \forall t \geq t_0 + T(\eta, c), \ \|x(t_0)\| < c. \tag{3.50}$$

To determine stability of equilibrium points, a Lyapunov function is used. Often, a Lyapunov function is taken as the total energy of the system, but this is not always the case. A function $V(x)$ can be chosen as a Lyapunov function candidate (LFC), and require that it satisfies the conditions given in the Lyapunov stability theorem. This theorem is now stated for an autonomous system

$$\dot{\mathbf{x}} = f(\mathbf{x}). \tag{3.51}$$

Theorem 1 (Lyapunov Stability) *[19] Let* $\mathbf{x} = \mathbf{0}$ *be an equilibrium point of* (3.51) *and* $D \subset \mathbb{R}^n$ *be a domain containing* $x = 0$. *Let* $V : D \to \mathbb{R}$ *be a continuously differentiable function such that*

$$V(0) = 0 \ \text{ and } \ V(x) > 0 \ \text{ in } \ D - \{0\}, \tag{3.52}$$

$$\dot{V}(x) \leq 0 \ \text{ in } \ D, \tag{3.53}$$

then, $x = 0$ *is stable. Moreover, if*

$$\dot{V}(x) < 0 \ \text{ in } \ D - \{0\}, \tag{3.54}$$

then $x = 0$ *is asymptotically stable.*

If the function $V(x)$ satisfies Equation (3.52) it is said to be *positive definite* and if $\dot{V}(x)$ satisfies Equation (3.53) this is said to be *negative semidefinite* and when it satisfies Equation (3.54) it is said to be *negative definite*. This stability theorem can also be extended to a non-autonomous system, and to also include uniform stability and uniform asymptotic stability and so this theorem is extended and formulated as follows.

Theorem 2 (Uniform Stability) *[21] Let* $x = 0$ *be an equilibrium point of* (3.46) *and* $D = \{x \in \mathbb{R}^n \mid |x| < r\}$. *Let* $V : D \times \mathbb{R}^n \to \mathbb{R}_+$ *be a continuously differentiable function such that* $\forall t \geq 0, \ \forall x \in D$,

$$\gamma_1(|x|) \leq V(x, t) \leq \gamma_2(|x|), \tag{3.55}$$

$$\frac{\partial V}{\partial t} + \frac{\partial V}{\partial x} f(x, t) \leq -\gamma_3(|x|). \tag{3.56}$$

Then the equilibrium $x = 0$ *is*

- *uniformly stable, if* γ_1 *and* γ_2 *are class* $\mathcal{K}$ *functions on* $[0, r)$ *and* $\gamma_3(\cdot) \geq 0$ *on* $[0, r)$;
- *uniformly asymptotically stable, if* γ_1, γ_2 *and* γ_3 *are class* $\mathcal{K}$ *functions on* $[0, r)$;
- *exponentially stable, if* $\gamma_i(\rho) = k_i \rho^\alpha$ *on* $[0, r), k_i > 0, \alpha > 0, i = 1, 2, 3$;

- *globally uniformly stable, if* $D = \mathbb{R}^n$, γ_1 *and* γ_2 *are class* $\mathcal{K}_\infty$ *functions, and* $\gamma_3(\cdot) \geq 0$ *on* $\mathbb{R}_{\geq 0}$;
- *globally uniformly asymptotically stable, if* $D = \mathbb{R}^n$, γ_1 *and* γ_2 *are class* $\mathcal{K}_\infty$ *functions, and* γ_3 *is a class* $\mathcal{K}$ *function on* $\mathbb{R}_{\geq 0}$; *and*
- *globally exponentially stable, if* $D = \mathbb{R}^n$ *and* $\gamma_i(\rho) = k_i \rho^\alpha$ *on* $\mathbb{R}_{\geq 0}, k_i > 0, \alpha > 0, i = 1, 2, 3$.

A desired stability property is to have a uniformly asymptotically stable equilibrium, because then disturbances are better dealt with [21]. Adaptive controllers will in general achieve less strong properties for the equilibrium than this but also more than uniform stability because an adaptive controller will force the tracking error to go towards zero. For a time-varying signal, this is called *tracking*. The following theorem is used for convergence analysis.

Theorem 3 (LaSalle-Yoshizawa) *[21] Let* $x = 0$ *be an equilibrium point of (3.46) and suppose* f *is Locally Lipschitz in* x *uniformly in* t. *Let* $V : \mathbb{R}^n \to \mathbb{R}_+$ *be a continuously differentiable, positive definite and radially unbounded function* $V(x)$ *such that*

$$\dot{V} = \frac{\partial V}{\partial x}(x) f(x,t) \leq -W(x) \leq 0, \quad \forall t \geq 0, \quad \forall x \in \mathbb{R}^n, \tag{3.57}$$

where W *is a continuous function. Then, all solutions of (3.46) are globally uniformly bounded and satisfy*

$$\lim_{t \to \infty} W(x(t)) = 0. \tag{3.58}$$

In addition, if $W(x)$ *is positive definite, then the equilibrium* $x = 0$ *is globally uniformly asymptotically stable (GUAS).*

The Lipschitz condition is a proof of existence and uniqueness of a solution to the differential equation (3.46) and the theorem for this is stated below.

Theorem 4 (Local Existence and Uniqueness) *[19] Let* $f(t,x)$ *be piecewise continuous in* t *and satisfy the Lipschitz condition*

$$||f(t,x) - f(t,y)|| \leq L||x - y||, \tag{3.59}$$

$\forall\ x, y \in B = \{x \in \mathbb{R}^n |\ ||x - x_0|| \leq r\},\ \forall\ t \in [t_0, t_1]$. *Then, there exists some* $\delta > 0$ *such that the state equation* $\dot{x} = f(t,x)$ *with* $x(t_0) = x_0$ *has a unique solution over* $[t_0, t_0 + \delta]$.

By assuming that $f(t,x)$ is piecewise continuous in t, allows including step changes with time for a time-varying input. The constant L is called the *Lipschitz constant*. A locally Lipschitz function on a domain $D \subset \mathbb{R}^n$ is Lipschitz on every subset of D that are closed and bounded.

3.4.2 Adaptive Backstepping Control

Adaptive backstepping is a recursive Lyapunov-based design method, stepping back towards the control input. The controller then has a dynamic feedback for estimating the parameters in form of an adaptive update law, and is a nonlinear dynamic feedback controller. One of the advantages with this controller is that it can avoid cancellations of nonlinearities and has the objective of stabilizing and tracking of a given reference signal.

To design a controller based on backstepping, some of the state variables are considered as virtual controls, and Lyapunov functions are utilized to design the control input and also an update law is chosen to ensure stability of the equilibrium point. Considering a second order system with state space model on the form

$$\begin{aligned} \dot{x}_1 &= x_2 \\ \dot{x}_2 &= u + \phi^T(x_1, x_2)\Theta \end{aligned} \tag{3.60}$$

where vector Θ is unknown and constant and vector ϕ contains known nonlinear functions. For this system, x_2 is first considered as a virtual control, used to stabilize x_1. This is solved with an adaptive controller with a control law $\alpha(x_1)$ and an update law $\dot{\hat{\Theta}} = f(x_1)$. The controller will guarantee boundedness of the plant state x and also stability, where a desired reference signal is tracked. This will be illustrated in the next section with a proof of stability and achieved reference tracking for the Aero system using constructed Lyapunov functions. The procedure for the design of the adaptive backstepping controller follows the procedure in [22].

3.4.3 Adaptive Backstepping Control of the Aero

The dynamical system for the Aero has a nonlinear model with several unknown parameters. The parameters can be estimated but there are uncertainties to the estimates. Because of this an adaptive controller is of high interest for controlling such a system. The nonlinear model given in Chapter 2.3.1 will be used for designing the adaptive controller, with the state variables defined as

$$\mathbf{x}^\top = [\theta, \psi, \omega_{by}, \omega_{bz}],$$

and with the equations for the model

$$\dot{\theta} = \dot{\omega}_{by}, \tag{3.61}$$
$$\dot{\psi} = \frac{1}{\cos\theta}\omega_{bz}, \tag{3.62}$$
$$\dot{\omega}_{by} = I_p^{-1}(K_{pp}V_p + K_{py}V_y - F_g l_{cm}\sin\theta - D_{Vp}\omega_{by}), \tag{3.63}$$
$$\dot{\omega}_{bz} = I_y^{-1}(K_{yy}V_y + K_{yp}V_p - D_{Vy}\omega_{bz}). \tag{3.64}$$

The Aero will now be considered as two second order systems on the form

$$\dot{\omega}_{by} = u_p + \Phi_1^\top(\theta, \omega_{by})\Theta_1, \tag{3.65}$$
$$\dot{\omega}_{bz} = u_y + \Phi_2^\top(\psi, \omega_{bz})\Theta_2, \tag{3.66}$$

where the variables u_p and u_y are the control inputs for pitch and yaw, Φ_1 and Φ_2 are known nonlinear functions and Θ_1 and Θ_2 are unknown vector constants. Equations (3.61) to (3.64) are rewritten into this form, giving the state space model

$$\dot{\mathbf{x}} = \begin{bmatrix} x_3 \\ \frac{1}{cos(x_1)}x_4 \\ u_p + \Phi_1^T(x_1, x_3)\Theta_1 \\ u_y + \Phi_2^T(x_2, x_4)\Theta_2 \end{bmatrix}, \tag{3.67}$$

where the variables u_p and u_y are equal to

$$u_p = \frac{1}{I_p}(K_{pp}u_1 + K_{py}u_2), \tag{3.68}$$
$$u_y = \frac{1}{I_y}(K_{yy}u_2 + K_{yp}u_1),$$

the vectors Φ_1^T and Φ_2^T are the known nonlinear functions

$$\Phi_1 = \begin{bmatrix} \sin x_1 \\ x_3 \end{bmatrix}, \qquad \Phi_2 = x_4, \tag{3.69}$$

and Θ_1 and Θ_2 are the unknown parameters

$$\Theta_1 = \frac{1}{I_p}\begin{bmatrix} -F_g l_{cm} \\ -D_{Vp} \end{bmatrix}, \qquad \Theta_2 = -\frac{D_{Vy}}{I_y}. \tag{3.70}$$

The control objective is to design a control law for $u_p(t)$ and $u_y(t)$ to force the outputs $y_1(t) = x_1(t)$, $y_2(t) = x_2(t)$, $y_3(t) = x_3(t)$ and $y_4(t) = x_4(t)$ and to asymptotically track the reference signals for

pitch and yaw, $x_{r1}(t)$ and $x_{r2}(t)$.

Assumption 1: The reference signals, $x_{r1}(t)$ and $x_{r2}(t)$ and first and second order derivative are piecewise continuous and bounded.

Now the adaptive backstepping control laws for the nonlinear system will be designed.

Step 1 - Design of virtual control
The state variables x_3 and x_4 are considered as control variables and will be used to stabilize x_1 and x_2. The coordinates are changed to

$$z_1 = x_1 - x_{r1}, \tag{3.71}$$
$$z_2 = x_2 - x_{r2}, \tag{3.72}$$
$$z_3 = x_3 - \alpha_1 - \dot{x}_{r1}, \tag{3.73}$$
$$z_4 = \frac{1}{\cos x_1} x_4 - \alpha_2 - \dot{x}_{r2}. \tag{3.74}$$

Here α_1 and α_2 are the virtual controls that will be chosen so that the error functions z_1 and z_2 converges towards zero. The derivative of the tracking errors z_1 and z_2 are

$$\dot{z_1} = x_3 - \dot{x}_{r1}, \tag{3.75}$$
$$\dot{z_2} = \frac{1}{\cos x_1} x_4 - \dot{x}_{r2}, \tag{3.76}$$

and by applying this to Equations (3.73) and (3.74) we have

$$z_3 = \dot{z}_1 - \alpha_1 \Leftrightarrow \dot{z}_1 = z_3 + \alpha_1, \tag{3.77}$$
$$z_4 = \dot{z}_2 - \alpha_2 \Leftrightarrow \dot{z}_2 = z_4 + \alpha_2. \tag{3.78}$$

A control Lyapunov function

$$V_1 = \frac{1}{2} z_1^2 + \frac{1}{2} z_2^2 \tag{3.79}$$

is chosen, and now we want the derivative of this function to be a negative definite function. The derivative of V_1 is

$$\begin{aligned} \dot{V}_1 &= z_1 \dot{z}_1 + z_2 \dot{z}_2, \\ &= z_1(z_3 + \alpha_1) + z_2(z_4 + \alpha_2). \end{aligned} \tag{3.80}$$

The virtual controls are now chosen to be

$$\alpha_1 = -c_1 z_1, \tag{3.81}$$
$$\alpha_2 = -c_2 z_2, \tag{3.82}$$

where c_1 and c_2 are positive constants and so

$$\begin{aligned} \dot{V}_1 &= z_1(z_3 - c_1 z_1) + z_2(z_4 - c_2 z_2), \\ &= -c_1 z_1^2 + z_1 z_3 - c_2 z_2^2 + z_2 z_4. \end{aligned} \tag{3.83}$$

If z_3 and z_4 are zero, then $\dot{V}_1$ is negative and z_1 and z_2 will converge towards zero as wanted.

Step 2 - Design control input and choose an update law
The derivative of z_3 and z_4 are expressed as

$$\begin{aligned}\dot{z_3} &= \dot{x}_3 - \dot{\alpha_1} - \ddot{x}_{r1} \\ &= u_p + \Phi_1^T(x_1, x_3)\Theta_1 - (-c_1\dot{z}_1) - \ddot{x}_{r1} \\ &= u_p + \Phi_1^T(x_1, x_3)\Theta_1 + c_1(x_3 - \dot{x}_{r1}) - \ddot{x}_{r1}, \end{aligned} \tag{3.84}$$

$$\begin{aligned}\dot{z_4} &= \dot{x}_4 - \dot{\alpha_2} - \ddot{x}_{r2} \\ &= u_y + \Phi_2^T(x_2, x_4)\Theta_2 - (-c_2\dot{z}_2) - \ddot{x}_{r2} \\ &= u_y + \Phi_2^T(x_2, x_4)\Theta_2 + c_2(\frac{1}{\cos x_1}x_4 - \dot{x}_{r2}) - \ddot{x}_{r2}. \end{aligned} \tag{3.85}$$

The control inputs u_p and u_y will now be designed so that z_1, z_2, z_3 and z_4 all converge towards zero. To do this, the following second Lyapunov function is utilized

$$V_2 = V_1 + \frac{1}{2}z_3^2 + \frac{1}{2}z_4^2 + \frac{1}{2}\tilde{\Theta}_1^\top\Gamma_1^{-1}\tilde{\Theta}_1 + \frac{1}{2}\tilde{\Theta}_2^\top\Gamma_2^{-1}\tilde{\Theta}_2, \tag{3.86}$$

where Γ_1 and Γ_2 are the adaption gain matrices, both positive definite, and were the matrices

$$\tilde{\Theta}_1 = \Theta_1 - \hat{\Theta}_1, \tag{3.87}$$

$$\tilde{\Theta}_2 = \Theta_2 - \hat{\Theta}_2, \tag{3.88}$$

and since Θ_1 and Θ_2 are constant, the time derivative of Equations (3.87) and (3.88) are

$$\dot{\tilde{\Theta}}_1 = -\dot{\hat{\Theta}}_1, \tag{3.89}$$

$$\dot{\tilde{\Theta}}_2 = -\dot{\hat{\Theta}}_2. \tag{3.90}$$

The derivative of Equation (3.86) gives

$$\begin{aligned}\dot{V}_2 =& \dot{V}_1 + z_3\dot{z}_3 + z_4\dot{z}_4 + \tilde{\Theta}_1^\top\Gamma_1^{-1}\dot{\tilde{\Theta}}_1 + \tilde{\Theta}_2^\top\Gamma_2^{-1}\dot{\tilde{\Theta}}_2 \\ =& - c_1z_1^2 + z_1z_3 - c_2z_2^2 + z_2z_4 + z_3(u_p + \Phi_1^\top(x_1, x_3)\Theta_1 + c_1(x_3 - \dot{x}_{r1}) - \ddot{x}_{r1}) \\ &+ z_4(u_y + \Phi_2^\top(x_2, x_4)\Theta_2 + c_2\left(\frac{1}{\cos x_1}x_4 - \dot{x}_{r2}\right) - \ddot{x}_{r2}) - \tilde{\Theta}_1^\top\Gamma_1^{-1}\dot{\hat{\Theta}}_1 - \tilde{\Theta}_2^\top\Gamma_2^{-1}\dot{\hat{\Theta}}_2. \end{aligned} \tag{3.91}$$

To ensure that the derivative of V_2 is negative definite, the control inputs are chosen to be

$$u_p = - z_1 - \Phi_1^\top\hat{\Theta}_1 - c_3z_3 - c_1(x_3 - \dot{x}_{r1}) + \ddot{x}_{r1}, \tag{3.92}$$

$$u_y = - z_2 - \Phi_2^\top\hat{\Theta}_2 - c_4z_4 - c_2\left(\frac{1}{\cos x_1}x_4 - \dot{x}_{r2}\right) + \ddot{x}_{r2}, \tag{3.93}$$

where c_3 and c_4 are positive constants. By inserting Equations (3.92) and (3.93) into Equation (3.91) we obtain

$$\begin{aligned}\dot{V}_2 &= -c_1z_1^2 - c_2z_2^2 - c_3z_3^2 - c_4z_4^2 + \Phi_1^\top(\Theta_1 - \hat{\Theta}_1)z_3 + \Phi_2^\top(\Theta_2 - \hat{\Theta}_2)z_4 - \tilde{\Theta}_1^\top\Gamma_1^{-1}\dot{\hat{\Theta}}_1 - \tilde{\Theta}_2^\top\Gamma_2^{-1}\dot{\hat{\Theta}}_2, \\ &= -c_1z_1^2 - c_2z_2^2 - c_3z_3^2 - c_4z_4^2 + \Phi_1^\top\tilde{\Theta}_1z_3 + \Phi_2^\top\tilde{\Theta}_2z_4 - \tilde{\Theta}_1^\top\Gamma_1^{-1}\dot{\hat{\Theta}}_1 - \tilde{\Theta}_2^\top\Gamma_2^{-1}\dot{\hat{\Theta}}_2, \\ &= -c_1z_1^2 - c_2z_2^2 - c_3z_3^2 - c_4z_4^2 - \tilde{\Theta}_1^\top\Gamma_1^{-1}(\dot{\hat{\Theta}}_1 - \Gamma_1\Phi_1z_3) - \tilde{\Theta}_2^\top\Gamma_2^{-1}(\dot{\hat{\Theta}}_2 - \Gamma_2\Phi_2z_4), \end{aligned} \tag{3.94}$$

and now the update laws are chosen to be

$$\dot{\hat{\Theta}}_1 = \Gamma_1\Phi_1z_3, \tag{3.95}$$

$$\dot{\hat{\Theta}}_2 = \Gamma_2\Phi_2z_4, \tag{3.96}$$

where the update laws eliminate the last two terms in Equation (3.94). Then

$$\dot{V}_2 = -c_1z_1^2 - c_2z_2^2 - c_3z_3^2 - c_4z_4^2. \tag{3.97}$$

The adaptive backstepping design is summarized in Table 3.1.

Table 3.1: Adaptive Backstepping Control Scheme

Change of coordinates:

$$z_1 = x_1 - x_{r1} \tag{3.71}$$
$$z_2 = x_2 - x_{r2} \tag{3.72}$$
$$z_3 = x_3 - \alpha_1 - \dot{x}_{r1} \tag{3.73}$$
$$z_4 = \frac{1}{\cos x_1} x_4 - \alpha_2 - \dot{x}_{r2} \tag{3.74}$$

Adaptive Control Law:

$$u_p = -z_1 - \Phi_1^\top \hat{\Theta}_1 - c_3 z_3 - c_1(x_3 - \dot{x}_{r1}) + \ddot{x}_{r1} \tag{3.92}$$
$$u_y = -z_2 - \Phi_2^\top \hat{\Theta}_2 - c_4 z_4 - c_2 \left(\frac{1}{\cos x_1} x_4 - \dot{x}_{r2} \right) + \ddot{x}_{r2} \tag{3.93}$$

with virtual controls

$$\alpha_1 = -c_1 z_1 \tag{3.81}$$
$$\alpha_2 = -c_2 z_2 \tag{3.82}$$

Parameter update laws:

$$\dot{\hat{\Theta}}_1 = \Gamma_1 \Phi_1 z_3 \tag{3.95}$$
$$\dot{\hat{\Theta}}_2 = \Gamma_2 \Phi_2 z_4 \tag{3.96}$$

Theorem 5 *Considering the closed loop adaptive system consisting of the plant* (3.67)*, the adaptive controllers* (3.92) *and* (3.93)*, the virtual control laws* (3.81) *and* (3.82)*, the parameter updating laws* (3.95) *and* (3.96) *and Assumption 1. All signals in the closed loop system are ensured to be globally bounded. Furthermore, asymptotic tracking is achieved, i.e.*

$$\lim_{t \to \infty} = [y_i(t) - x_{ri}(t)] = 0 \quad \textit{for} \quad i = 1, 2. \tag{3.98}$$

Proof: The stability properties of the equilibrium follows from Equations (3.86) and (3.97) and invoking the stability theorem (Theorem 2). By applying the LaSalle-Yoshizawa theorem (Theorem 3), $V_2(t)$ is globally uniformly bounded. This implies that z_1, z_2, z_3, z_4 are bounded and are asymptotically stable and z_1, z_2, z_3, $z_4 \to 0$ as $t \to \infty$ and also $\hat{\Theta}_1$ and $\hat{\Theta}_2$ are bounded. Since $z_1 = x_1 - x_{r1}$ and $z_2 = x_2 - x_{r2}$, tracking of the reference signals is also achieved, and x_1 and x_2 are also bounded since z_1 and z_2 are bounded and since x_{r1} and x_{r2} are bounded by definition, cf. Assumption 1. The virtual controls α_1 and α_2 are also bounded from Equation (3.81) and (3.82) and then x_3 and x_4 are also bounded. From Equations (3.92) and (3.93) it follows that the control inputs also are bounded.

Remark 1. The theorem states a global boundedness of the Lyapunov function $V_2(t)$. Because the model has a singularity for a pitch angle of $\pm$ 90 degrees, the equation explodes at this point. For this to be global, the singularity can not be present. By using quaternion method for the attitude parameterization, this singularity will be avoided [15].

Now, considering the error state $\mathbf{z}$ including the tracking errors. The adaption gain matrices are considered as $\Gamma_1 = \gamma I$ and $\Gamma_2 = \gamma I$. Bounds for transient performance can be derived, and bound on the $\mathcal{L}_2$ norm will now be proven, similar to [23] and [24].

Theorem 6 *[21] In the adaptive system* (3.67)*,* (3.95)*,* (3.96)*,* (3.92)*,* (3.93)*,*(3.81) *and* (3.82)*, the*

following inequalities hold for the transient tracking errors

$$||y_1(t) - y_{r1}(t)||_2 \leq \frac{|\tilde{\Theta}_1(0)| + |\tilde{\Theta}_2(0)|}{\sqrt{2c_1\gamma}}, \tag{3.99}$$

$$||y_2(t) - y_{r2}(t)||_2 \leq \frac{|\tilde{\Theta}_1(0)| + |\tilde{\Theta}_2(0)|}{\sqrt{2c_2\gamma}}, \tag{3.100}$$

and the following inequalities hold for the transient velocity tracking errors

$$||\dot{y}_1(t) - \dot{y}_{r1}(t)||_2 \leq \left(\frac{1}{\sqrt{c_3}} + \sqrt{c_1}\right) \frac{|\tilde{\Theta}_1(0)| + |\tilde{\Theta}_2(0)|}{\sqrt{2\gamma}}, \tag{3.101}$$

$$||\dot{y}_2(t) - \dot{y}_{r2}(t)||_2 \leq \left(\frac{1}{\sqrt{c_4}} + \sqrt{c_2}\right) \frac{|\tilde{\Theta}_1(0)| + |\tilde{\Theta}_2(0)|}{\sqrt{2\gamma}}. \tag{3.102}$$

with initial values for $\mathbf{z}$ *set to* $z_i(0) = 0,\ i = 1, 2, 3, 4.$

Proof: The Lyapunov function V_2 is non increasing from (3.97) and bounded from below by zero, and then

$$||z_1||_2^2 = \int_0^\infty |z_1(\tau)|^2 d\tau \leq \frac{1}{c_1} V_2(0), \tag{3.103}$$

$$||z_2||_2^2 = \int_0^\infty |z_2(\tau)|^2 d\tau \leq \frac{1}{c_2} V_2(0), \tag{3.104}$$

$$||z_3||_2^2 = \int_0^\infty |z_3(\tau)|^2 d\tau \leq \frac{1}{c_3} V_2(0), \tag{3.105}$$

$$||z_4||_2^2 = \int_0^\infty |z_4(\tau)|^2 d\tau \leq \frac{1}{c_4} V_2(0). \tag{3.106}$$

With the initial values for $\mathbf{z}$ set to $z_i(0) = 0,\ i = 1, 2, 3, 4$, the initial value for Equation (3.86) will be

$$V_2(0) = \frac{1}{2\gamma}(|\tilde{\Theta}_1(0)|^2 + |\tilde{\Theta}_2(0)|^2), \tag{3.107}$$

that are independent of $c_i,\ i = 1, 2, 3, 4$, and decreasing with γ. From (3.103), (3.104) and (3.107) this results in

$$||z_1||_2 \leq \frac{1}{\sqrt{c_1}} \frac{|\tilde{\Theta}_1(0)| + |\tilde{\Theta}_2(0)|}{\sqrt{2\gamma}}, \tag{3.108}$$

$$||z_2||_2 \leq \frac{1}{\sqrt{c_2}} \frac{|\tilde{\Theta}_1(0)| + |\tilde{\Theta}_2(0)|}{\sqrt{2\gamma}}, \tag{3.109}$$

where the bounds can be reduced by increasing c_1 and c_2 or by increasing γ. For the velocity tracking errors we have

$$||\dot{y}_1 - \dot{y}_{r1}|| = ||\dot{z}_1||_2 = ||z_3 - c_1 z_1||_2 \leq ||z_3||_2 + c_1||z_1||_2 \tag{3.110}$$

$$= \left(\frac{1}{\sqrt{c_3}} + \sqrt{c_1}\right) \frac{|\tilde{\Theta}_1(0)| + |\tilde{\Theta}_2(0)|}{\sqrt{2\gamma}}, \tag{3.111}$$

$$||\dot{y}_2 - \dot{y}_{r2}|| = ||\dot{z}_2||_2 = ||z_4 - c_2 z_2||_2 \leq ||z_4||_2 + c_2||z_2||_2 \tag{3.112}$$

$$= \left(\frac{1}{\sqrt{c_4}} + \sqrt{c_2}\right) \frac{|\tilde{\Theta}_1(0)| + |\tilde{\Theta}_2(0)|}{\sqrt{2\gamma}}, \tag{3.113}$$

where the bounds depend on $c_i,\ i = 1, 2, 3, 4$ and γ. The $\mathcal{L}_2$ transient performance of the $\mathbf{z}$ system can be improved by increasing the control parameters c_i or by increasing the adaptation gain γ.

Remark 2. The tracking error can be made smaller by increasing the design parameters c_i and γ.

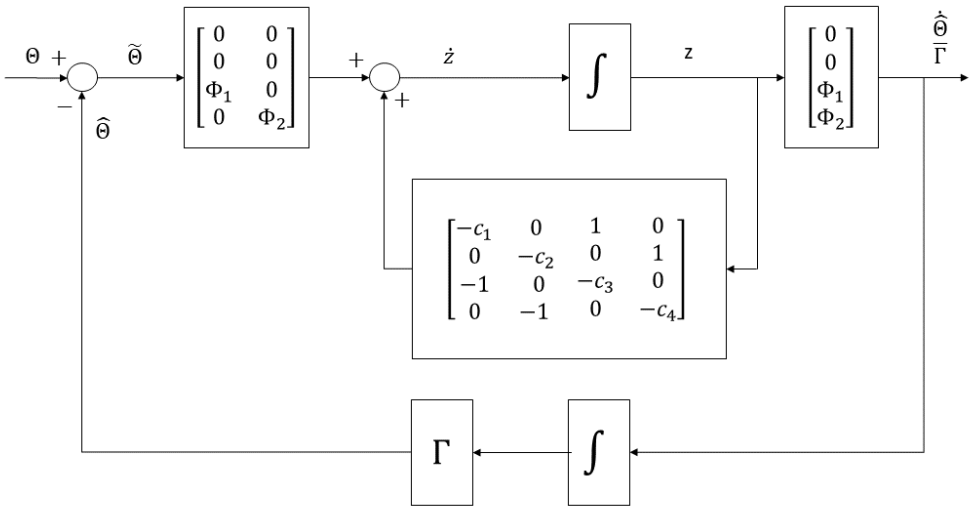

Figure 3.4: Block diagram of the closed loop adaptive backstepping for the Aero

The closed loop system of the Aero in matrix form looks like

$$\dot{\mathbf{z}} = \begin{bmatrix} -c_1 & 0 & 1 & 0 \\ 0 & -c_2 & 0 & 1 \\ -1 & 0 & -c_3 & 0 \\ 0 & -1 & 0 & -c_4 \end{bmatrix} \mathbf{z} + \begin{bmatrix} 0 & 0 \\ 0 & 0 \\ \Phi_1 & 0 \\ 0 & \Phi_2 \end{bmatrix} \begin{bmatrix} \Theta_1 - \hat{\Theta}_1 \\ \Theta_2 - \hat{\Theta}_2 \end{bmatrix}, \tag{3.114}$$

$$\dot{\hat{\mathbf{\Theta}}} = \begin{bmatrix} 0 \\ 0 \\ \Gamma_1 \Phi_1 \\ \Gamma_2 \Phi_2 \end{bmatrix} \mathbf{z}, \tag{3.115}$$

and a block diagram of the closed loop adaptive backstepping control is shown in Figure 3.4.

Chapter 4

Simulation and Testing on the Aero

All controllers were simulated with the use of Simulink and MATLAB. In Table 4.1 the parameters used for the simulation and for the implemented controllers are given. For simulation and implementation on the Aero, a fixed sample time of 0.002 s was used with the solver ODE1 (Euler) that uses the Euler integration method to compute the model state at the next time step based on the current value of the state and the state derivatives. The initial condition for angles and angular velocities were set to zero.
First a verification of models is given in Section 4.1 and also an openloop test of the system. In Section 4.2 the trajectories that the Aero will follow both for simulation and testing are given. Then the controllers PID and PV are simulated and tested to see if it is possible to use these as controllers for the Aero in Sections 4.3 and 4.4. Next, the LQR and adaptive controller will be simulated and tested in Sections 4.5 and 4.6, before different physical disturbances are added to the Aero and tested with LQR and adaptive control in Section 4.7. In the last Section 4.8, the two controllers will be compared based on total error and total voltage for all tests.

4.1 Verification of Models

The nonlinear and the linearized model have both been simulated to check that the behavior was as expected. For both models different tests that are summarized in Table 4.2 were checked. All models used in simulation and testing have a saturation for input voltages to ± 24 V, implemented to prevent over-voltage, and saturation for the pitch angle to ± 60 deg. The nonlinear model is based on the simplified model from Equation (2.33) and with the linearized estimates for the main and cross-torques. The linearized estimates was chosen since the behavior was quite similar as for the polynomial estimates when this was simulated. Both nonlinear and linear model had a behavior as expected.

The linear state space model for the Aero from Section 2.3.2 with

$$\dot{\mathbf{x}} = \mathbf{A}\mathbf{x} + \mathbf{B}\mathbf{u}$$
$$\mathbf{y} = \mathbf{C}\mathbf{x} + \mathbf{D}\mathbf{u}$$

and Equation (2.36) and (2.37) shows that $\mathbf{A}$ is a 4×4 matrix, and $\mathbf{u}$ is a 2-vector and $\mathbf{C}$ is a 2×4 matrix. According to the definitions of controllability and observability given in Section 3.1, if the rank of the controllability matrix is n, that in this case is 4, the system is controllable and if the rank of the observability matrix is n, the system is observable. The rank of the controllability and observability matrix is 4 and so the system is fully controllable and observable.

4.1.1 Openloop Test of Model

After the models were verified, an openloop test of the nonlinear and linear model together with Aero were tested. The results for this is shown in Figure 4.1. The models both have the same

Table 4.1: Parameters used for the controllers

Parameter	**Value**	**Description**
I_p	0.0217	Inertia about the pitch axis
I_y	0.0217	Inertia about the yaw axis
D_{Vp}	0.007	Viscous damping about the pitch axis
D_{Vy}	0.0095	Viscous damping about the yaw axis
m_b	1.075	Mass of the Aero body
g	9.81	Constant of acceleration due to gravity
l_{cm}	0.0038	Distance to center of mass in z_b-direction
K_{pp}	0.0012	Torque trust gain from the main motor acting on pitch
K_{yy}	0.00176	Torque trust gain from the tail motor acting on yaw
K_{py}	0.0012	Cross-torque thrust gain acting on pitch from tail motor
K_{yp}	-0.0014	Cross-torque thrust gain acting on yaw from main motor
PID	**Constants**	
p_0	1	zero pole
ζ	1	damping
ω_n	2	frequency
LQR	**Constants**	
Q-matrix	$\begin{bmatrix} 250 & 0 & 0 & 0 \\ 0 & 70 & 0 & 0 \\ 0 & 0 & 0 & 0 \\ 0 & 0 & 0 & 0 \end{bmatrix}$	
R-matrix	$\begin{bmatrix} 0.0029 & 0 \\ 0 & 0.0029 \end{bmatrix}$	
Adaptive Backstepping	**Constants**	
c_1	6	
c_2	6	
c_3	3	
c_2	3	
γ	1	

Table 4.2: Simulation test for the nonlinear and linear model to verify that the models behaves as expected

Test	**Expected behavior of model**	**Nonlinear Model**	**Linearized Model**
No inputs to the system.	Nothing should change.	√	√
Initial positive pitch angle.	Expected oscillation about pitch, going to zero.	√	√
Initial positive yaw angle.	No change for pitch, yaw stays at initial given angle.	√	√
Initial positive velocity for yaw.	Rotation about yaw in positive direction, going to a constant yaw angle. No change for pitch.	√	√
Initial positive velocity for pitch.	Pitch angle change in positive direction, oscillating back to zero. No change for yaw.	√	√
Positive input V_p.	Positive pitch and negative yaw.	√	√
Positive input V_y.	Positive pitch and positive yaw.	√	√

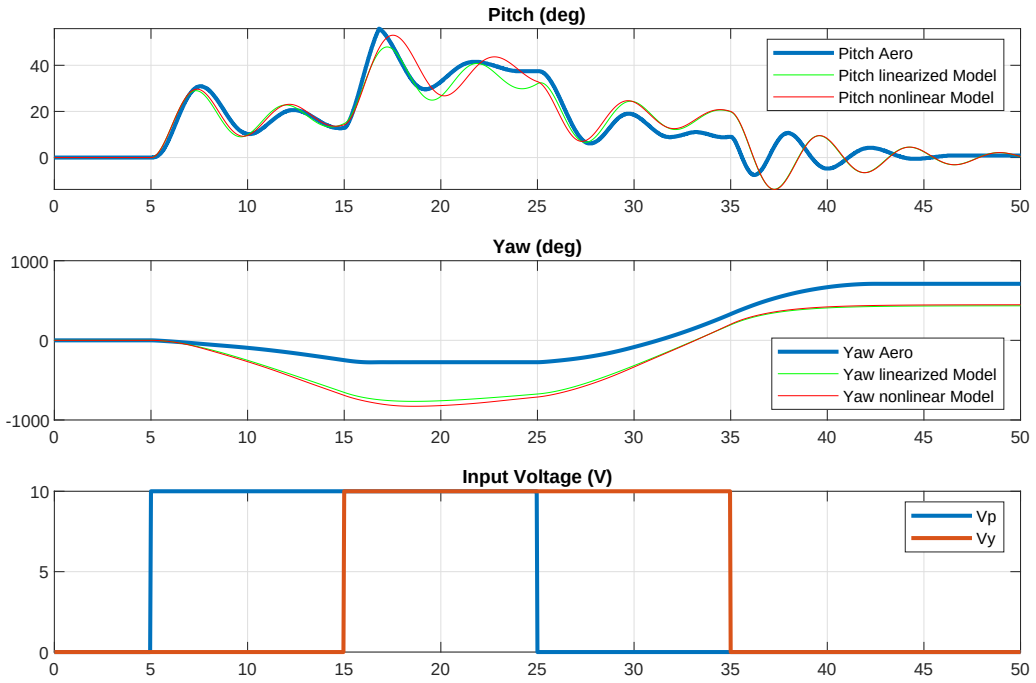

Figure 4.1: Openloop test to verify that the models behave as the Aero

behavior as the Aero, where the differences is due to unmodeled dynamics and is assumed to be mostly because of unmodeled Coulomb friction. This is especially seen in yaw, where the voltage needs an input V_y greater than 5.7 V to have a rotation, so the Aero have some static friction not taken into account.

4.2 Test Sequences for Simulation and Testing

The same test sequences were applied for control of Aero in simulation and testing. Three different desired trajectories were given to test and compare the linear and nonlinear controllers.

Test 1: The first test was a sine wave with amplitude of 40 degrees and frequency of 0.05 Hz applied to pitch, while there should be no rotation about yaw.
Test 2: The second test was different step inputs to pitch and yaw at different time instances.
Test 3: The third test was the same step sequence as in the second test but with smoother steps. To do so, the step functions from test 2 was gained with a second-order transfer function $\omega_{nt}^2/(s^2 + 2\zeta_t\omega_{nt}s + \omega_{nt}^2)$ so that the output of this is the new reference signal, giving a smoother transmission between the steps [19]. The cut-off frequency ω_{nt} was chosen to 1.5 and the damping ratio ζ_t was chosen to have a value of 1. The though is that the adaptive controller needs time to adapt to changes and adjust the estimated parameters $\hat{\Theta}_1$ and $\hat{\Theta}_2$. Assuming that step functions are not optimal for an adaptive controller, it is assumed that it will be better to give a smooth curve function to follow instead. This is due to the fact that the controller is designed as a tracking controller, i.e. following trajectories, i.e. it is not able to follow discrete changes. Then tracking errors are introduced that are injected into the adaptive law possibly causing divergence in the estimated parameters $\hat{\Theta}_1$ and $\hat{\Theta}_2$. Also when the reference trajectory is chosen, the performance of the system can be improved by choosing a gentler trajectory for the controller to follow.

For all the tests, the reference signals and first and second derivative of the signal are piecewise continuous and bounded.

The test was carried out by first a simulation of the system, then testing on the Aero. For two of the controllers, different disturbances were added to the system to see the behavior with this.

4.2.1 Filters to Reduce Noise from Gyros

When testing on the Aero, there is measurement noise from the different sensors. The signals for pitch and yaw angular velocities were filtered using a second order low-pass filter with a cut off frequency of 70 rad/s and a damping ratio of 0.8. This filter was added to reduce measurement noise from the gyros, and the same filter was added for both LQR and adaptive controller. A plot of the gyro signal before and after filtering is shown in Figure 4.2. This plot is from a test sequence with a smooth step.

The filtered gyro signal lags a bit behind the unfiltered signal, and also if a lower break frequency was chosen, this would have smoothen out the signal some. A lower break frequency of 50 (rad/s) was tested and result shown in Figure 4.3 so a smoother signal can be used.

4.3 Simulation with the Decoupled PID Controller

The decoupled PID controller from Chapter 3.2.1 was simulated and tested for control of the Aero. One PID compensator was designed for pitch and one for yaw for the main torques, and so the cross-coupling torques were disregarded. This means it was treated as two SISO systems, and since the controller did not take into account the cross coupling, unwanted motion was expected. The results from the simulation are shown in Appendix A, Figures A.1 to A.3 where all three test sequences were simulated. When tested on the Aero, a first-order highpass filter on the form $\omega_{np}s/(s+\omega_{np})$ was used to compute the velocities of the errors, where ω_{np} is the cut-off frequency, set to 100 rad/s.

The simulation results show a good tracking performance for both pitch and yaw for all three test sequences. When the PID controllers were tested for control of the Aero, the performance was not good and the input voltage had a chattering behavior. The bad performance was assumed to be because the gains were to high and also since the cross coupling was not taken into account for the closed loop. Further tuning to have a better performance was not looked into.

4.4 Simulation and Testing with the PV Controller

The decoupled PV controller as described in Chapter 3.2.2 was also simulated and tested for control of the Aero. This was a decoupled controller only taking into account the main torques, and so control of the Aero was treated as two SISO systems. Here the same highpass filter as for the PID was applied to compute the velocities of the errors. The results from the simulation and testing are presented in Appendix B.

Results for test 1 are shown in Figures B.1 and B.2. The Aero was able to follow the given trajectory both when simulating and testing with this control structure. The maximal error in pitch was about 8 deg for the simulation and 10 deg when tested on the Aero, and there was a maximal error in yaw of about 7 deg for the simulation and 5 deg for testing. The input voltages from simulation in Figure B.2 had nice sine-curves, and the input voltages from testing had the same sine-curves but with more chattering.

The results from simulation and testing of test 2 are shown in Figures B.3 and B.4. From the simulation a maximal steady state error of 4.8 deg in pitch can be observed after the first step and a maximal steady state error of 5.5 deg in yaw is observed after the first step in yaw. From the test, these errors are slightly higher with a maximal steady state error of 5.7 deg in pitch and 6.2 deg in yaw.

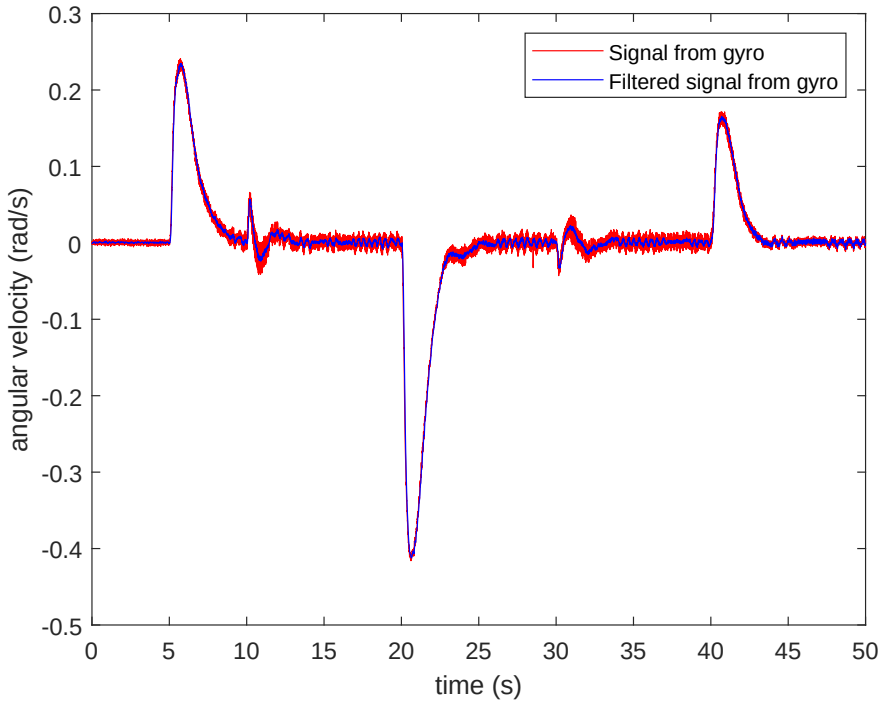

(a) Signals from gyro

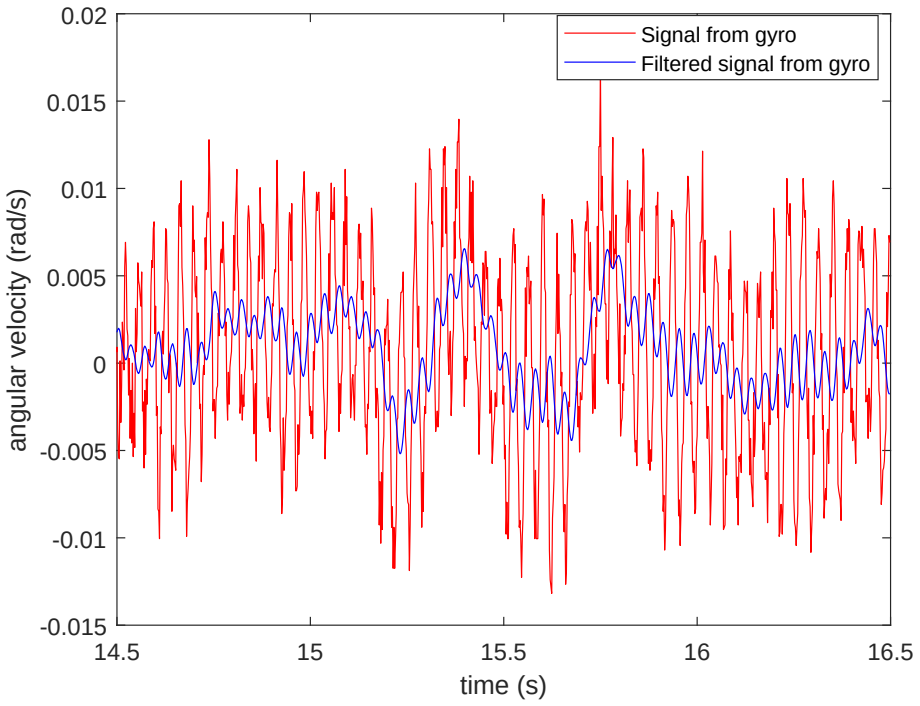

(b) Close up of gyro signals

Figure 4.2: Signals from gyro, unfiltered (red) and filtered (blue)

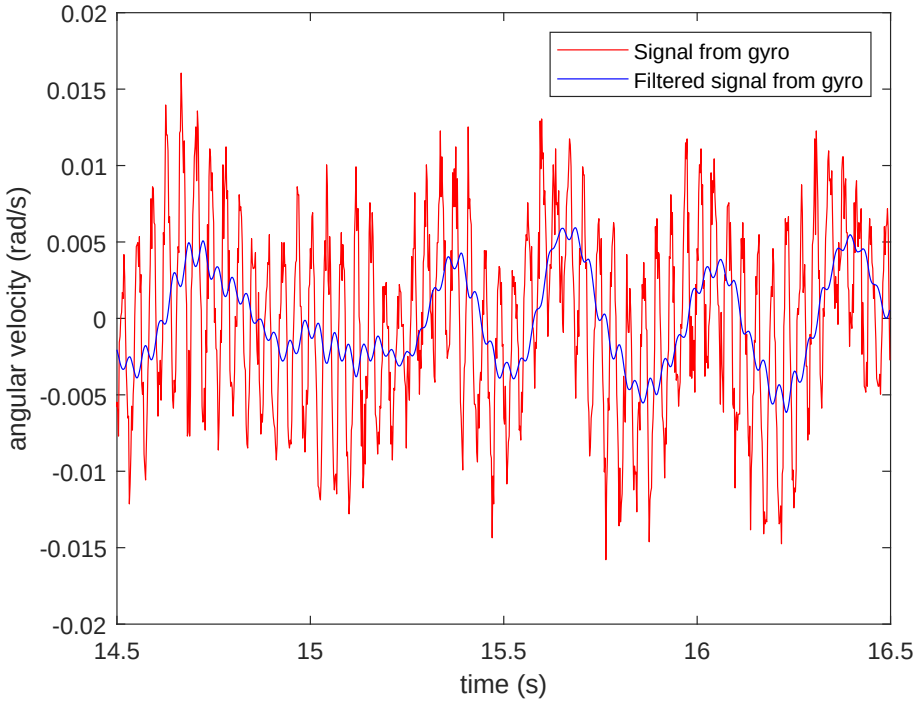

Figure 4.3: Close up of gyro signals with reduced break frequency, unfiltered (red) and filtered (blue)

The results from the simulation and testing of test 3 are shown in Figures B.5 and B.6. From the simulation, the same steady state error is observed for pitch and yaw as in test 2. From the testing, the maximal steady state error in pitch is 5.4 deg and about 7.8 deg for yaw.

4.5 Simulation and Testing with the LQR

To simulate the system with the LQR, the weighting matrices $\mathbf{Q}$ and $\mathbf{R}$ were first needed. The simulation was first tested with values for these matrices given from Quanser, and was modified some, resulting in the matrices in Table 4.1. The values for the two matrices were adjusted so that the performance of the controller had similar performance for the test sequence from test 2 with step inputs, as the adaptive controller, that will be discussed in Chapter 4.6. The total squared voltage was similar here and this will be shown later in Chapter 4.8 when the controllers are compared. From this the $\mathbf{K}$ and $\mathbf{P}$ matrices could be found with MATLAB, and also giving four eigenvalues, all negative.

The results from simulation and testing on the Aero with the LQR is shown in Figures 4.4 to 4.9 for the three different test sequences, sine wave, step function and smooth step function.

For test 1, the biggest error in pitch angle was when reaching the maximum and minimum points of 40 degrees on the pitch trajectory. Then the error was around 3 deg. This is seen in Figure 4.4a. When running on the Aero, this error was some delayed. The yaw angle only had small errors that was less than 1 deg, seen in Figure 4.4b.

For test 2, the steady-state error in pitch was about 2.5 deg when pitch was not zero, while yaw followed the desired angle fine. The biggest errors were of course when there was a change in step. There were also small errors in pitch when yaw had a change of angle, and the same applied for yaw when pitch changed angles and was due to the cross coupling effect. This can be seen for pitch in Figure 4.6a at time $10s$, $30s$ and $40s$ when yaw had change in step, and for yaw in Figure 4.6b at time $5s$, $20s$ and $40s$.

For test 3, the steady-state error in pitch was similar to test 2, but the biggest errors that could be seen for the step function when changing steps, were not here any more. The smoother transition between steps gets rid of these errors.

4.6 Simulation and Testing with the Adaptive Backstepping Controller

To simulate the system with the adaptive backstepping control, a Simulink model was build with the system setup as described in Chapter 3.4.3. The values for the constants c_1, c_2, c_3 and c_4 and for the adaption gain γ were found by trial and error. First all the gains were set equal to 1, and then adjusted to meet the same performance as the LQR for the step functions. The initial conditions for the estimated parameters were set to $\hat{\Theta}_1(0) = \Theta_1$ and $\hat{\Theta}_2(0) = \Theta_2$, since they already had been estimated. This is not required for the controller to work, but now the controller does not have to estimate values from zero, reducing the error in the beginning since $\hat{\Theta}_1$ ans $\hat{\Theta}_2$ are closer to Θ_1 and Θ_2.

The results from simulation and testing on the Aero with the adaptive controller is shown in Figures 4.10 to 4.18 for the three different test sequences.

Looking at the plots for the sine wave trajectory (test 1) shown in Figure 4.10a, the absolute error was ≤ 2 deg for pitch angle and ≤ 0.9 deg for yaw angle. The maximum error occurred when the input voltages changed sign, seen in Figure 4.11, meaning this was when the rotors changed direction. Both simulation and testing on the Aero showed that the desired trajectory for a sine wave in pitch could be followed using the adaptive controller. The input voltages were similar for both simulation and testing as Figure 4.11 shows. In Figure 4.12, $\hat{\Theta}_1$, was adapting to changes as the pitch angle changed, while $\hat{\Theta}_2$ was not changing since there wa no change for the trajectory of the yaw angle.

For test 2, the desired trajectory was followed closely as Figure 4.13 shows. The biggest error was at the time of a step both during simulation and testing, and there was also a cross-coupling effect that could be seen as pitch and yaw changed position. This cross coupling effect was only seen when tested on the Aero. Input voltages from simulation and testing showed a similar behavior, this can be seen in Figure 4.14. The $\hat{\Theta}_i, i = 1, 2$, were adapting at every step, shown in Figure 4.15. Also $\hat{\Theta}_1$ was changing in between time $20 - 40s$. At that time there was a small error in the pitch angle, that was reduced over the same time period.

For the third test, the desired trajectory was followed smoothly as Figure 4.16 shows. The biggest error was 2.5 deg for pitch at the time of the biggest change in pitch from a positive pitch of 30 deg to a negative pitch of 20 deg. Input voltages shown in Figure 4.17 had a similar behavior for simulation and testing. The only difference was from time $45s$ to $50s$ where the desired pitch and yaw angles were zero and inputs were zero for simulation but $V_p = 4V$ and $V_y = -4V$ for testing, and giving the same output angles. This was probably due to the error in yaw that the controller was trying to compensate for, and yaw was assumed not changing since there was static friction in the system, and a higher voltage would be needed to have a rotation. The equal inputs with different sign would not change the pitch angle since the main and cross-torque gains for pitch were equal, $K_{pp} = K_{py}$. The $\hat{\Theta}_i, i = 1, 2$ were adapting during the simulation and testing as Figure 4.18 shows.

For all three trajectories tested here, the output tracked the desired reference signal and the tracking error was bounded.

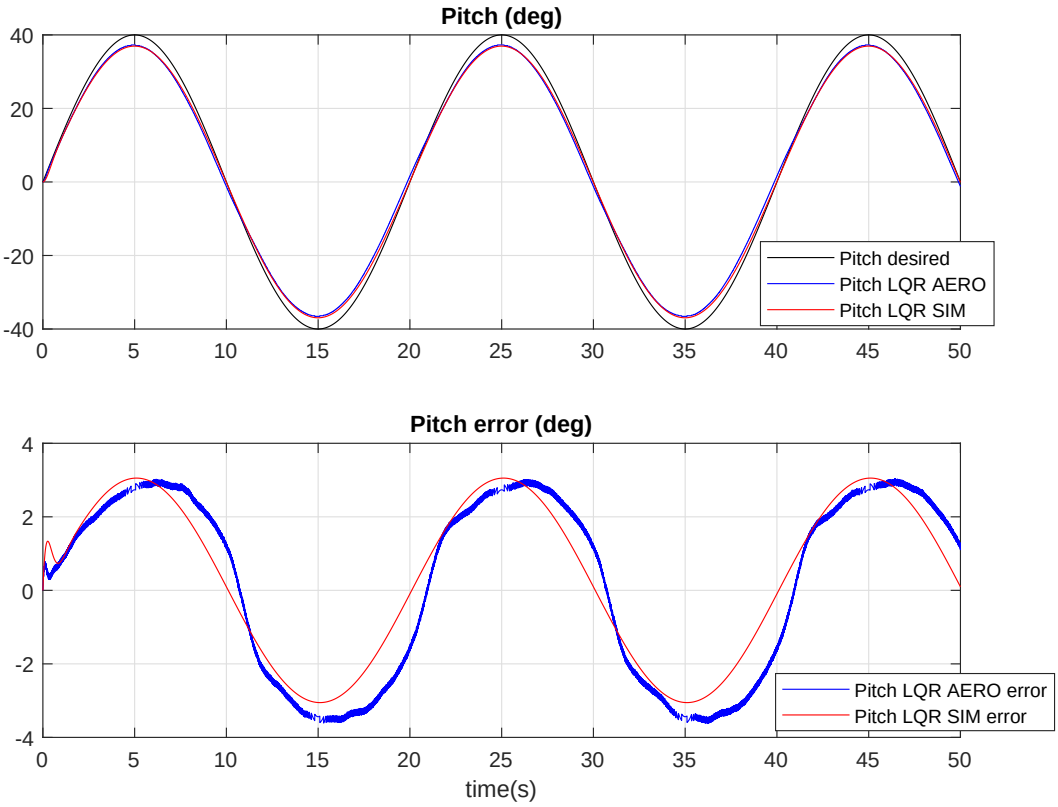

(a) Pitch angle and error for test 1 (sine wave) with the LQR

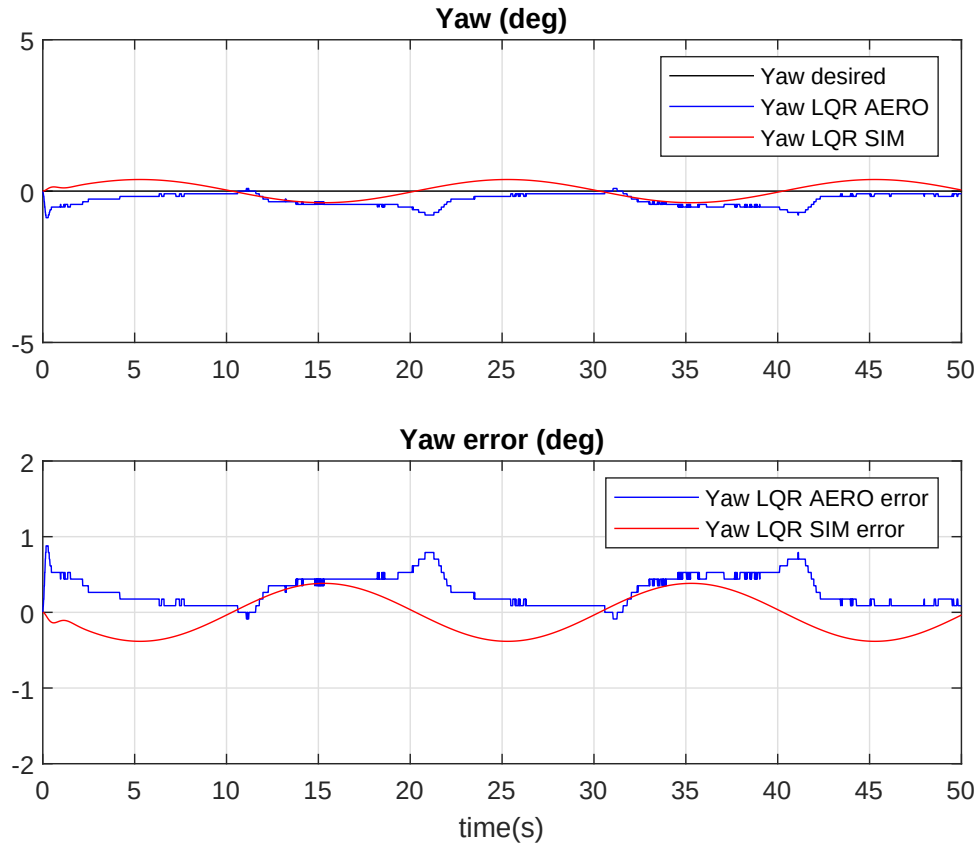

(b) Yaw angle and error for test 1 (sine wave) with the LQR

Figure 4.4: Angles and errors for test 1 (sine wave) with the LQR, both simulated and tested on the Aero

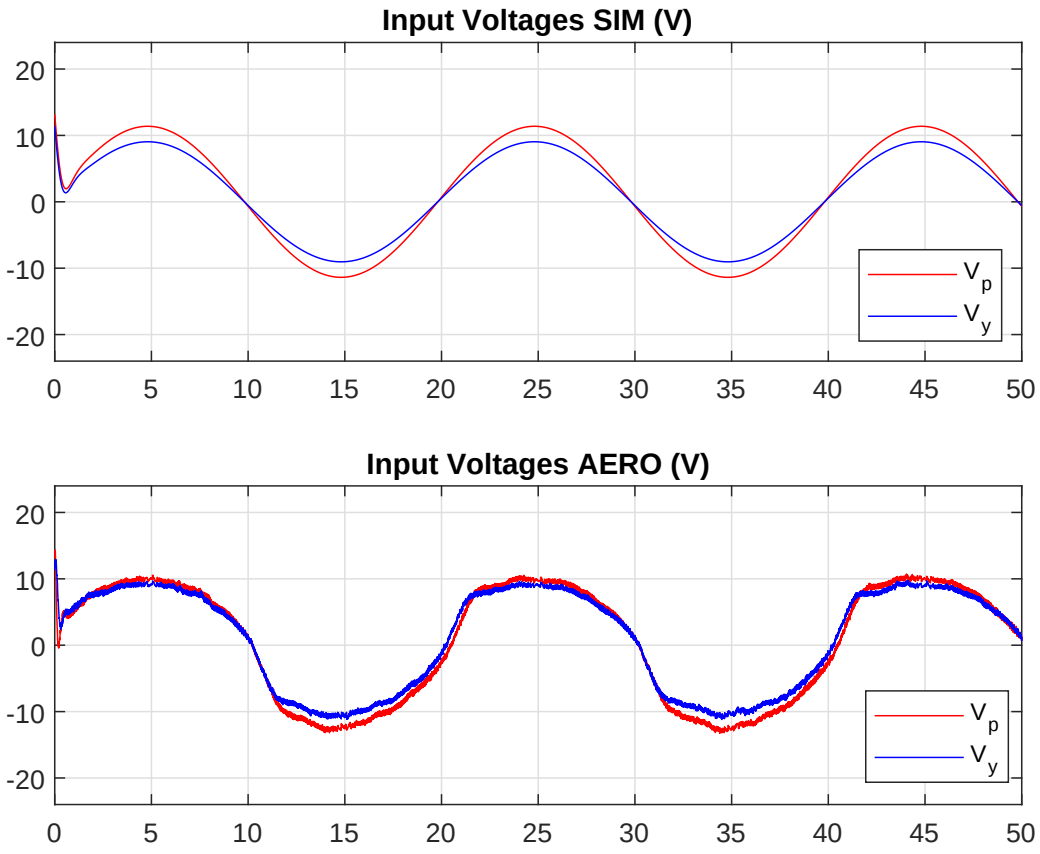

Figure 4.5: Voltage for test 1 (sine wave) with the LQR, when tested on the Aero

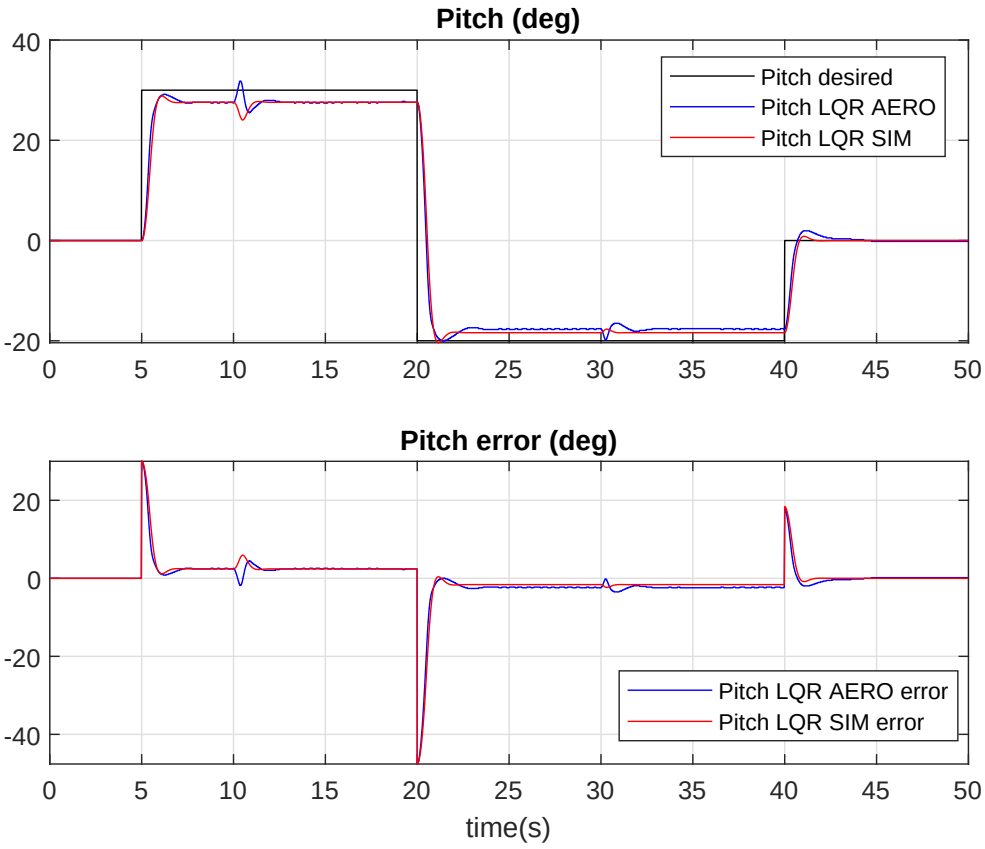

(a) Pitch angle and error for test 2 (step sequence) with the LQR

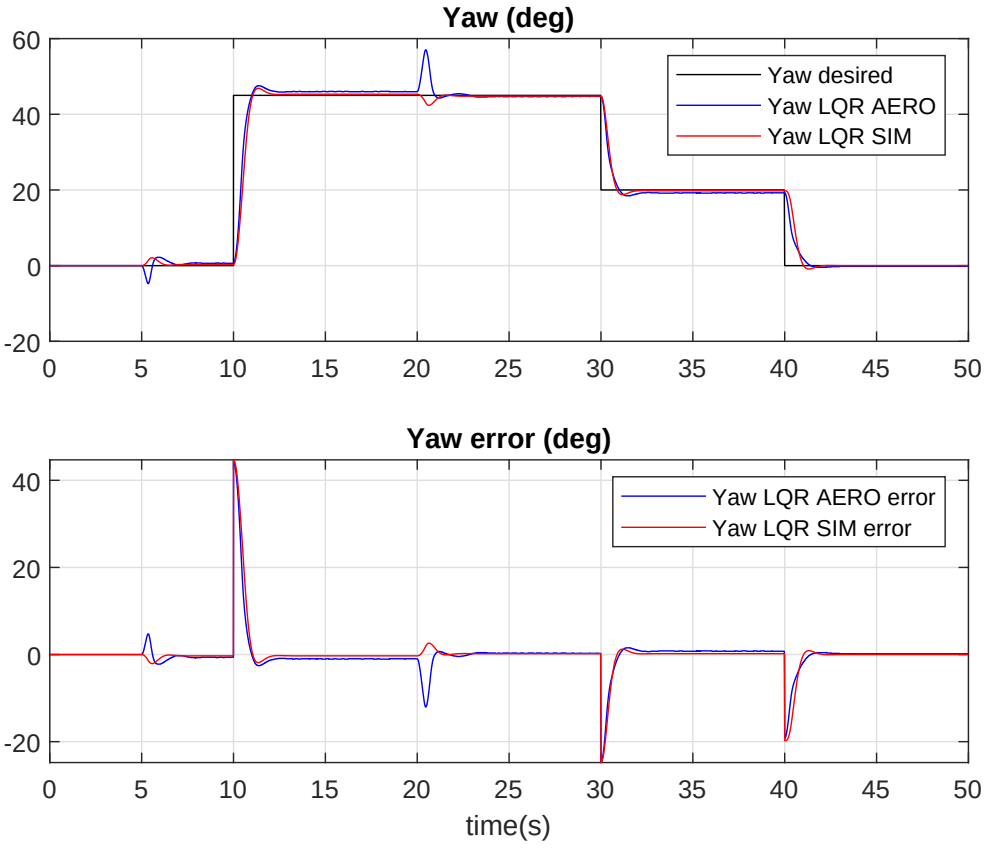

(b) Yaw angle and error for test 2 (step sequence) with the LQR

Figure 4.6: Angles and errors for test 2 (step sequence) with the LQR, both simulated and tested on the Aero

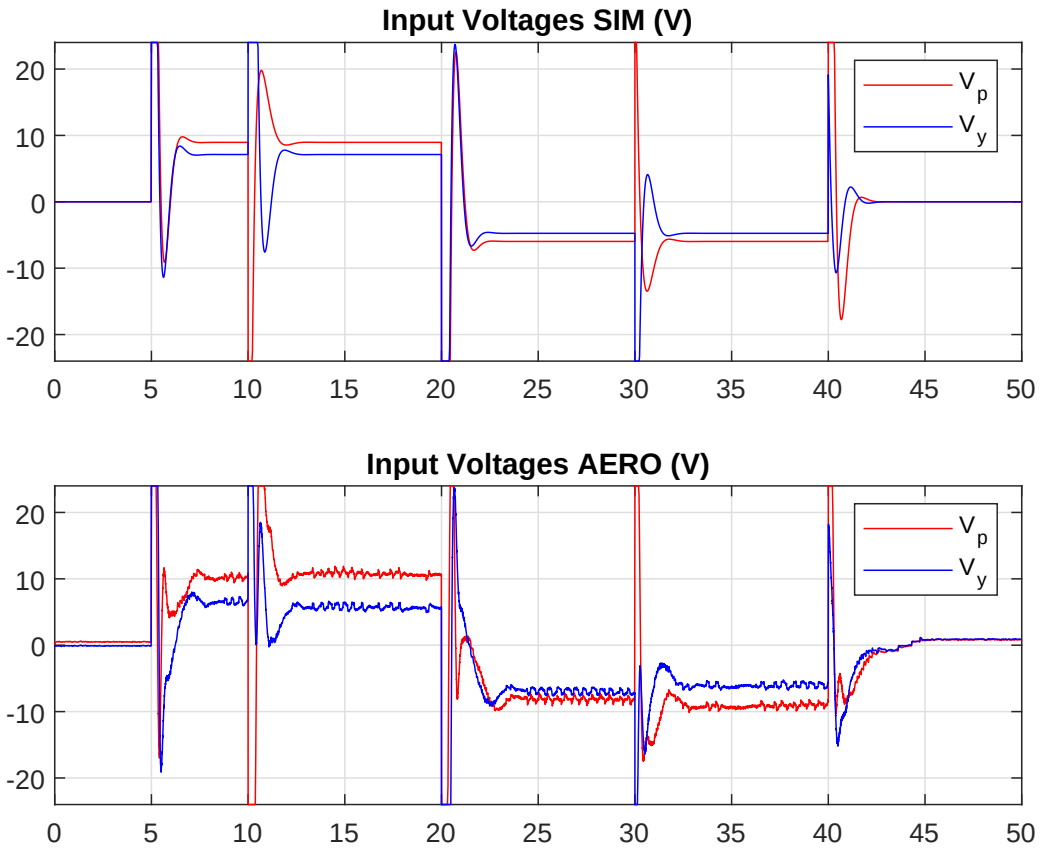

Figure 4.7: Voltage for test 2 (step sequence) with the LQR, when tested on the Aero

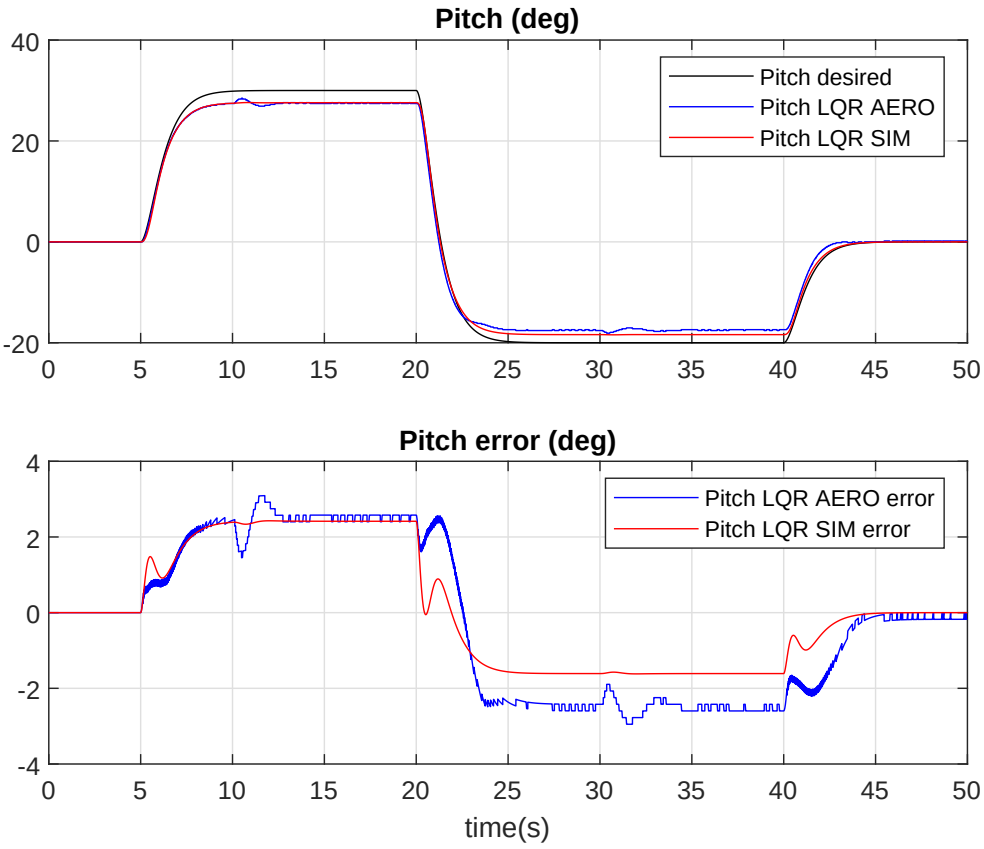

(a) Pitch angle and error for test 3 (smooth step) with the LQR

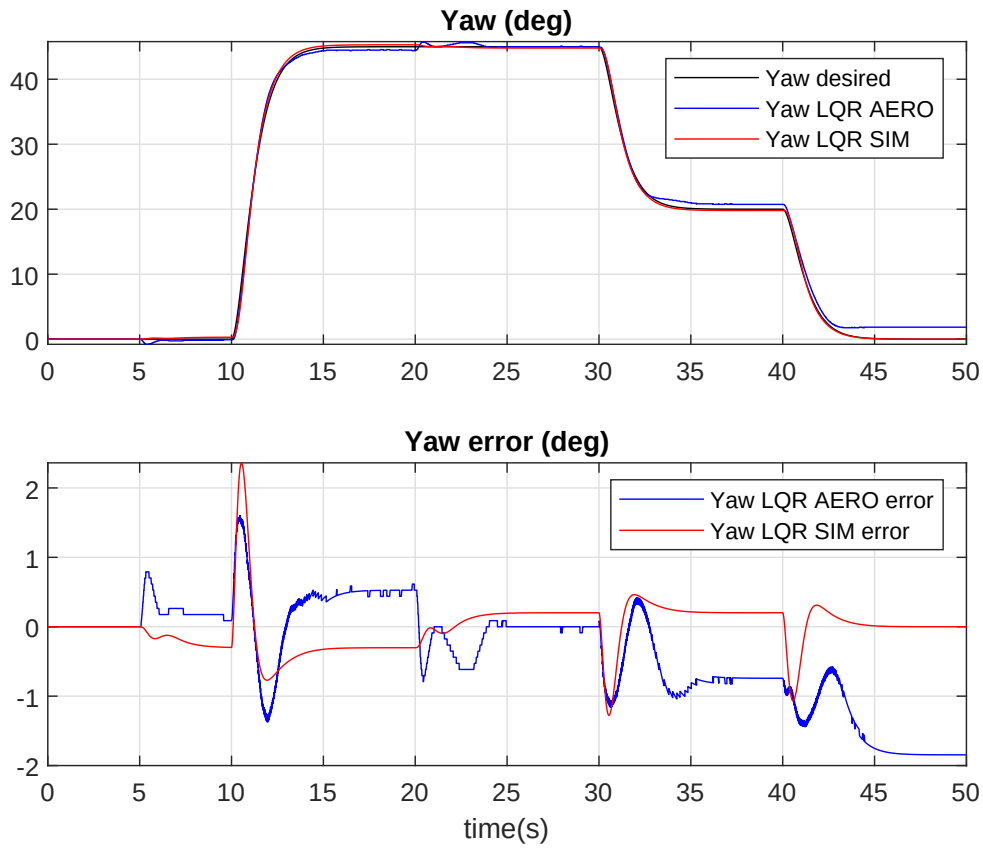

(b) Yaw angle and error for test 3 (smooth step) with the LQR

Figure 4.8: Angles and errors for test 3 (smooth step) with the LQR, both simulated and tested on the Aero

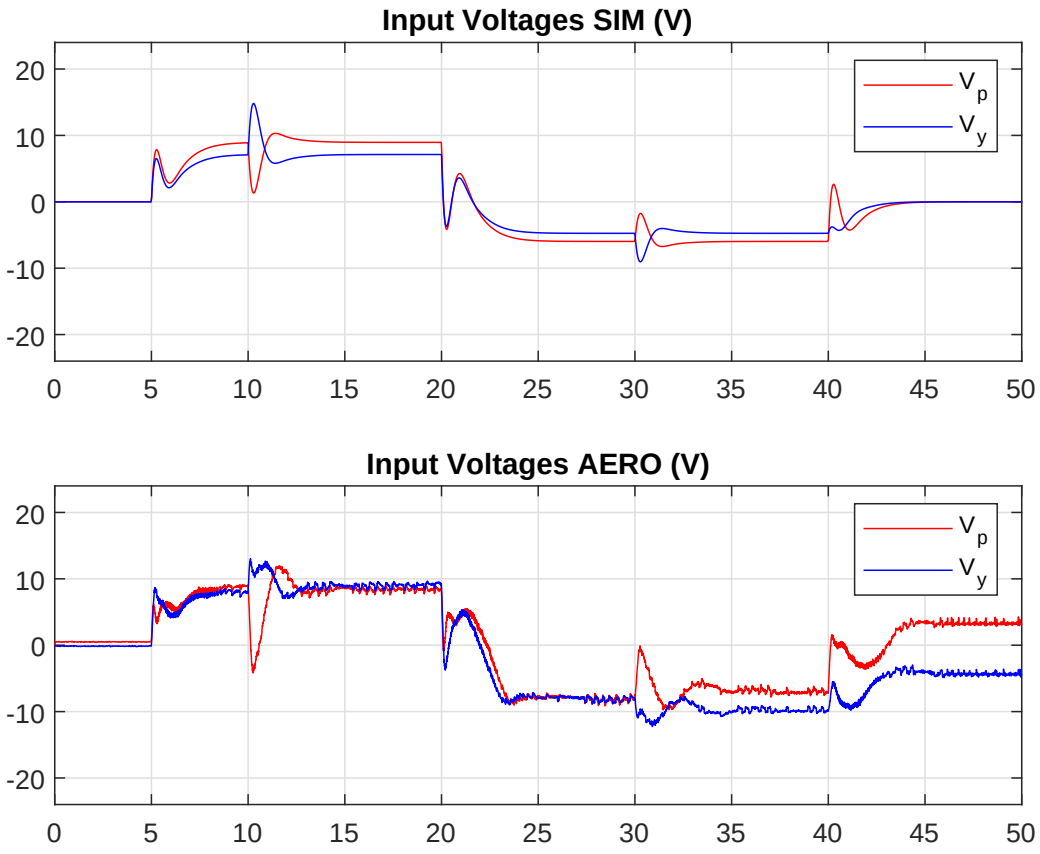

Figure 4.9: Voltage for test 3 (smooth step) with the LQR, when tested on the Aero

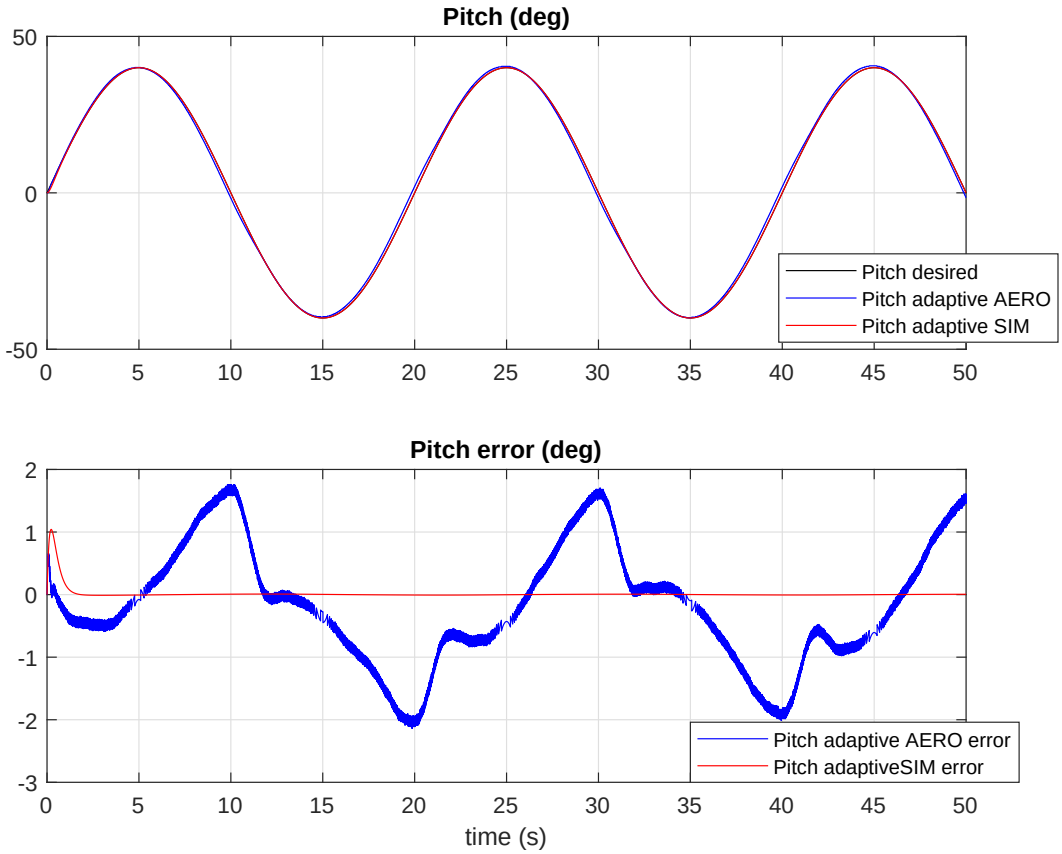

(a) Pitch angle and error for test 1 (sine wave) with adaptive backstepping control

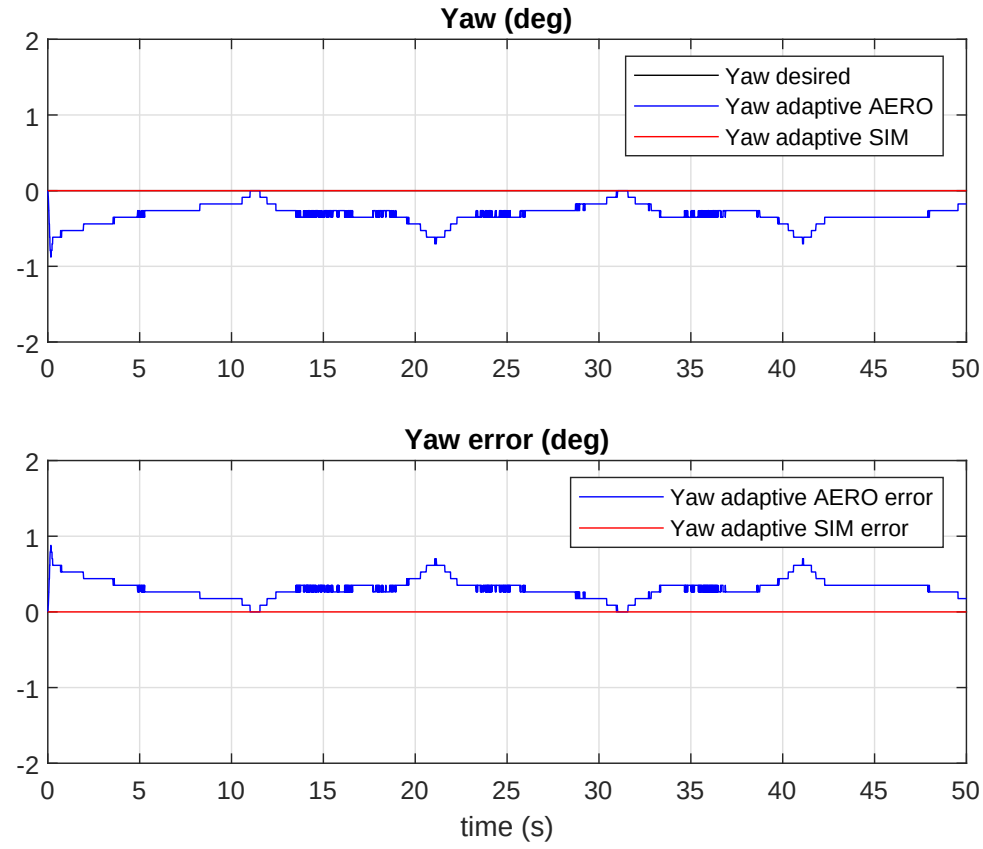

(b) Yaw angle and error for test 1 (sine wave) with adaptive backstepping control

Figure 4.10: Angles and errors for test 1 (sine wave) with adaptive backstepping control, both simulated and tested on the Aero

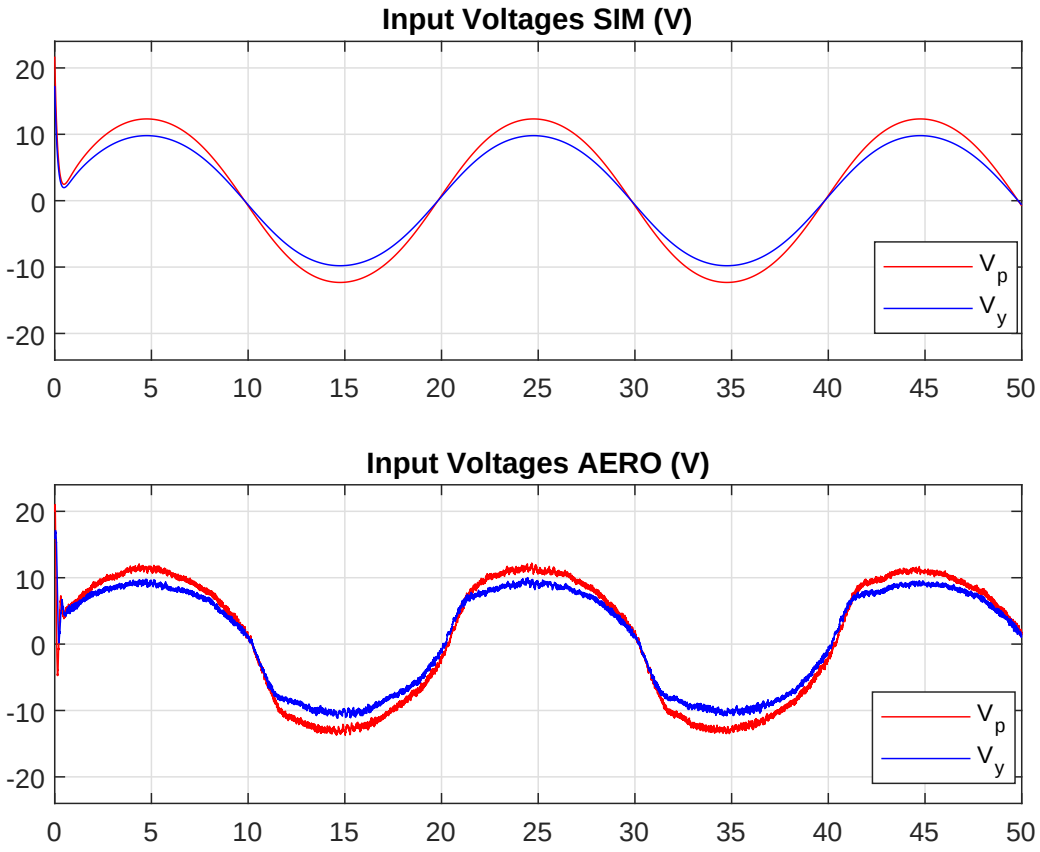

Figure 4.11: Voltage for test 1 (sine wave) with adaptive backstepping control, when tested on the Aero

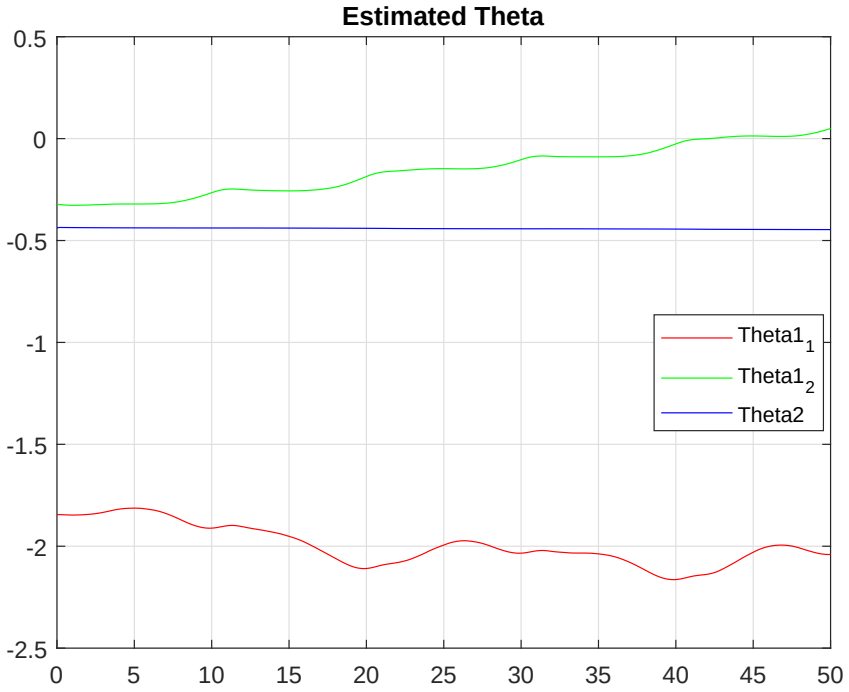

Figure 4.12: Estimated theta for test 1 (sine wave)

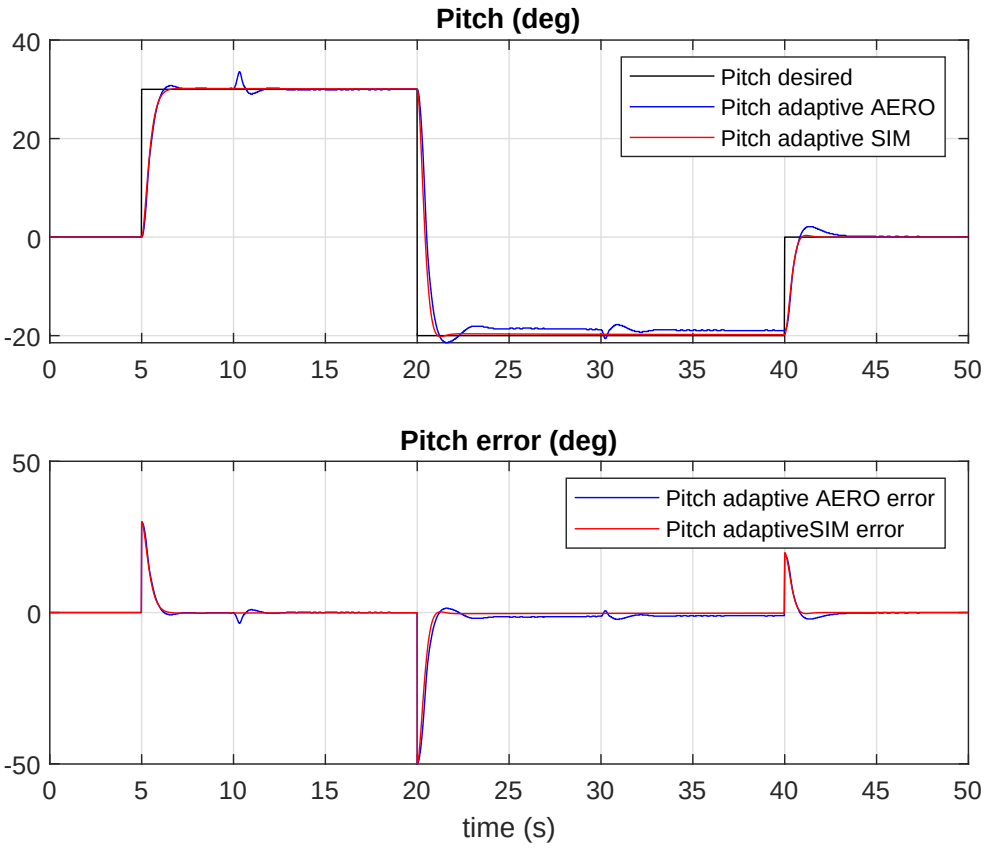

(a) Pitch angle and error for test 2 (step sequence) with adaptive backstepping control

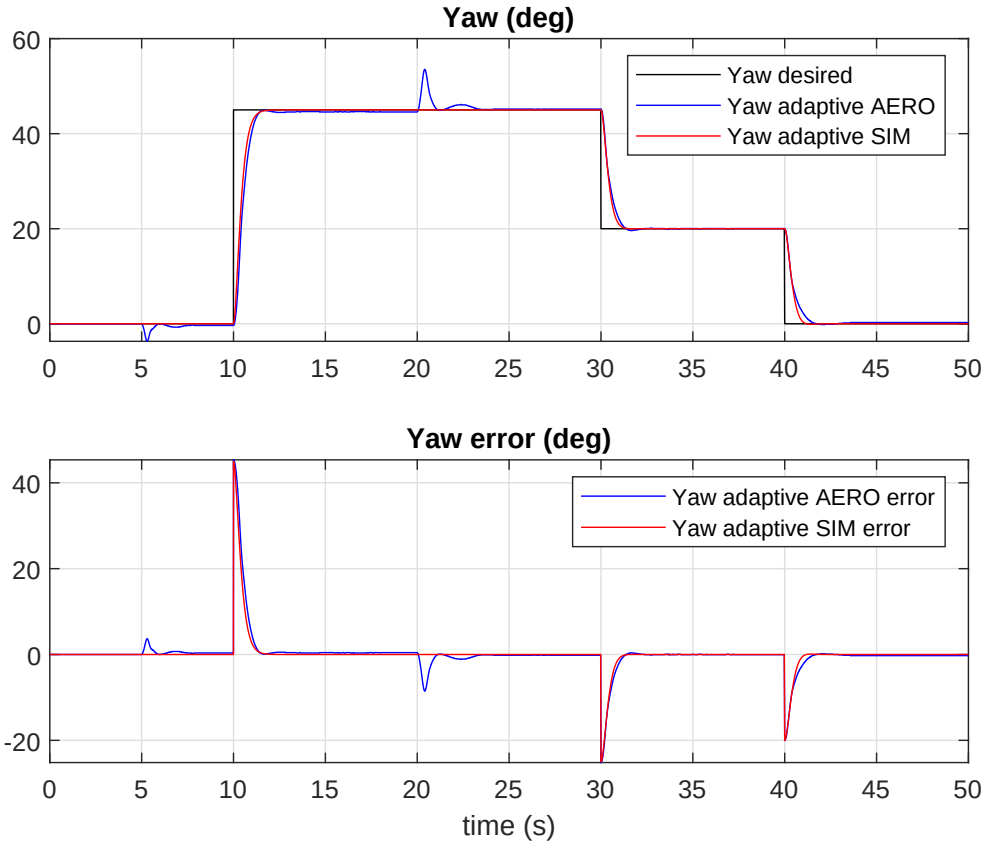

(b) Yaw angle and error for test 2 (step sequence) with adaptive backstepping control

Figure 4.13: Angles and errors for test 2 (step sequence) with adaptive backstepping control, both simulated and tested on the Aero

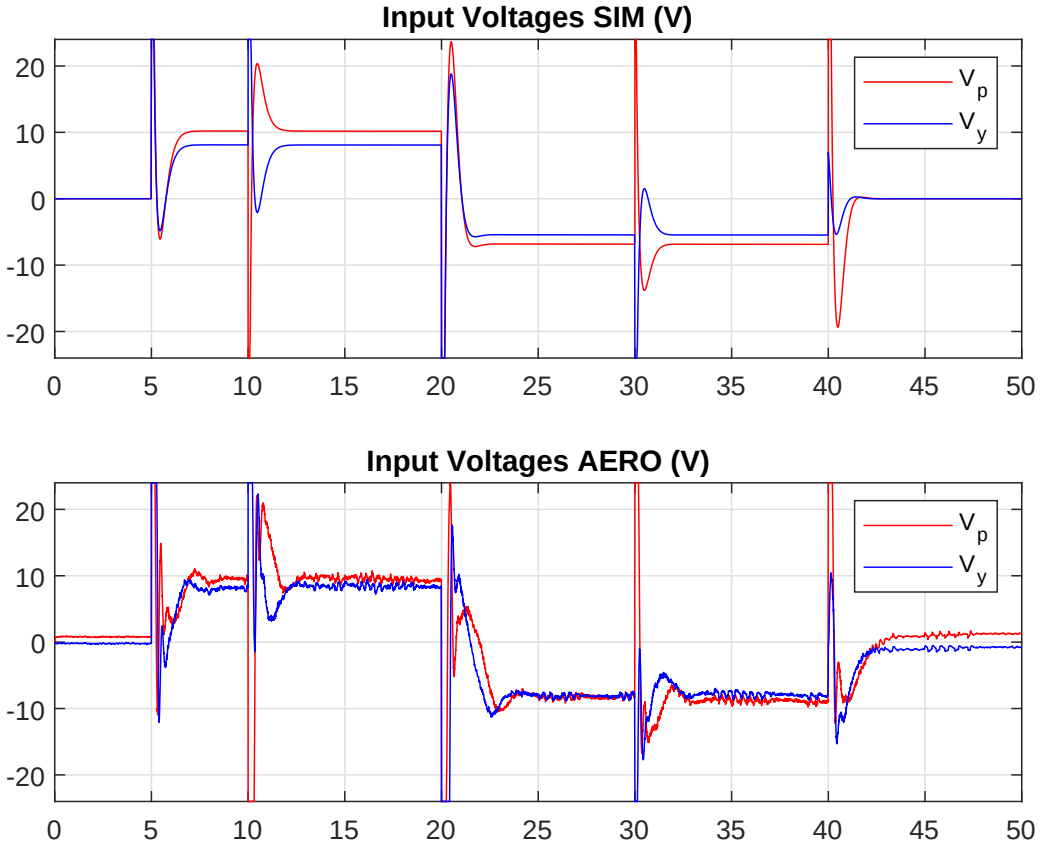

Figure 4.14: Voltage for test 2 (step sequence) with adaptive backstepping control

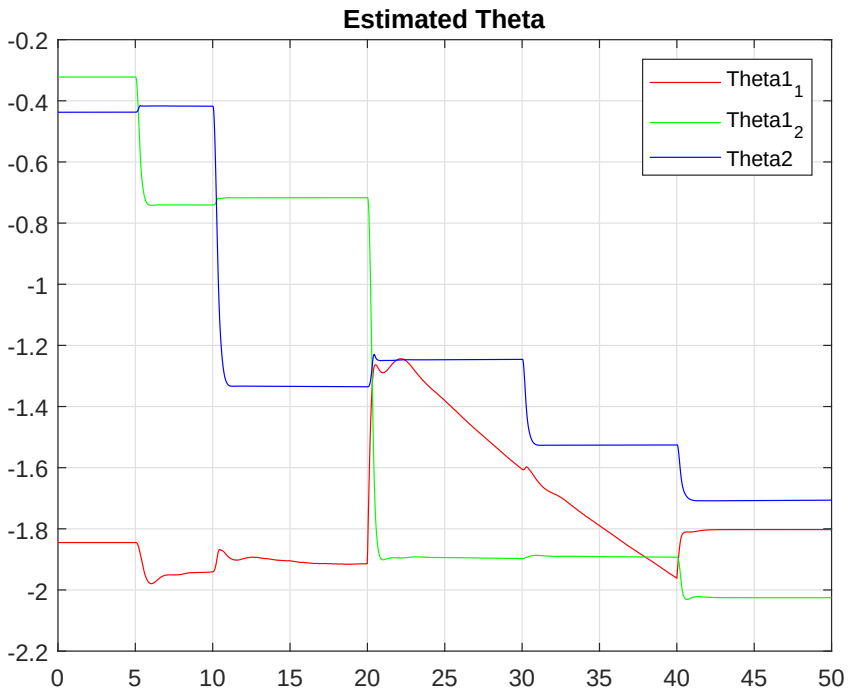

Figure 4.15: Estimated theta for step sequence with adaptive backstepping control

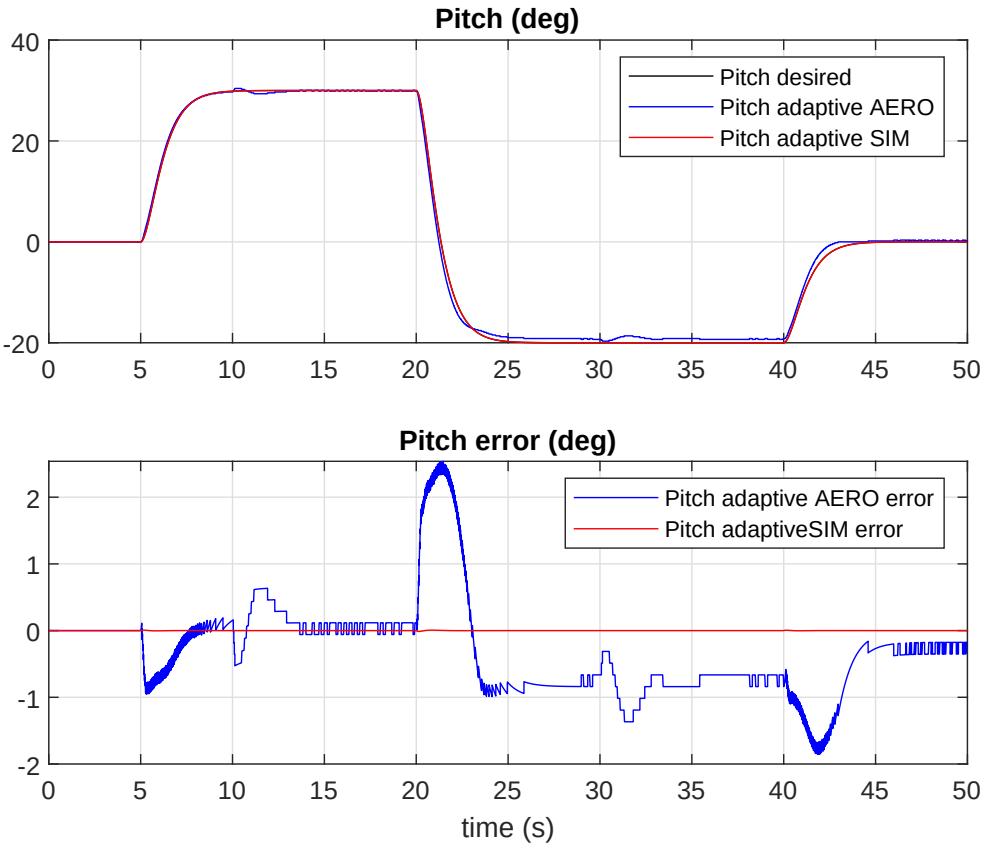

(a) Pitch angle and error for test 3 (smooth step) with adaptive backstepping control

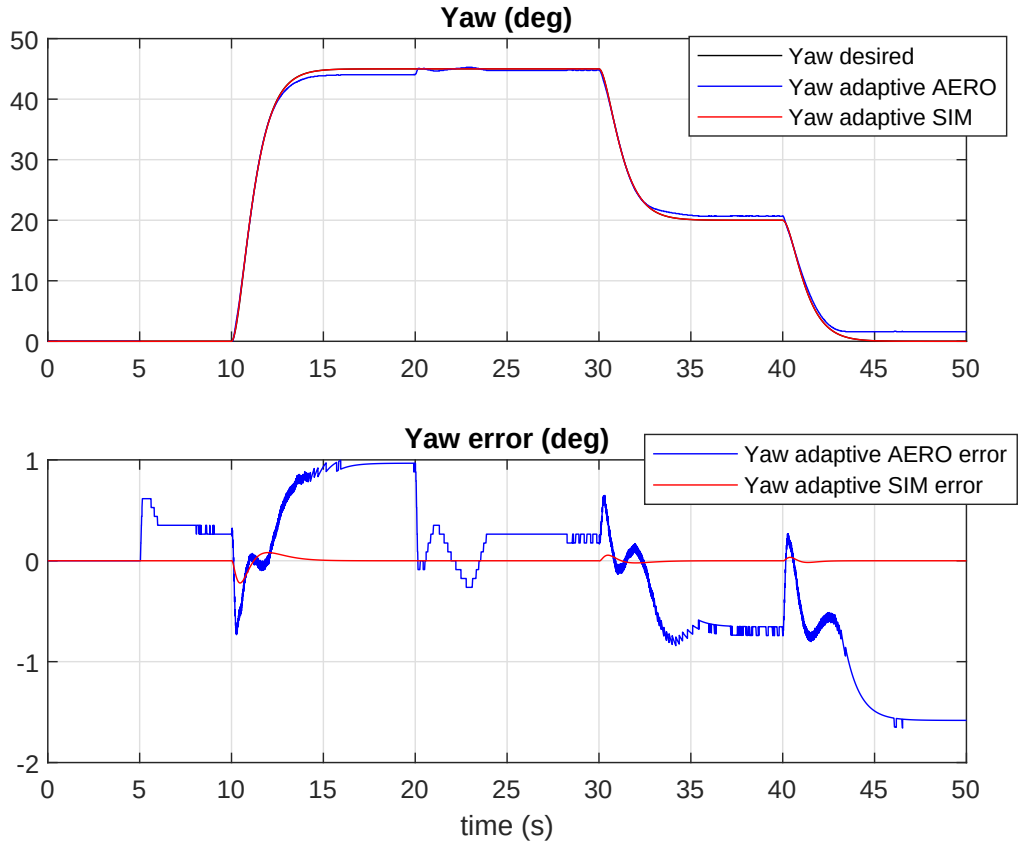

(b) Yaw angle and error for test 3 (smooth step) with adaptive backstepping control

Figure 4.16: Angles and errors for test 3 (smooth step) with adaptive backstepping control, both simulated and tested on the Aero

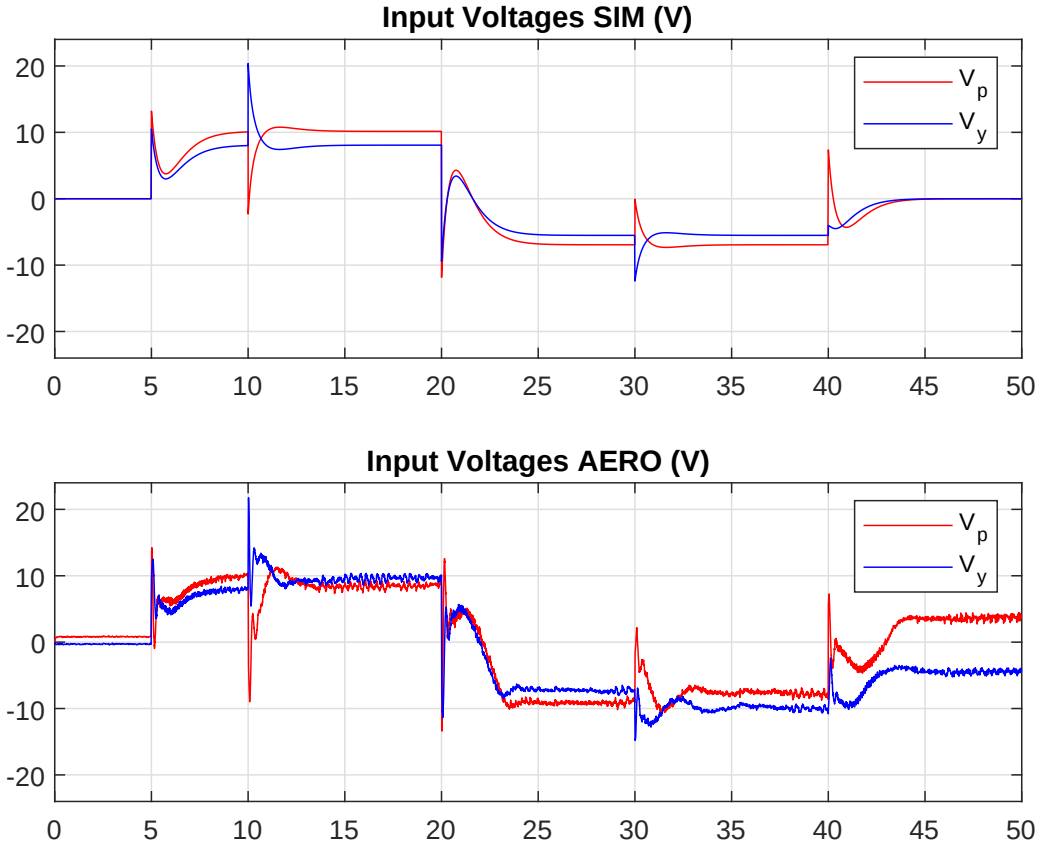

Figure 4.17: Voltage for test 3 (smooth step) with adaptive backstepping control,

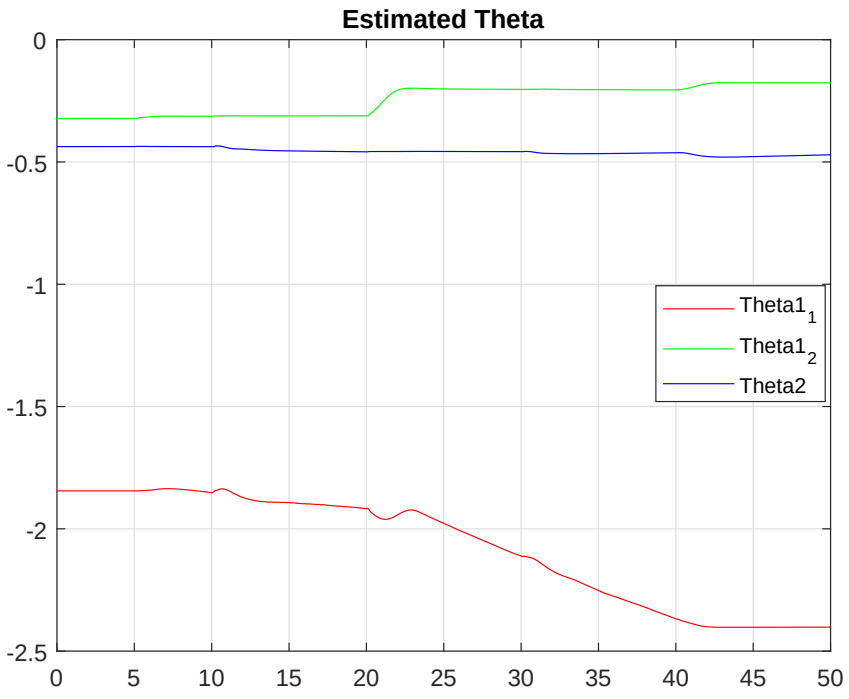

Figure 4.18: Estimated theta smooth step with adaptive backstepping control

4.7 Test on the Aero with Disturbances

Different disturbances were added to the Aero to test how well the LQR and the adaptive controller could cope with disturbances. The adaptive controller should be able to adjust its estimates to meet the disturbances. The gains for the two controllers were not changed. Four different disturbances were added, changing the system in different ways, and the different disturbances and results from this will be shown in the next sections.

4.7.1 Disturbance of Added Mass

Negative Torque

A mass of 5.8 grams in form of a washer was added to the main thruster, a distance of 23.8 cm from the pivot point. This means a negative torque was added for pitch that is not included in the model. The added mass also have impact on several of the parameters in the model, affecting both the Aero mass, m_b and the inertia $\mathbf{I}_{b/o}$ and also changing the center of mass $\mathbf{r}_{cm}$. When this mass was added, the equilibrium moved from zero degrees to a negative pitch angle of 24.5 deg. To test the same sequences as without this physical disturbance, the Aero was hold in horizontal position at startup and then let go when running the control so that the disturbance was added after approximately 1 second after start of the desired trajectory. This gave a disturbance in form of load variation. The results from this test can bee seen in Appendix C where Figures C.1 to C.3 show the first test sequence, Figures C.4 to C.6 show test sequence two and C.7 to C.9 show the third test.

For the first test, both controllers had a maximal error that was less than 1 degree for yaw. Both followed the sine wave, and both had a maximal error of approximately 4 deg. The LQR had the biggest error when the pitch trajectory reached max and min values, while the adaptive controller had the biggest error around where the Aero had its equilibrium point, a pitch angle of -24.5 deg. This was also when the rotors changed from a positive to a negative voltage. The plotted $\hat{\Theta}_i, i = 1, 2$ in Figure C.3 show how the update law was changing with time and by comparing these values with the values from no disturbances presented in Figure 4.12, $\hat{\Theta}_1$ was changing more now, with increasing values.

For the second test, when the mass was added in the beginning, both controllers had an error in pitch angle of about 2.5 deg. When there was a step in pitch for 30 deg, the adaptive controller had almost zero error at the end of the step. After the next step, the adaptive controller had a bigger error than LQR, but one can see that the error was reduced with time, going towards zero. The $\hat{\Theta}_i, i = 1, 2$ in Figure C.6 shows that $\hat{\Theta}_1$ had changed behavior for the first estimate relative to what was the result from this test without disturbances. The two other estimates were relatively equal as without disturbance. This seems to be a correct behavior since the parameter that changed, was the parameter that was relating to the pitch angle, i.e. state variable x_1.

For the third test, the plot in Figure C.7a shows the same error in pitch angle in the first 5 seconds, when pitch angle should be zero, as test two. After the pitch angle was changed at time 5 s, the error for the adaptive controller was going towards zero. For the last time period where the pitch angle should be zero, both the LQR and the adaptive controller had an error just as in the beginning, first 5 seconds, when the desired pitch angle was zero. The errors were much smaller than it was for test two, just as it was without disturbances.

Positive Torque

A similar disturbance with the same mass was also tested. Now the mass was added to the tail thruster at the same distance as in the previous test. This gave a positive torque to the Aero and a new equilibrium point, moved from zero degrees to a positive pitch angle of 24.5 deg. The same procedure was followed when the test sequences was tried as for the previous test. The results are shown in Appendix D Figures D.1 to D.9. The results for this disturbance was similar to the one with a negative torque, with the main difference of changed sign for errors.

From test one, the LQR had same behavior as before, with largest errors for max and min points on the pitch trajectory, while the adaptive controller had largest error when the Aero had a pitch angle of 24.5 deg, which was at the new equilibrium point of the Aero in pitch. The $\hat{\Theta}_i, i = 1, 2$ were changing as they did for the previous disturbance, but $\hat{\Theta}_1$ for x_1 was changed in a negative direction now.

For test two, when mass was added in the beginning, both controllers had an error in pitch angle just as they had for a negative torque, with the difference of changed sign of error and also $\hat{\Theta}_1$ had changed direction.

A similar behavior can be seen for the third test as for the negative torque. A closer look at the pitch error in time period 25 to 40 s, one can see that the LQR had a steady-state error of about 4 deg, while the adaptive controller is reducing the error with time, and also that the estimated parameter $\hat{\Theta}_1$ was changing for the same time-period. This can also be seen for the step function in test two.

Both controllers seemed to handle the added mass, and follow the given trajectories. Both controllers had a steady state error when the desired pitch angle was zero.

4.7.2 Disturbance of Changing Tail Propeller

The tail propeller was changed from a low- to high efficiency propeller, meaning that the main and cross-torque gains produced by the input V_y were changed. The new propeller also had different airfoils, that is the cross sectional shape of blades on the propeller, than the old propeller, and so this will change the aerodynamic force also. Because this new propeller had a lower weight, a mass was also included to the tail thruster so that the Aero retained a horizontal position when at rest. This disturbance illustrate actuator damage where the dynamics were changed. Results from testing are shown in Appendix E.

For test 1 one can see from Figure E.1 that both controllers were able to follow the desired sine curve trajectory. Once again the LQR had biggest error when the pitch trajectory reached maximum and minimum values, with a maximal error of 4 deg, a little higher than without added disturbance. The adaptive controller had biggest error at the equilibrium point with maximal error of 2 deg, just as without the disturbance. From Figure E.2 one can see that a higher voltage was needed to reach the highest points on the curve, where both input voltages had increased for both controllers, but input V_y had changed most. Figure E.3 shows that the estimated parameter $\hat{\Theta}_1$ was slightly changed relative to without disturbance.

For test 2, Figure E.4 shows that the cross-coupling effect between pitch and yaw gave bigger errors than without disturbance. For the applied voltages seen in Figure E.5, input V_y had increased values now, this seems fair based on the changed propeller. Also the $\hat{\Theta}_i, i = 1, 2$ seen in Figure E.6, were changing more now.

For test 3, the results are shown in Figures E.7, E.8 and E.9, and both controllers were able to follow the desired trajectory. The errors were some higher and the estimated parameters were changing more now due to this disturbance relative to before the propeller was changed.

4.7.3 Disturbance of Changing both Propellers

Both propellers were changed to high efficiency propellers, and so main and cross torque gains produced by both inputs were changed. Also the mass of the Aero body was changed since the new propellers were lighter than the old. Results from tests are given in Appendix F.

Looking at the plot of input voltages in Figure F.2 for test one, saturation was reached when pitch angle was going below approximately - 25 deg, as seen in Figure F.1. This gave big errors for

Table 4.3: Compare total error of the LQR and the adaptive backstepping controller

Total error						
Test	Controller	No disturbance	Disturbance, added mass -	Disturbance, added mass +	Disturbance, changed tail propeller	Disturbance, changed both propellers
Sine	LQR	0.0938	0.1228	0.1245	0.1625	1.2054
	Adaptive	0.0153	0.0616	0.1001	0.0195	1.2825
Step	LQR	**0.6974**	0.7912	0.8337	1.0352	1.6936
	Adaptive	**0.7228**	0.8109	0.8611	1.0402	1.2752
Smooth step	LQR	0.0727	0.1092	0.1477	0.2589	0.2719
	Adaptive	0.0175	0.0869	0.1383	0.1024	0.1095

both controllers since it was not possible to reach the desired reference, because a higher voltage was needed than what could be applied.

In Figure F.4, showing angles and errors from test two, a bigger overshoot can be seen for both controllers, and also a bigger steady state error for the pitch angle. Figure F.5 shows that higher values of input was needed and Figure F.6 shows changes in the estimated values.

The last test sequence had smallest errors when the propellers were changed, with biggest absolute error in pitch at 6.5 deg for the LQR and 4.9 deg for the adaptive controller at time 31.5 s as seen in Figure F.7. The LQR had bigger steady state errors than the adaptive. Figure F.8 shows that there was a bigger need of inputs than before. The parameter $\hat{\Theta}_1$ had a bigger change now than before.

4.8 Comparing the Controllers

The LQR and adaptive backstepping controller were compared with a measurement of tracking error, i.e. the error between reference signal of pitch and yaw and actual pitch and yaw. Also the total voltage used is measured. Both are used when comparing results from the controllers. The more accurate the controller is, meaning the error is smaller, the more voltage is needed to hold the trajectory closer to the reference and so there is a trade-off between these two. The measurement of the total error is

$$\|\mathbf{z}_\gamma\|^2 = \int_0^t |\mathbf{z}_\gamma(t)|^2 dt, \tag{4.1}$$

and the measurement of the total voltage, i.e. input to the system, is

$$\|\mathbf{u}\|^2 = \int_0^t |\mathbf{u}(t)|^2 dt. \tag{4.2}$$

In Table 4.3 the total tracking errors from Equation (4.1) are included from each test without and with the different disturbances for both the LQR and the adaptive backstepping controller. Table 4.4 shows the measurement of the total voltage from Equation (4.2). The gains for the two controllers were adjusted to have a similar performance for the step sequence in test two, and the highlighted values in Tables 4.3 and 4.4 show where the two controllers had a similar performance. Looking at these results one can see that for all the tests, both controllers had a better performance with both a lower total error and lower total voltage for the smooth step compared to ordinary step.

In Figure 4.19 the results from test one are plotted, where the blue plots are for the LQR and the red plots are for the adaptive backstepping controller. For four out of five of the tests, the adaptive controller had a lower error than the LQR. For the last test, where both propellers were changed, saturation was reached that resulted in big errors and high voltage usage.

Table 4.4: Compare total voltage of the LQR and the adaptive backstepping controller

Total voltage						
Test	Controller	No disturbance	Disturbance, added mass -	Disturbance, added mass +	Disturbance, changed tail propeller	Disturbance, changed both propellers
Sine	LQR	6572	8953	8623	11666	22848
	Adaptive	7244	9107	9028	11848	24252
Step	LQR	**6716**	9253	11925	13433	20376
	Adaptive	**6722**	8640	11513	13704	20406
Smooth step	LQR	4875	7435	9905	13914	17552
	Adaptive	5392	7593	10127	14308	19770

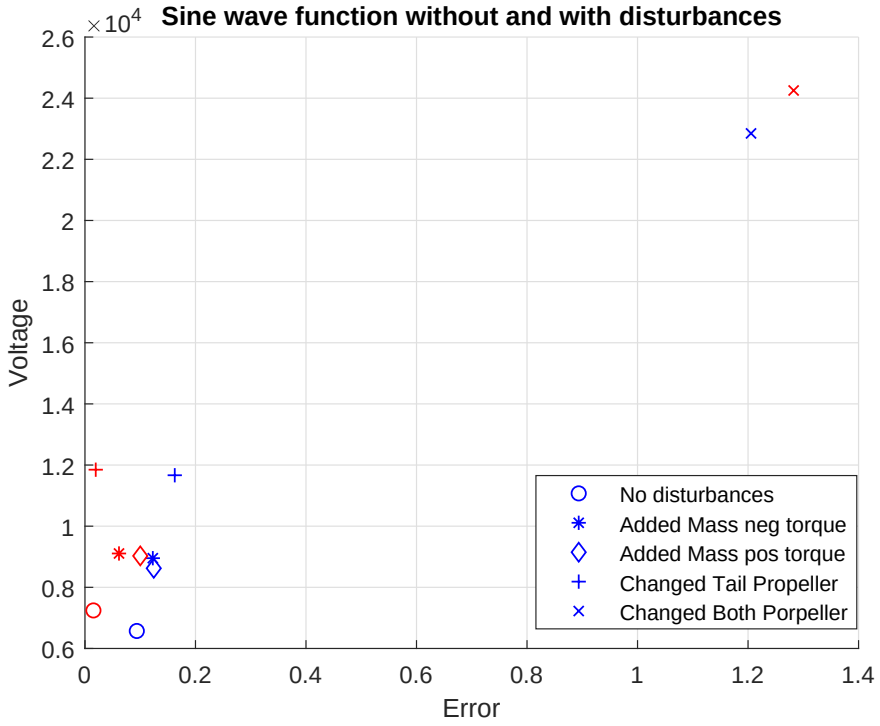

Figure 4.19: Comparing the LQR (blue plots) and the adaptive backstepping controller (red plots) for test 1

Figure 4.20 shows the compared results from test two. The two controllers had similar performance for four of the tests, but when both propellers were changed the adaptive controller had a better performance.

Last is the smooth step, and a compared plot in Figure 4.21. The adaptive controller had a better performance for all the tests relative to error, but used more input than the LQR.

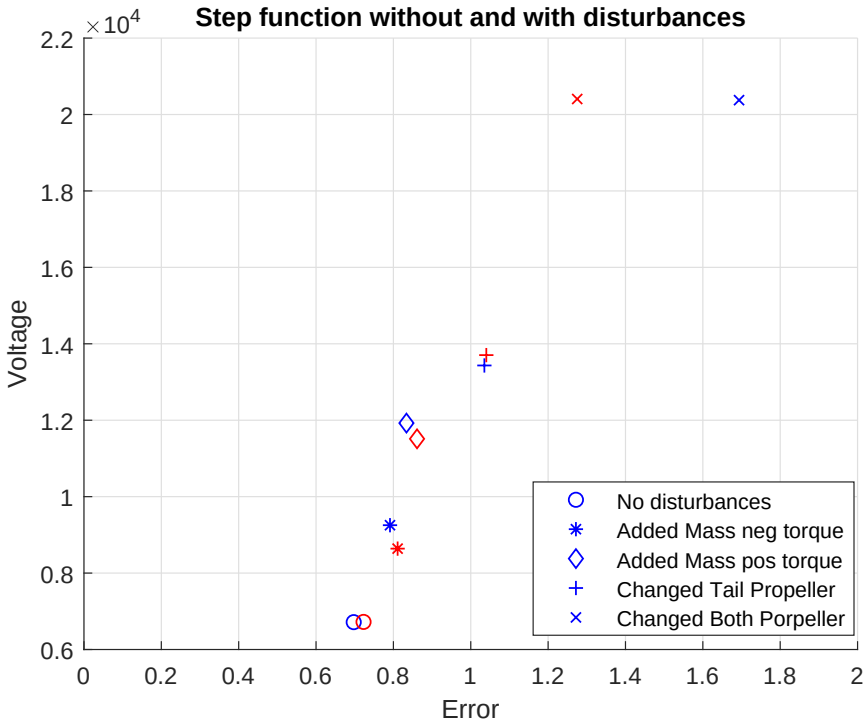

Figure 4.20: Comparing the LQR (blue plots) and the adaptive backstepping controller (red plots) for test 2

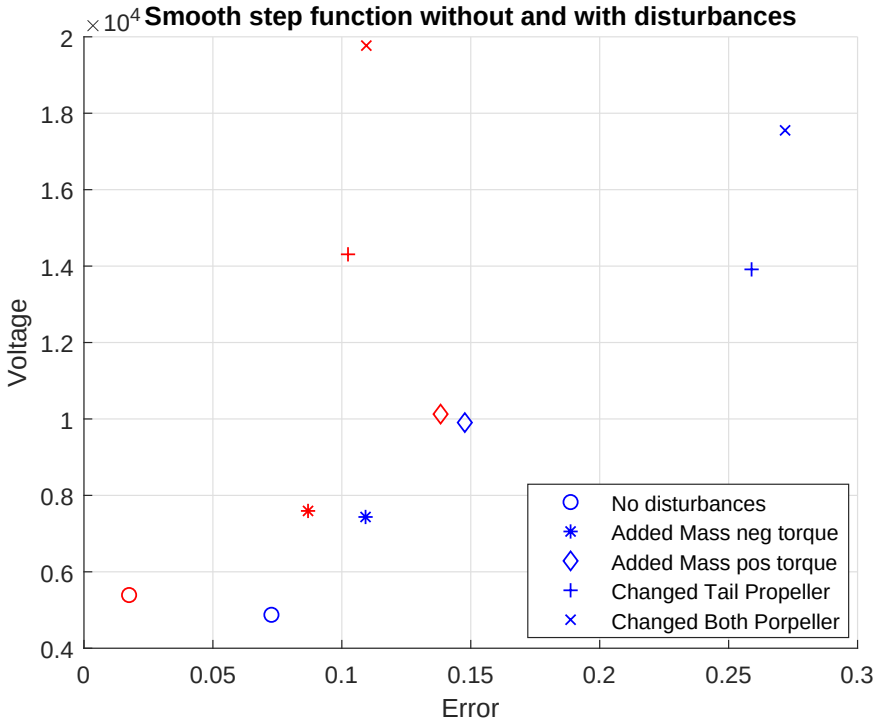

Figure 4.21: Comparing the LQR (blue plots) and the adaptive backstepping controller (red plots) for test 3

Chapter 5

Conclusion

In this thesis an adaptive backstepping controller has been proposed as a control structure for the Quanser Aero laboratory equipment. A mathematical model was first derived, where the kinematics and dynamics of the system were looked into, and a nonlinear model was derived. Some simplifications were done to the model, where for instance all the mass components were simplified when looking at the inertia for the Aero body and Coulomb friction was not included. The support yoke which is rotating with a rotation in yaw was also neglected to simplify the model. The nonlinear model was also linearized, so that a linear controller could be tested for control of the Aero.

All parameters for the model were estimated and the parameters have uncertainties to their value. All mass components were assumed to have the weight given by Quansers documentation, but have not been verified by weighting. The center of mass was estimated with two different approaches, giving two different estimates. The real value is probably somewhere in between these two. Viscous damping was estimated with the same test performed five times, averaging the value to reduce uncertainty. The main torques were estimated resulting in nonlinear function for this. For simplicity, the linear estimates for this were used for the controllers.

Four different controllers have been proposed for control of the Aero including two PID based controllers that are not model-based, one linear controller, LQR, requiring a linear model with estimated parameters to be able to calculate the feedback matrix $\mathbf{K}$ and a nonlinear controller based on adaptive backstepping where the nonlinear model was used. The latter controller does not require any estimated values.

The purpose of the simulation and testing with the decoupled PID and PV was to illustrate that control of a MIMO system using SISO systems not necessarily is a good idea since this will be harder to control than using a holistic approach for control. The PV controller showed that control using two SISO systems, controlling pitch and yaw separately, is possible but also causes bigger deviations from the desired trajectory than for controlling as a MIMO system. For this control method, the cross-coupling between inputs and outputs was neglected.

The LQR and the adaptive backstepping controller were simulated and tested and the performance compared. The LQR was minimizing the error in trajectory, velocity of trajectory and the inputs, while the adaptive controller only took the tracking errors and velocity of tracking errors into account when adapting its estimates. Three different desired trajectories in form of a sine wave for the pitch angle, different step inputs to pitch and yaw at different time instances and the same step sequence but with smoother step were simulated and tested. The reference signals and first and second derivative of the signal were piecewise continuous and bounded. Gyro signals were used to measure the angular velocities for pitch and yaw. To reduce measurement noise from the gyros, the rate signals were filtered by a second order low-pass filter. A test with lower break frequency showed that the signals could have been smoother.

Different physical disturbances were also added to the Aero to test if the adaptive controller was able to adapt to these changes. First a mass was added to the main thruster, giving a negative torque, then the same mass was added to the tail thruster, giving a positive torque. The third disturbance tested was changing the tail propeller from a low- to a high-efficiency propeller, and the last disturbance test was changing both propeller from low- to high-efficiency propellers.

For all tests with and without added disturbances, both controllers were able of tracking the desired reference signal. The results from a desired trajectory in form of a sine wave for the pitch angle showed that the LQR had biggest deviation when reaching the maximum and minimum points on the trajectory while the adaptive controller had biggest deviation around the equilibrium point for the Aero. The adaptive controller had a lower error for four out of the five tests with the sine wave. For the step sequence, the two controllers had a similar performance and for the smoother step the adaptive controller had a better performance relative to error than the LQR.

When the goal is to get from one desired reference angle to a new desired angle, a step function is often used. If one can plan the path between the two points, a smoother function can be used that will give a better performance for the system with both smaller errors and with lower consumption of input voltages. This was verified by simulation and testing of the step and the smooth step inputs, where a second order lowpass filter was used after the referenced step input. Also, giving a step function means that there will be a sudden change in the wanted pitch and yaw angles and this means the function is not continuous at that point. For the adaptive controller continuity is a need, but the Lipschitz condition reduces this to piecewise functions so that an adaptive controller can work even if the trajectory is not continuous at every point. But when we have a step function, the adaptive controller will perhaps need some time to adapt its estimated values. The smoother step function does not have this sudden change, and so the adaptive can change along the new reference trajectory. The smoother step seems to be a better solution for both the LQR and adaptive controller showing better performance, resulting in less errors both in tracking and less voltage use. The better performance can be seen for all the tests without and with disturbances.

The main focus has been to the adaptive backstepping controller and a stability proof have been given using constructed Lyapunov functions. It is shown that all signals in the closed loop system are bounded and asymptotic tracking of a reference signal is achieved. Simulation and testing confirms that this is so. The transient performance for the $\mathbf{z}$ system including the tracking errors in terms of $\mathcal{L}_2$ norm have been derived, where the performance can be improved by increasing the control parameters $c_i, i = 1, 2, 3, 4$ or by increasing the adaptation gain γ, and so the tracking errors can be made smaller.

5.1 Future Work

The nonlinear model used in this thesis included several simplifications, and there were unmodel components not included. All small deviations from the real system give small error in the model. A suggestion is to add more terms to the nonlinear model and then try to improve the adaptive backstepping control scheme. Motor dynamic is one of the things that can be include.

It is further suggested to look into what caused the adaptive backstepping controller to give an error in pitch angle around the equilibrium point of the Aero, and also why there is an error in the pitch angle after an added mass, when the desired angle is zero.

Another suggestion is to investigate the estimated parameters and see how they behave. Are they converging to their true values for any initial conditions? What is the relationship between the potential number of estimated parameters and measurements? How does the model formulation impact the behaviour of the estimated parameters?

Other disturbances can be tested, like wind.

Another thing is to try the proposed adaptive backstepping control scheme for a quad-copter with 3DOF (rotation) or 3+3DOF (rotation and translation). Then it is also suggested to change the attitude parameterization to a quaternion method or SO(3) for 3DOF (rotation) or SE(3) for 6DOF [14], this to avoid having singularities so that the quad-copter can turn however it wants.

References

[1] C. Woodford, "*Helicopters.*" https://www.explainthatstuff.com/helicopter.html. Accessed: 10.02.2019.

[2] S. K. Pandey and V. Laxmi, "Optimal control of twin rotor mimo system using lqr technique," in *Computational Intelligence in Data Mining*, 2014.

[3] A. P. S. Ramalakshmi and P. S. Manoharan, "Non-linear modeling and pid control of twin rotor mimo system," IEEE International Conference on Advanced Communication Control and Computing Technologies (ICACCCT), 2012.

[4] J. Frasik and S. I. L. Gabrielsen, "Practical application of advanced control, an evaluation of control methods on a quanser aero," Master's thesis, University of Agder, 2018.

[5] P. Chalupa, J. Přikryl, and J. Novák, "Modelling of twin rotor mimo system," in *Procedia Engineering*, vol. 100, pp. 249–258, 2015.

[6] P. Chalupa, J. Přikryl, and J. Novák, "Adaptive control of twin rotor mimo system," in *International Conference on Process Control (PC)*, 2015.

[7] A. P. S. Ramalakshmi, P. S. Manoharan, K. Harshath, and M. Varatharajan, "Model predictive control of 2dof helicopter," *International Journal of Innovation and Scientific Research*, vol. 24, pp. 337 – 346, June 2016.

[8] A. S. Dutka, A. W. Ordys, and M. J. Grimble, "Non-linear predictive control of 2 dof helicopter model," in *Proceedings of the 42nd IEEE Conference on Decision and Control Mad, Hawaii USA, December 2003*, 2003.

[9] Q. Ahmed, S. Iqbal, A. I. Bhatti, and I. Kazmi, "2-sliding mode based robust control for 2-dof helicopter," in *11th IEEE Workshop on Variable Structure Systems Mexico City, Mexico*, June 26-28, 2010.

[10] R. Patel, D. Deb, H. Modi, and S. Shah, "Adaptive backstepping control scheme with integral action for quanser 2-dof helicopter," 2017.

[11] Y. Zou and W. Huo, "Adaptive tracking control for a model helicopter with disturbances," 2015.

[12] M. Lopéz-Martinéz, C. Vivas, and M. G. Ortega, "A multivariable nonlinear $\mathcal{H}\infty$ controller for a laboratory helicopter," 2005.

[13] R. S. Burns, *Advanced Control Engineer.* Butterworth-Heinemann, 2001.

[14] O. Egeland and J. T. Gravdahl, *Modeling and Simulation for Automatic Control.* Marine Cybernetics AS, 2003.

[15] M. J. Sidi, *Spacecraft Dynamics & Control - A practical Engineering Approach.* Cambridge University Press, 2005.

[16] T. Glad and L. Ljung, *Control Theory - Multivariable and Nonlinear Methods.* Taylor and Francis, 2000.

[17] *Quanser AERO - 2DOF Lab Guide.*

[18] S. S. Rao, *Mechanical Vibrations.* Pearson Education, 2011.

[19] H. K. Khalil, *Nonlinear Systems, third edition.* Pearson Education International Inc., 2002.

[20] K. Ogata, *Modern Control Engineering.* Pearson, 2010.

[21] M. Krstić, I. Kanellakopoulos, and P. Kokotović, *Nonlinear and Adaptive Control Design.* 1995.

[22] J. Zhou and C.Wen, *Adaptive Backstepping Control of Uncertain Systems.* Springer, Berlin, Heidelberg, 2008.

[23] J. Zhou and C. Wen, "Adaptive feedback control of magnetic suspension system preceded by bouc-wen hysteresis," in *12th International Conference on Control Automation Robotics & Vision (ICARCV)*, 2012.

[24] J. Zhou, C. Wen, and W. Wang, "Adaptive control of uncertain nonlinear systems with quantized input signal," in *Automatica*, vol. 95, pp. 152–162, Sept. 2018.

Appendix A

Simulation of PID Controller

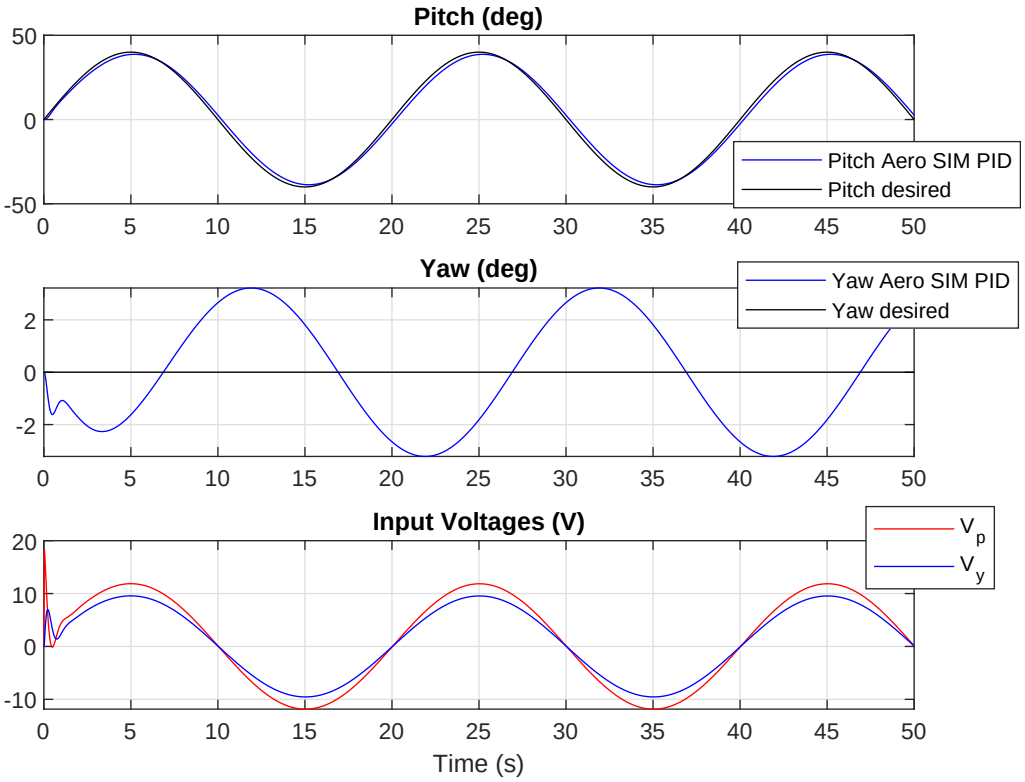

Figure A.1: Simulation of decoupled PID for Aero, Sine wave

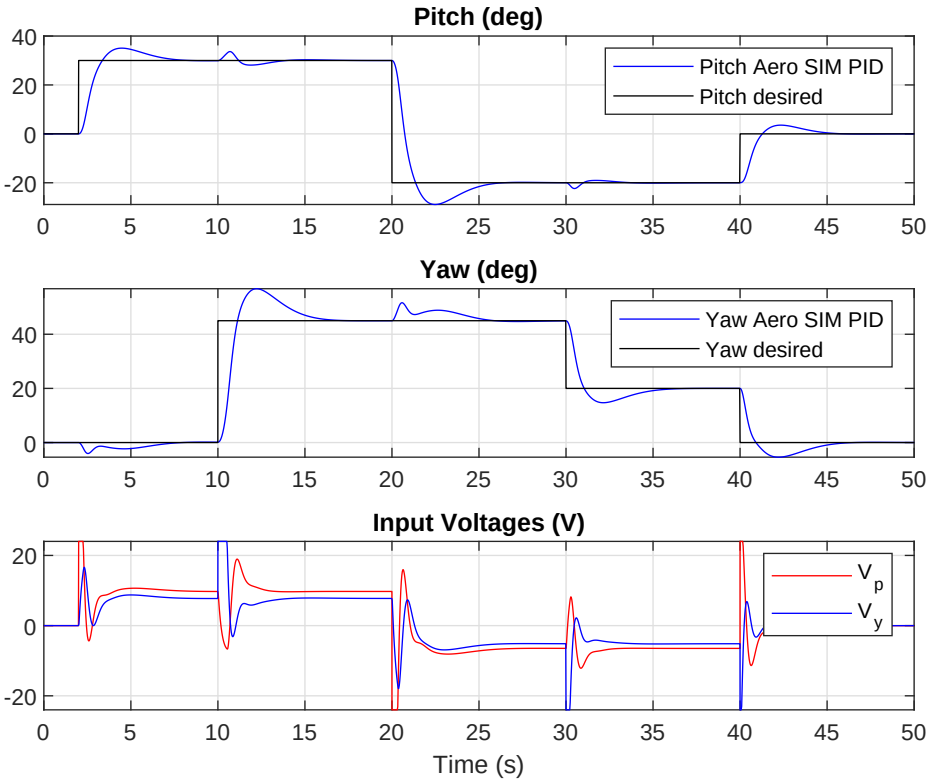

Figure A.2: Simulation of decoupled PID for Aero, Step sequence

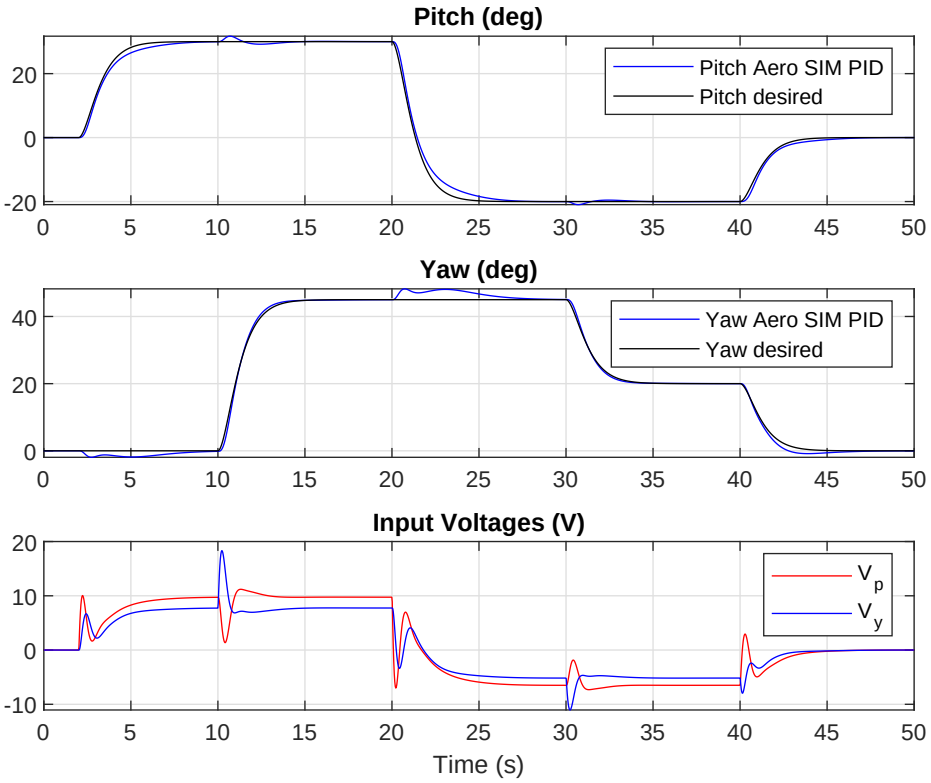

Figure A.3: Simulation of decoupled PID for Aero, smooth step sequence

Appendix B

Simulation and Testing of PV Controller

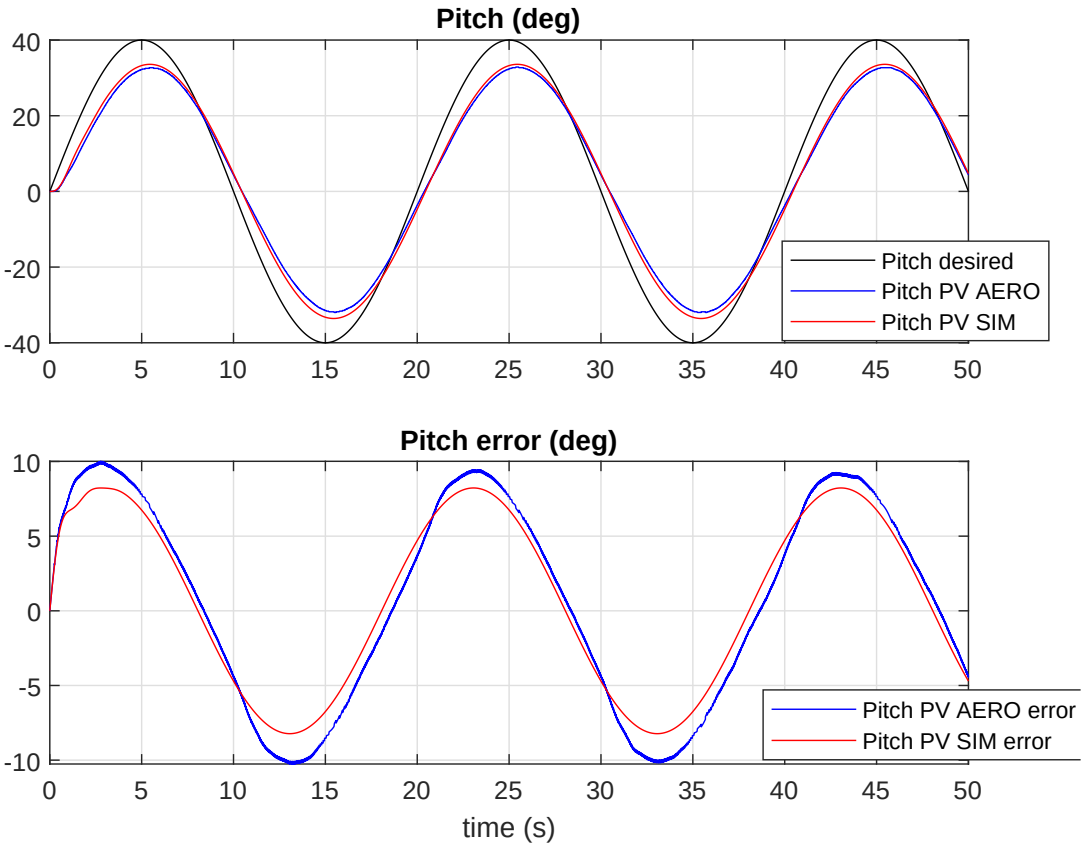

(a) Pitch angle and error for test 1 (sine wave) with PV control

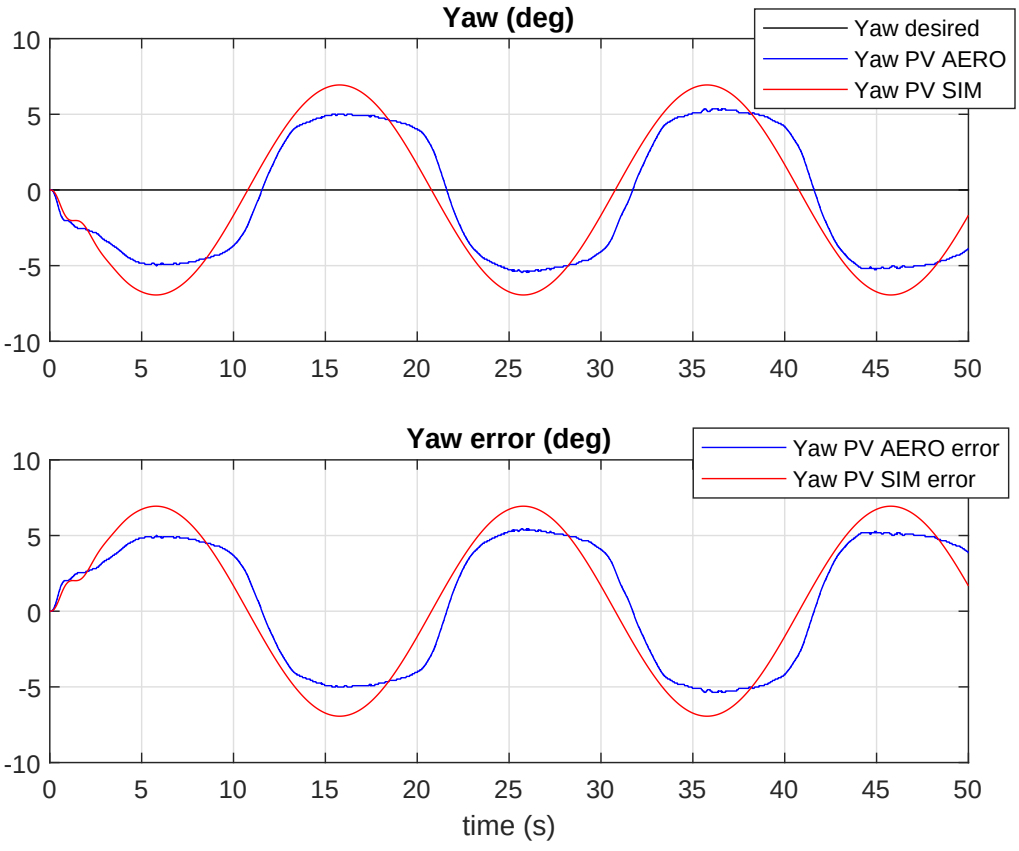

(b) Yaw angle and error for test 1 (sine wave) with PV control

Figure B.1: Angles and errors for test 1 (sine wave) with PV control, both simulated and tested on Aero

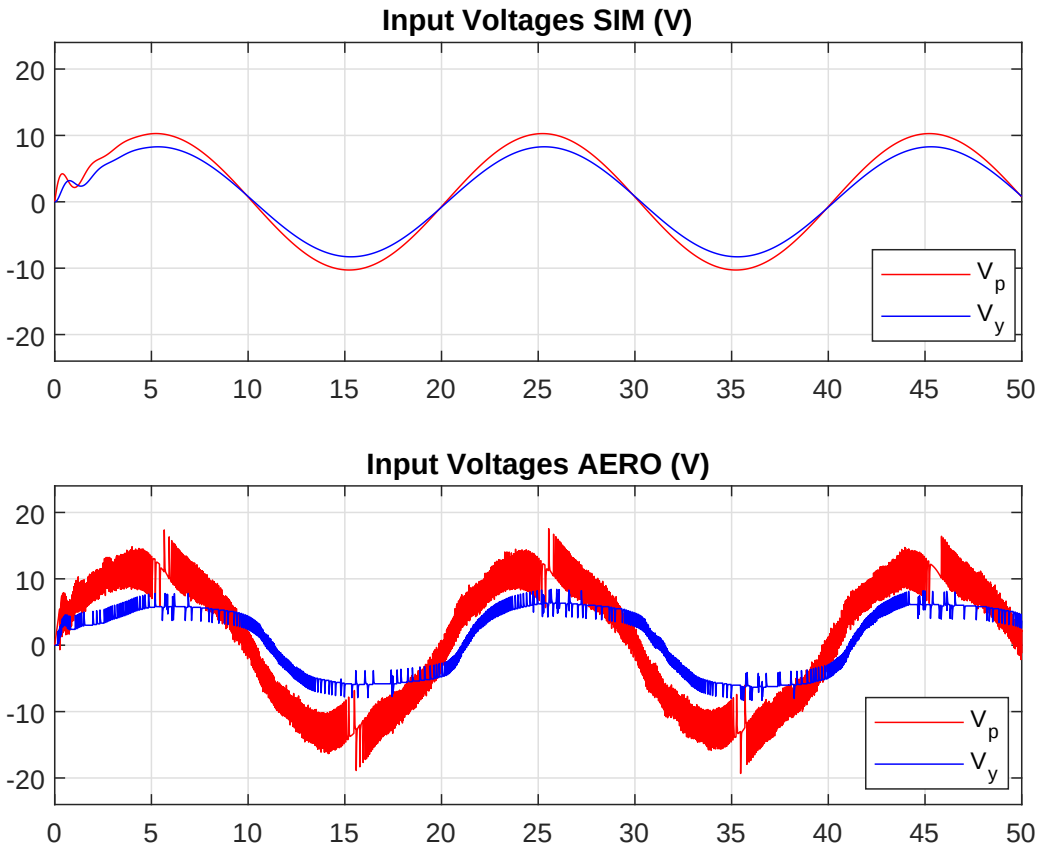

Figure B.2: Voltage for test 1 (sine wave) with PV control, when tested on Aero

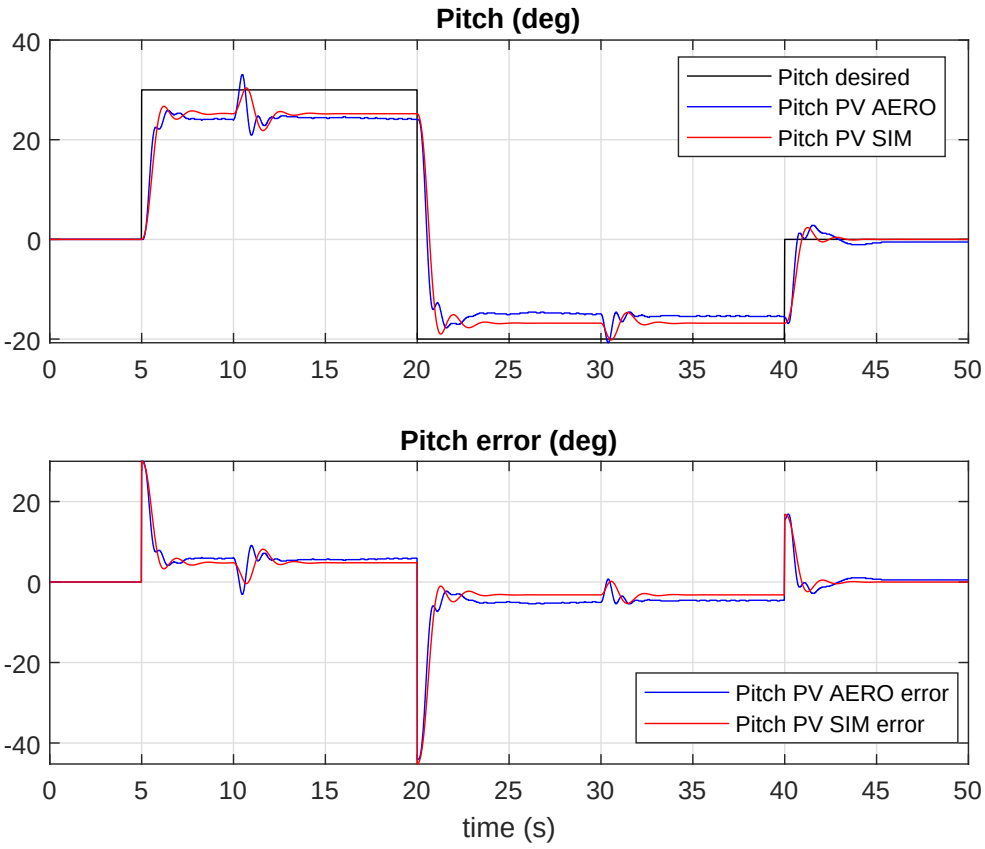

(a) Pitch angle and error for test 2 (step sequence) with PV control

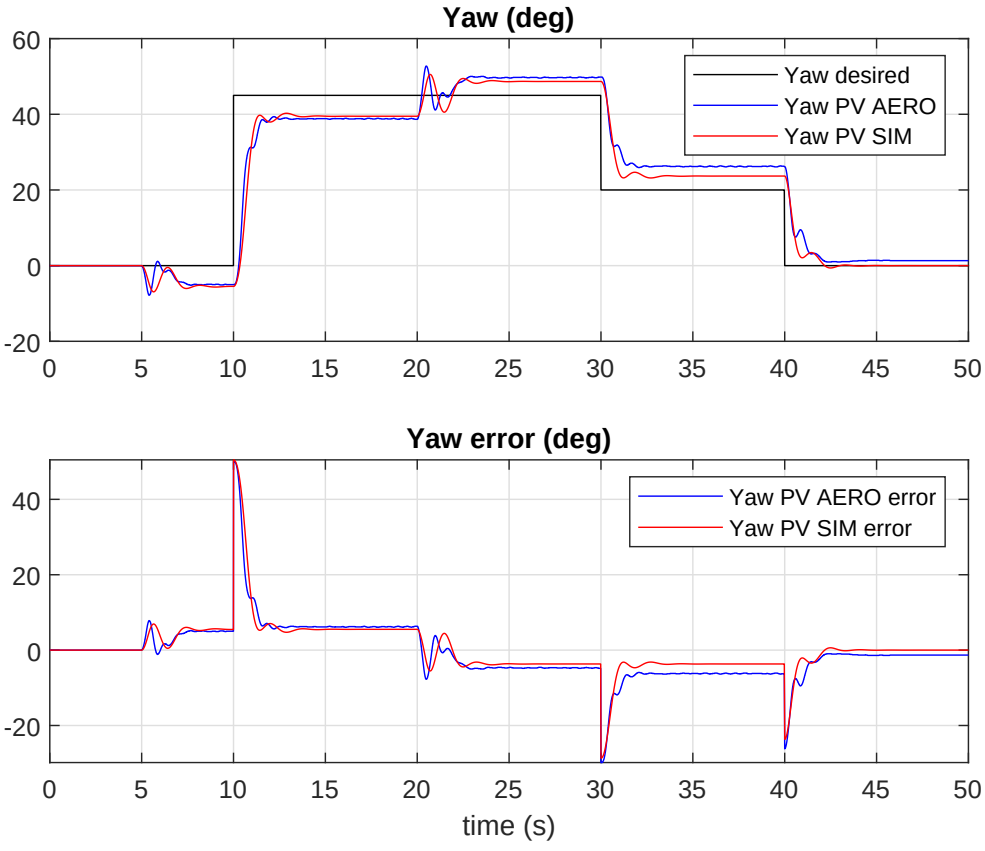

(b) Yaw angle and error for test 2 (step sequence) with PV control

Figure B.3: Angles and errors for test 2 (step sequence) with PV, both simulated and tested on Aero

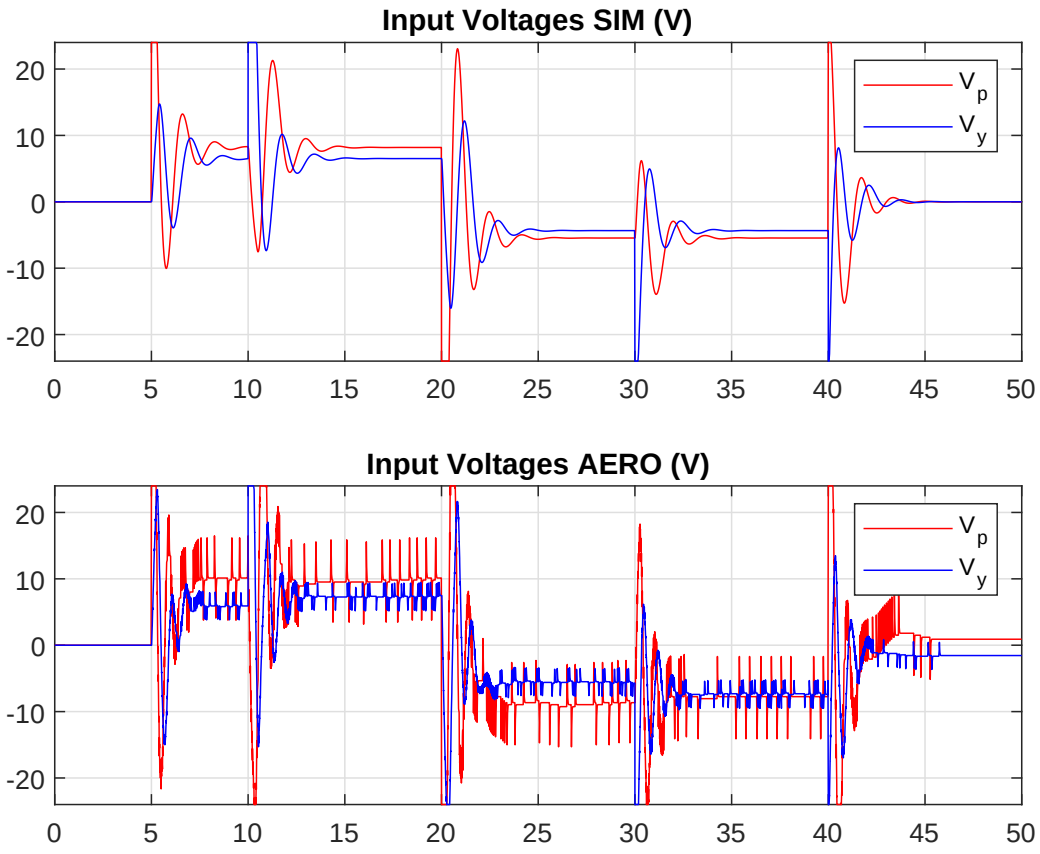

Figure B.4: Voltage for test 2 (step sequence) with PV control, when tested on Aero

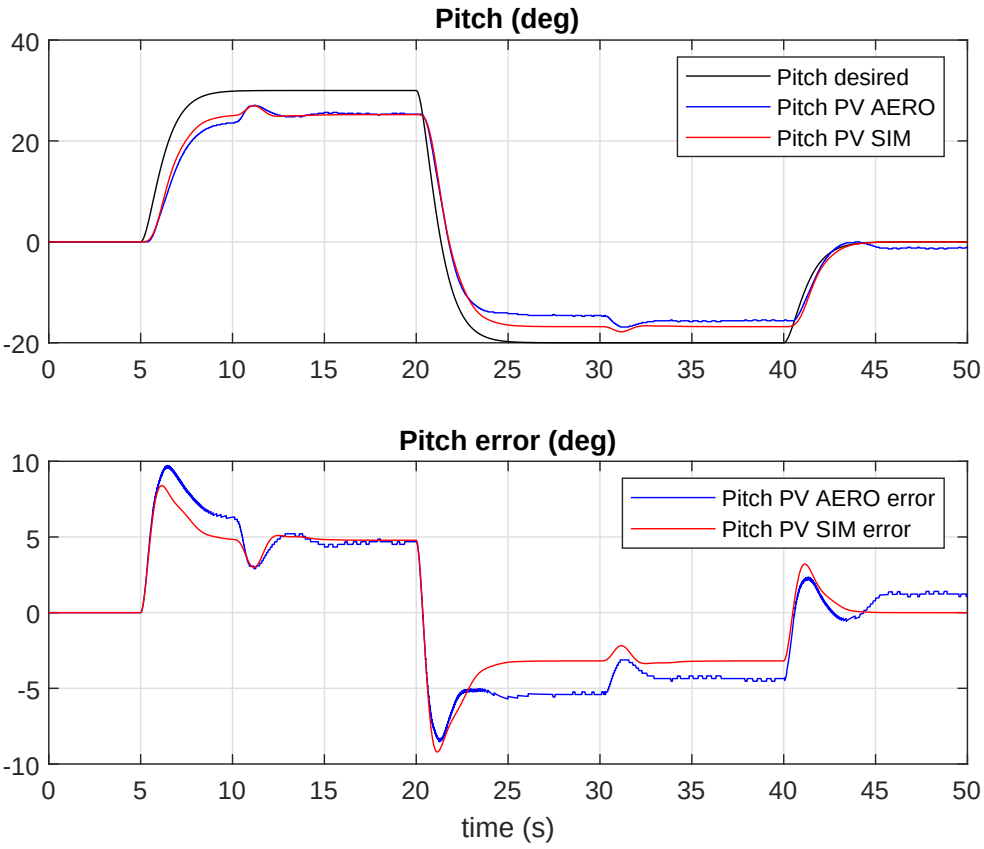

(a) Pitch angle and error for test 3 (smooth step) with PV control

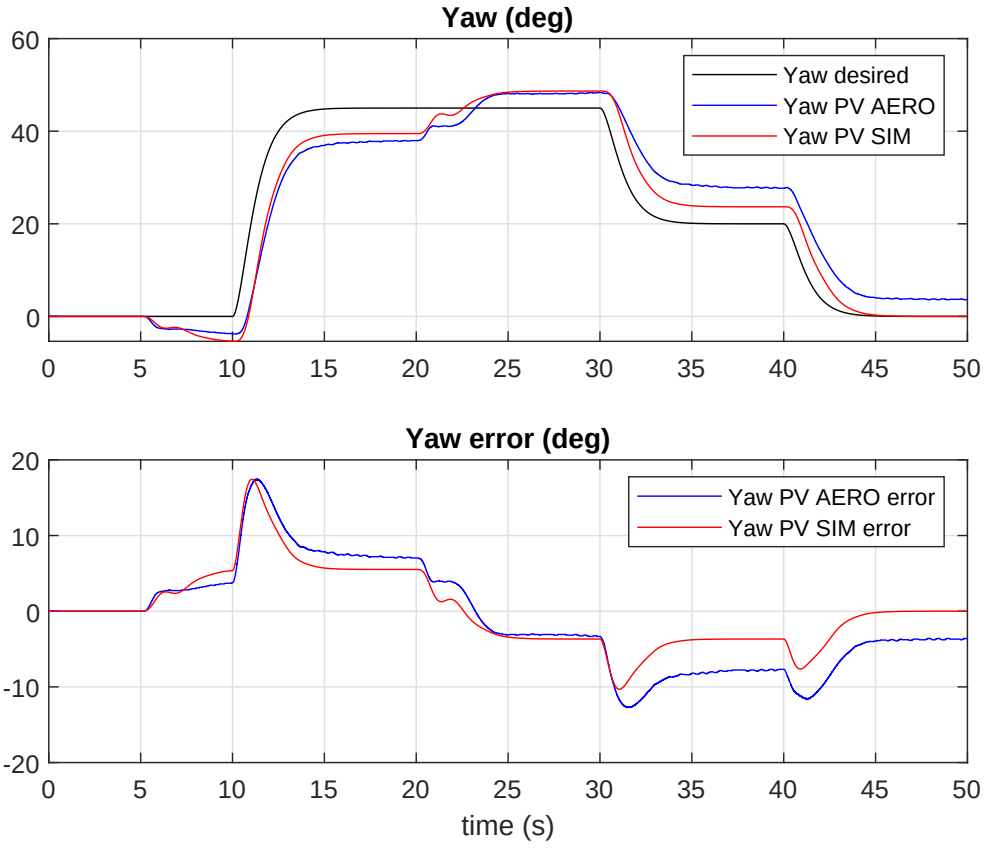

(b) Yaw angle and error for test 3 (smooth step) with PV control

Figure B.5: Angles and errors for test 3 (smooth step) with PV control, both simulated and tested on Aero

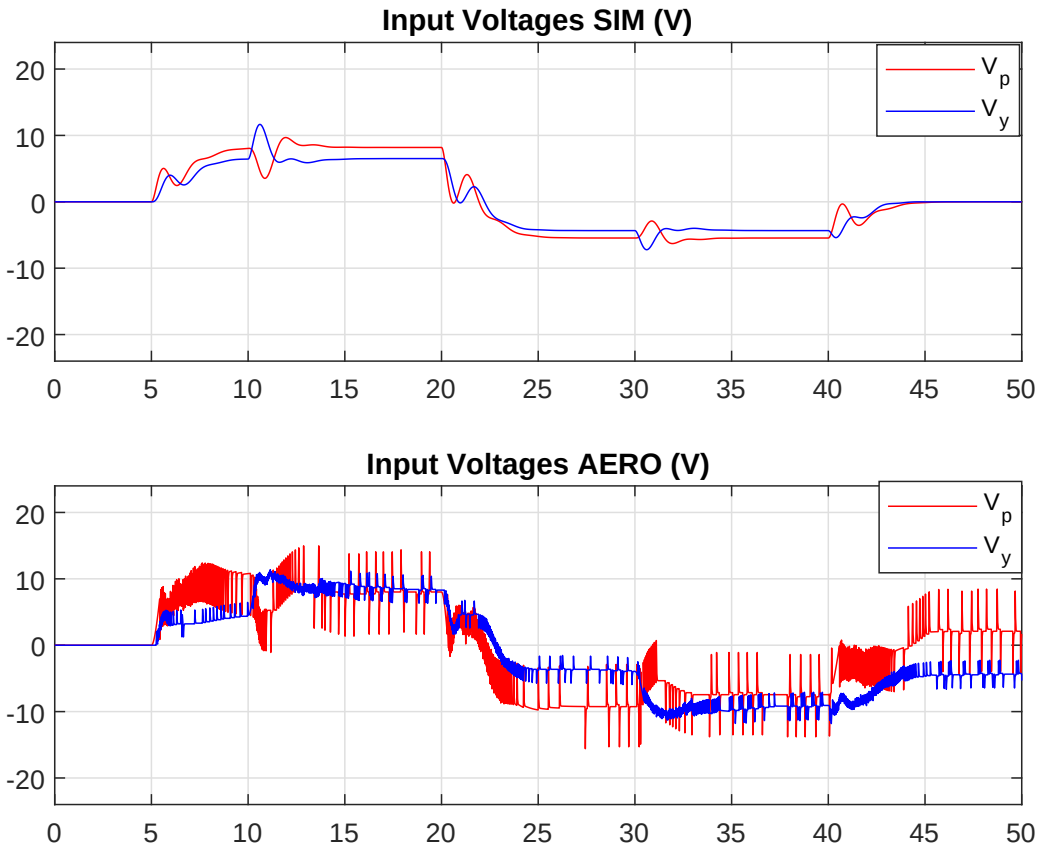

Figure B.6: Voltage for test 3 (smooth step) with PV control, when tested on Aero

Appendix C

Test with Disturbance of Added Mass, Negative Torque

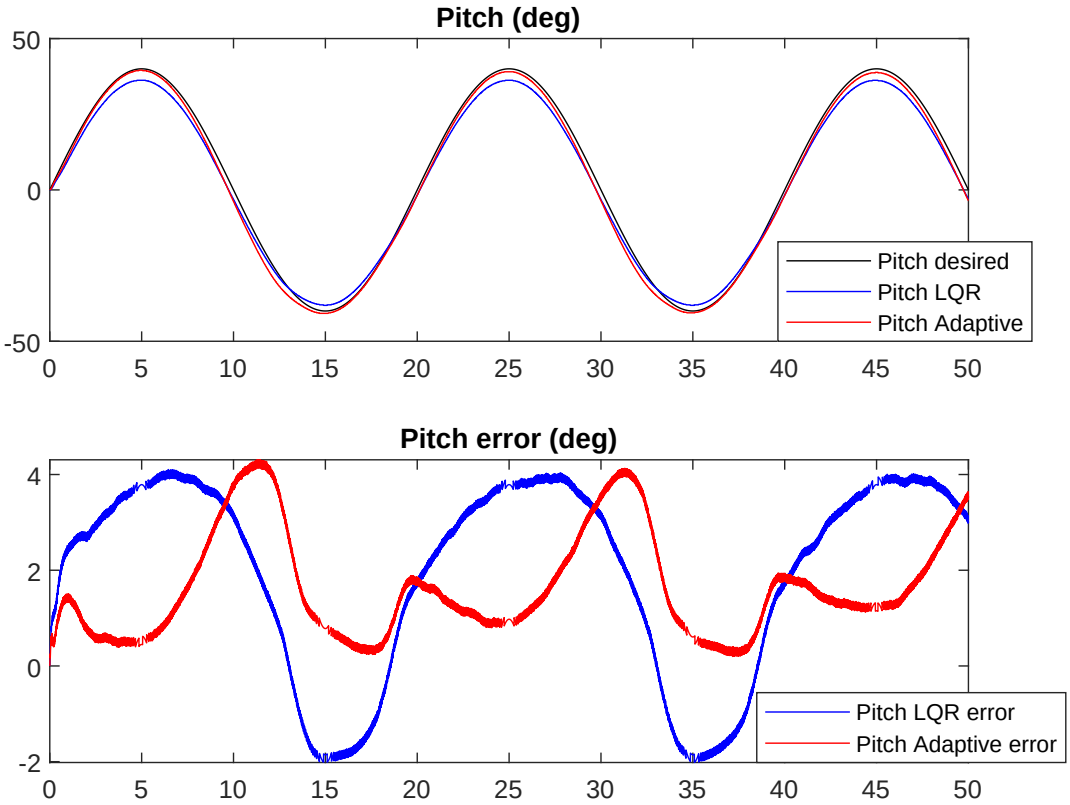

(a) Pitch angle and error for test 1 (sine wave) with disturbance of added mass, negative torque

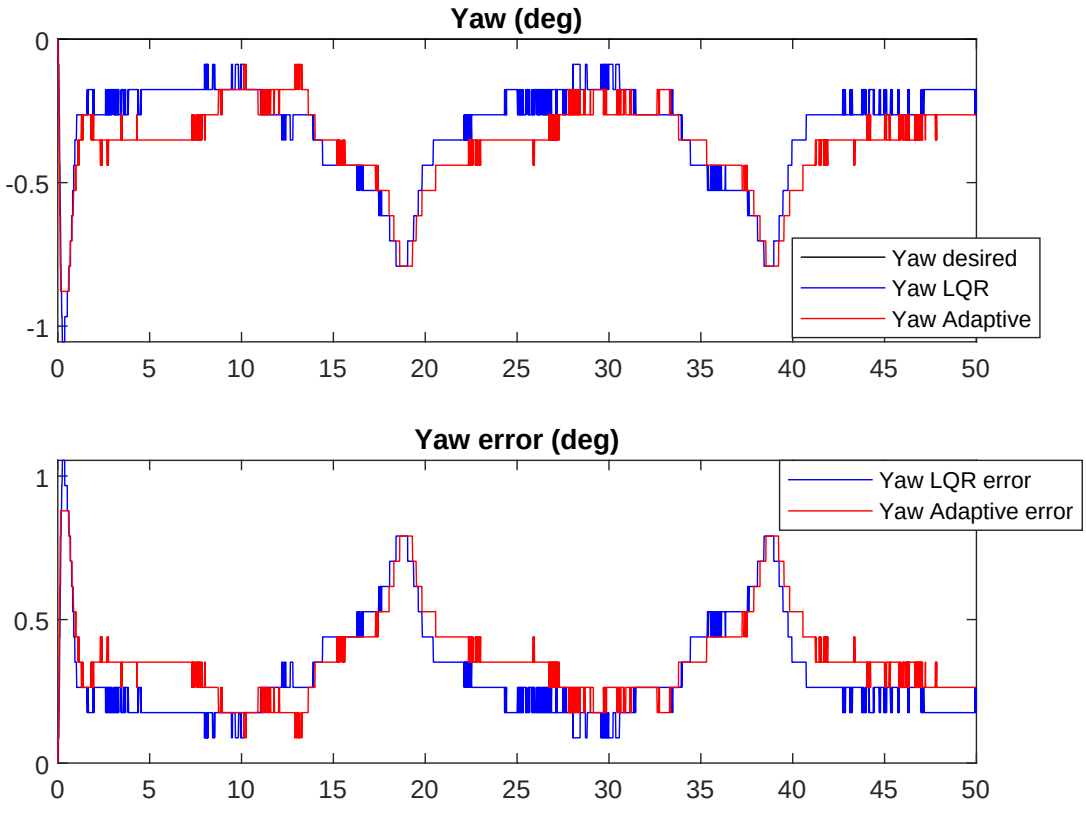

(b) Yaw angle and error for test 1 (sine wave) with disturbance of added mass, negative torque

Figure C.1: Angles and errors for test 1 (sine wave) with disturbance of added mass, negative torque

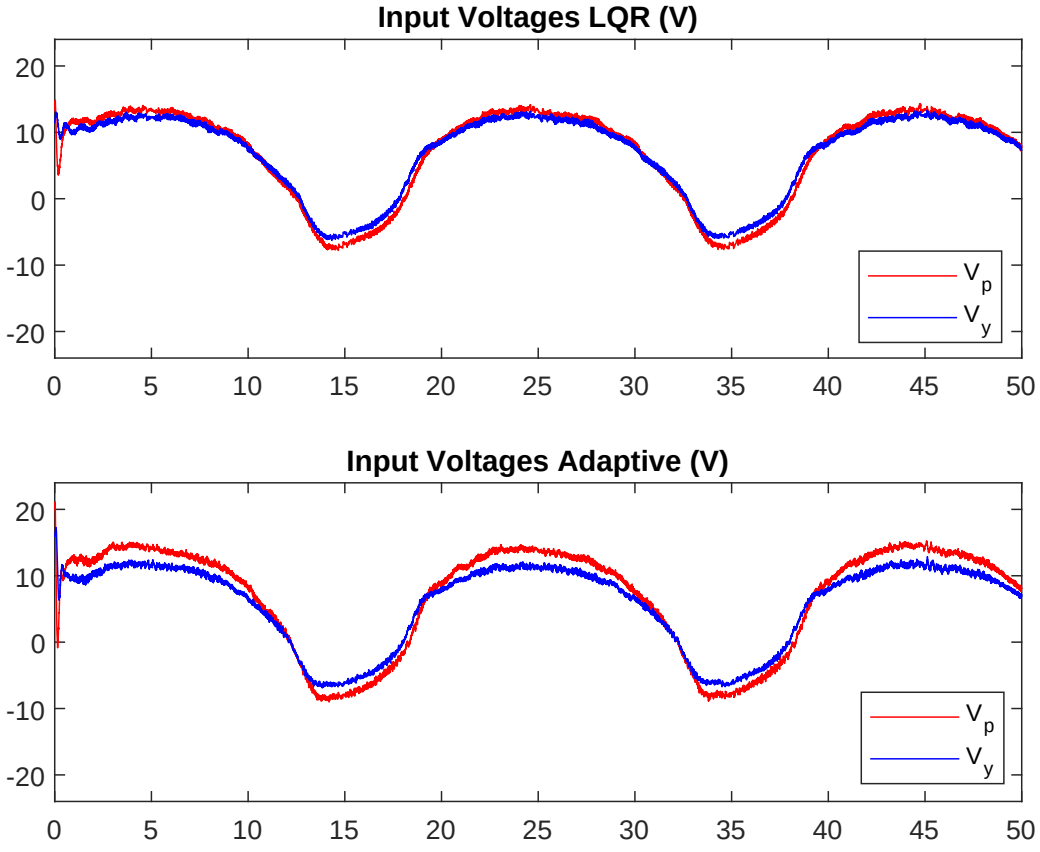

Figure C.2: Voltage for test 1 (sine wave) with disturbance of added mass, negative torque

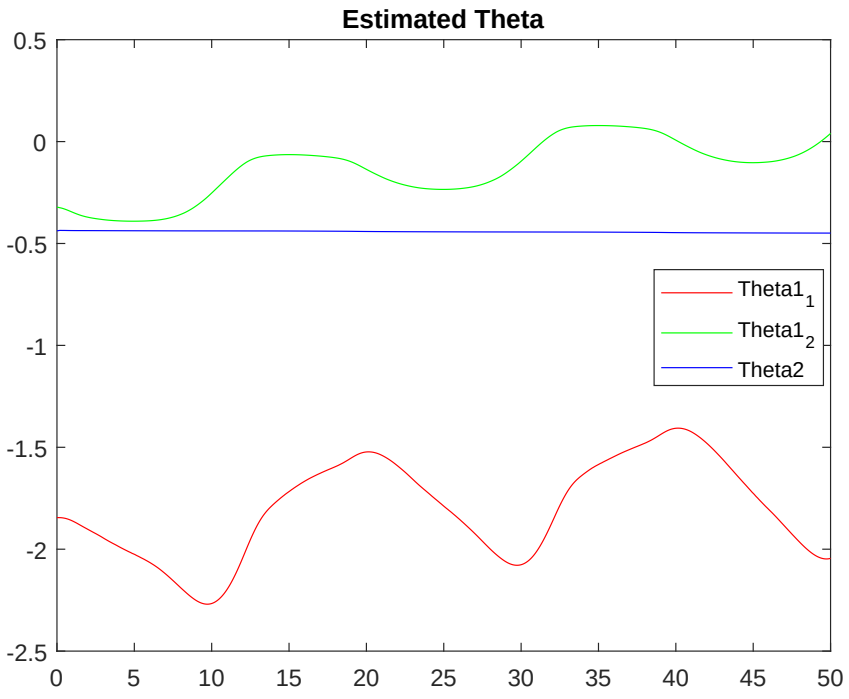

Figure C.3: Estimated theta for test 1 (sine wave) with disturbance of added mass, negative torque

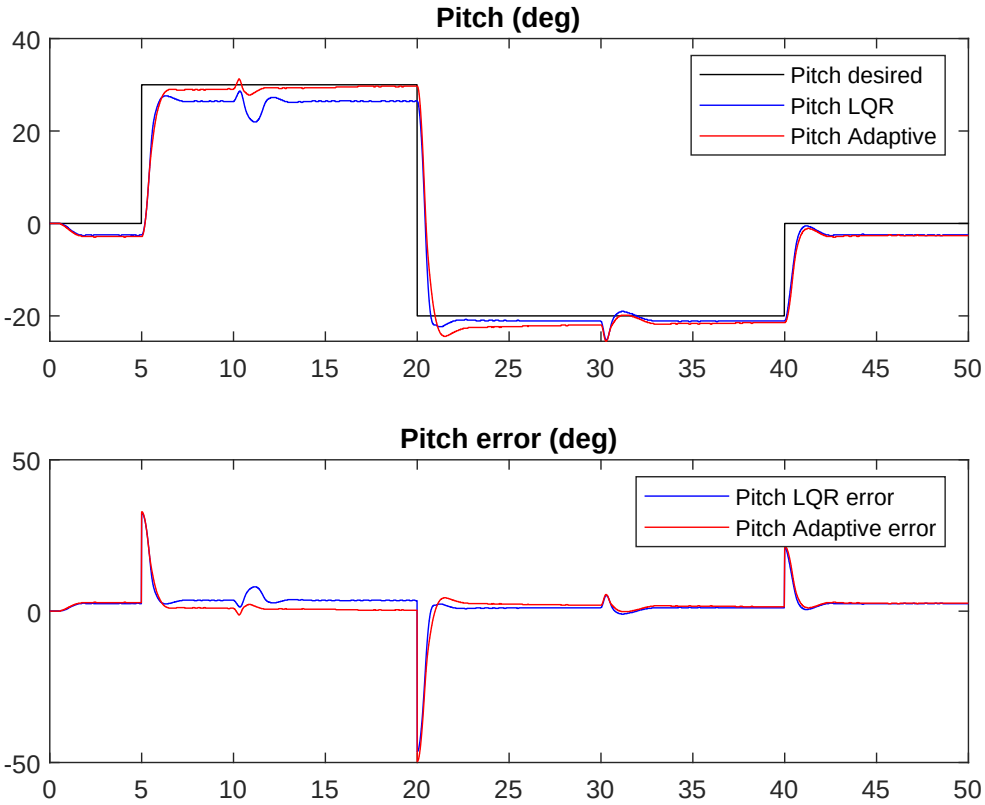

(a) Pitch angle and error for test 2 (step) with disturbance of added mass, negative torque

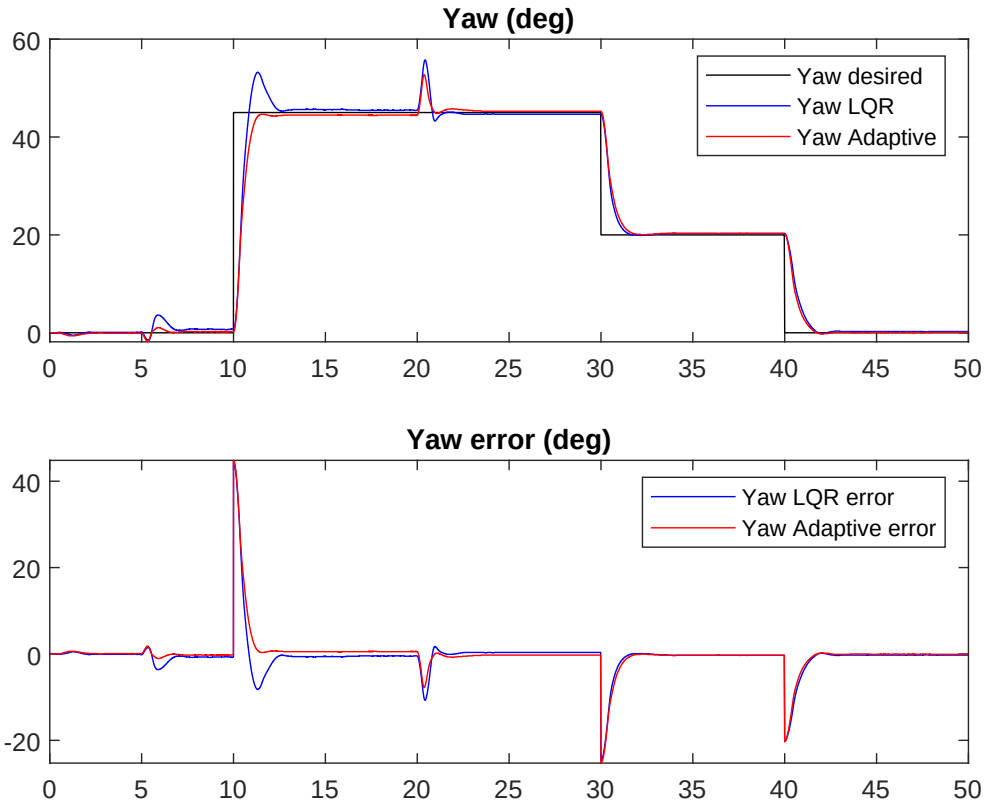

(b) Yaw angle and error for test 2 (step) with disturbance of added mass, negative torque

Figure C.4: Angles and errors for test 2 (step) with disturbance of added mass, negative torque

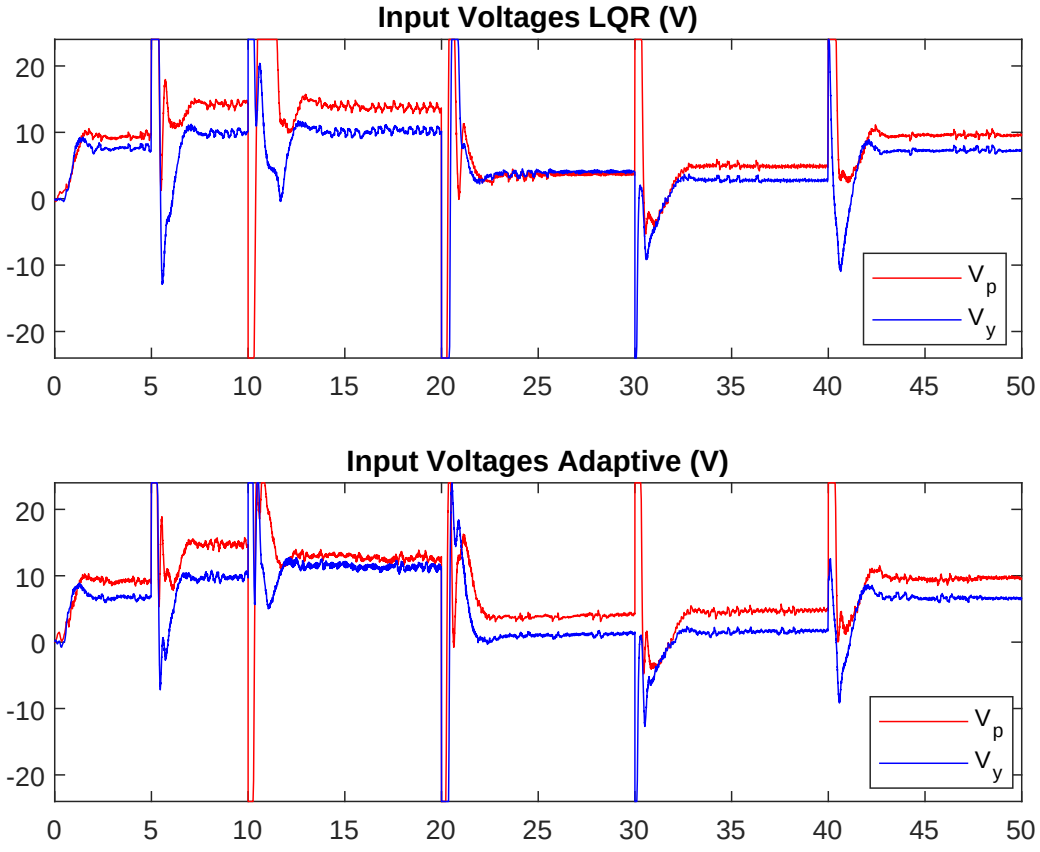

Figure C.5: Voltage for test 2 (step) with disturbance of added mass, negative torque

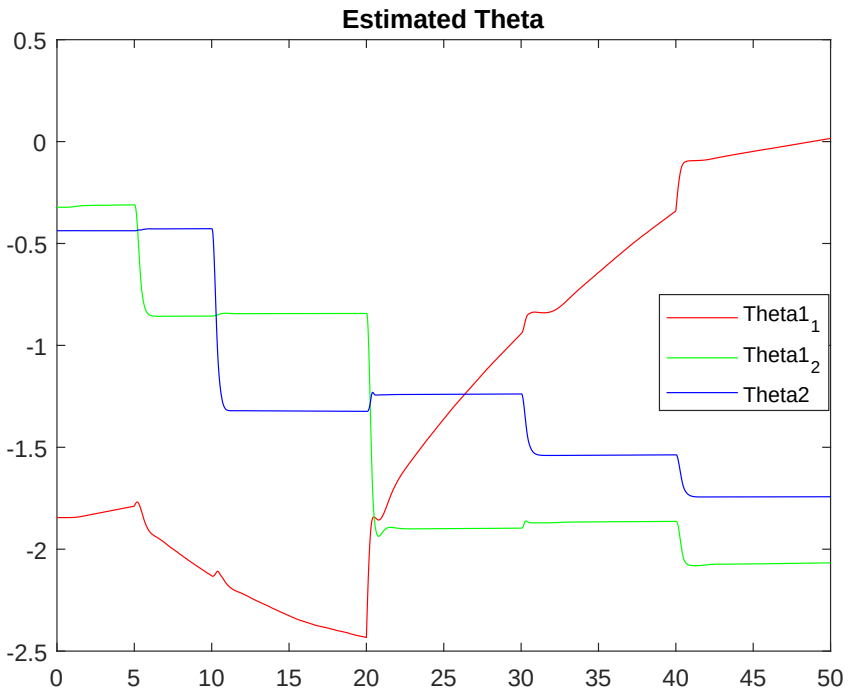

Figure C.6: Estimated theta for test 2 (step) with disturbance of added mass, negative torque

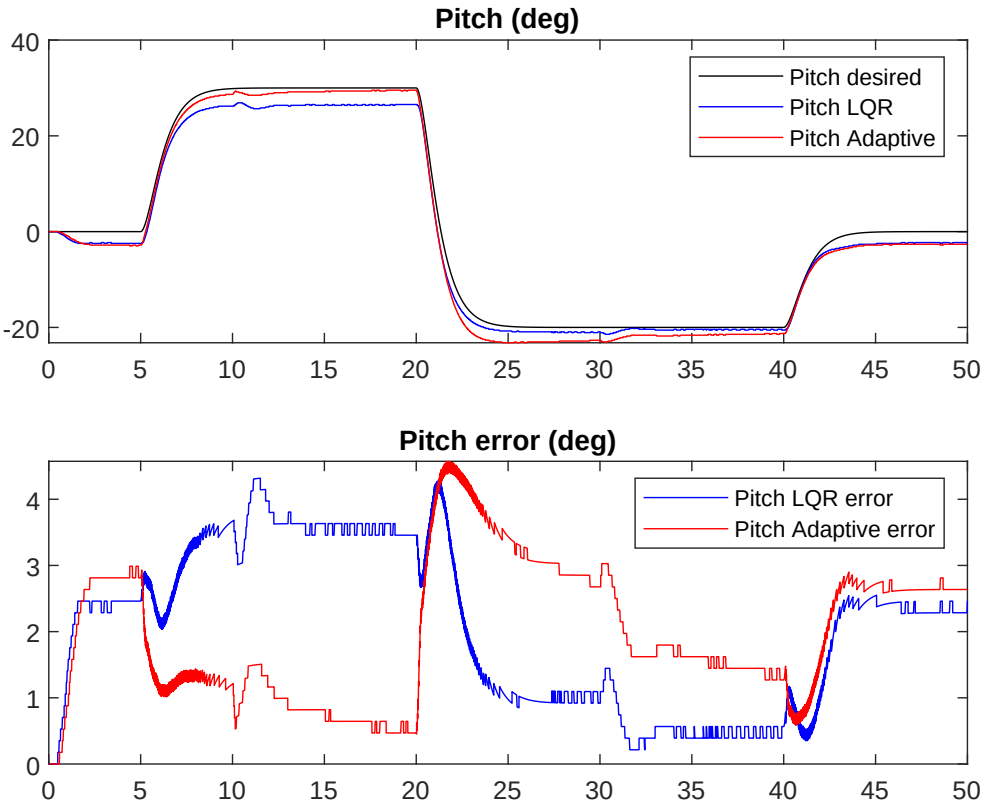

(a) Pitch angle and error for test 3 (smooth step) with disturbance of added mass, negative torque

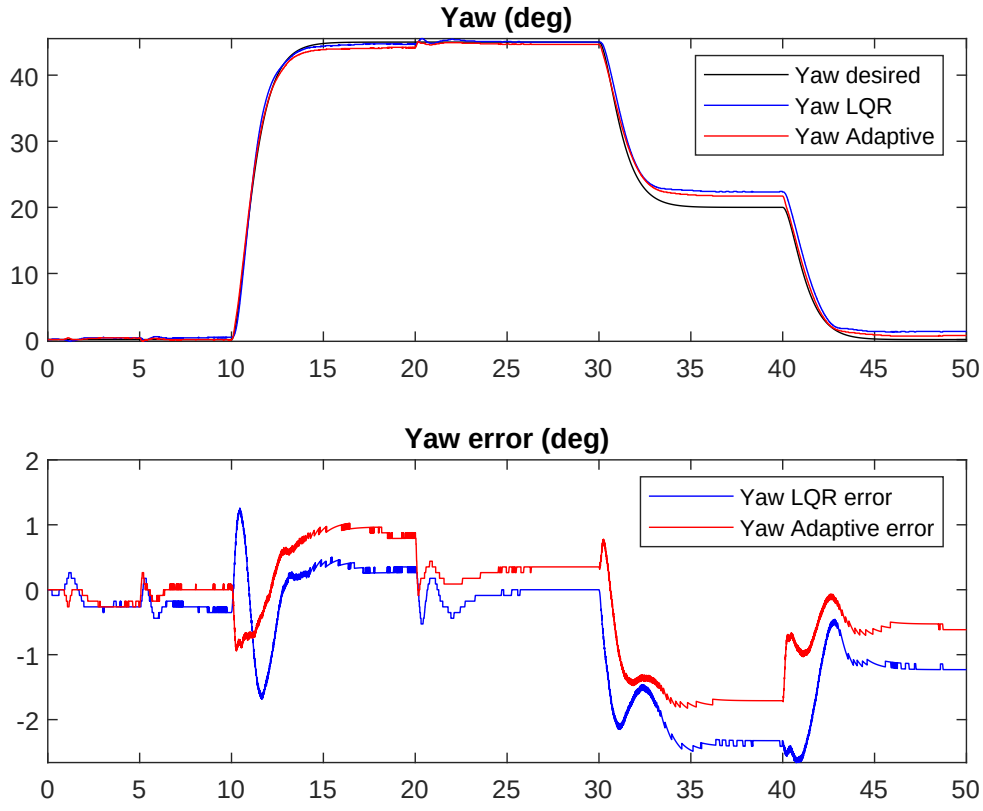

(b) Yaw angle and error for test 3 (smooth step) with disturbance of added mass, negative torque

Figure C.7: Angles and errors for test 3 (smooth step) with disturbance of added mass, negative torque

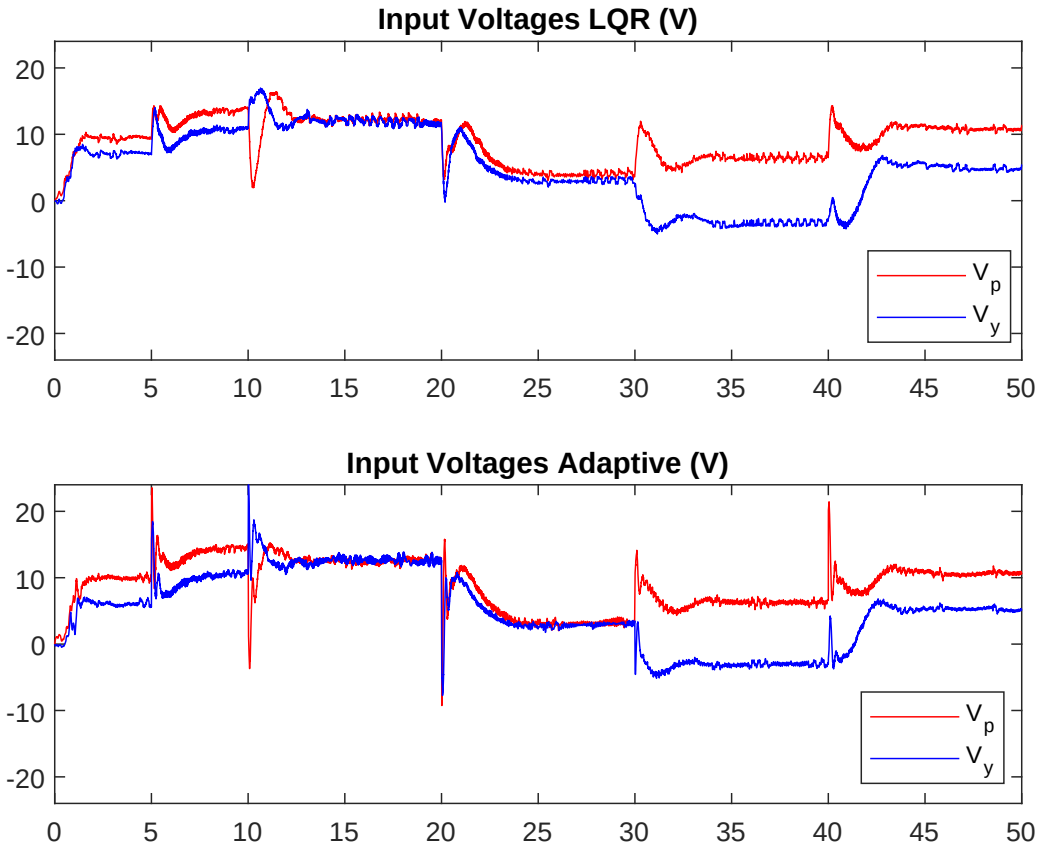

Figure C.8: Voltage for test 3 (smooth step) with disturbance of added mass, negative torque

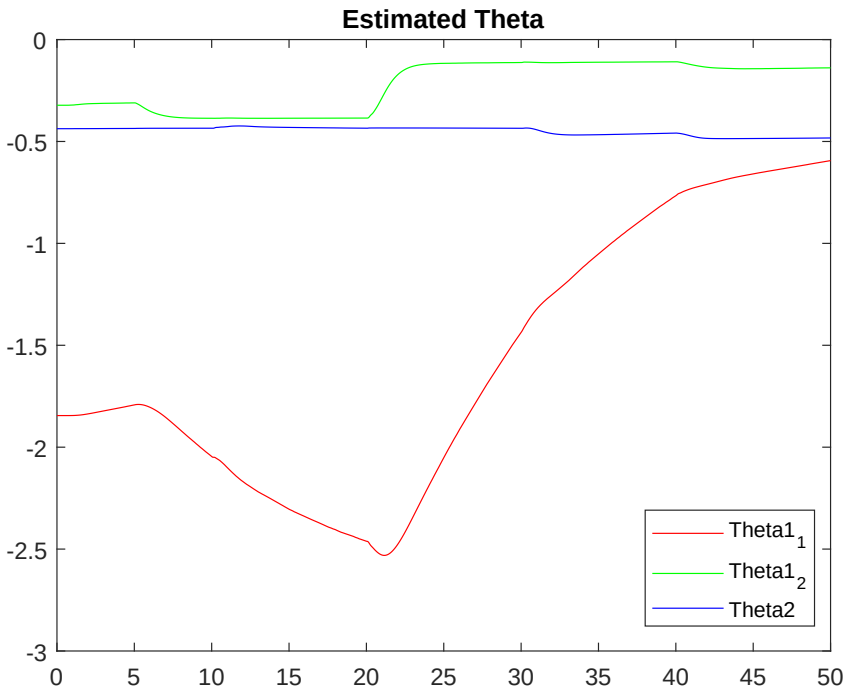

Figure C.9: Estimated theta for test 3 (smooth step) with disturbance of added mass, negative torque

Appendix D

Test with Disturbance of Added Mass, Positive Torque

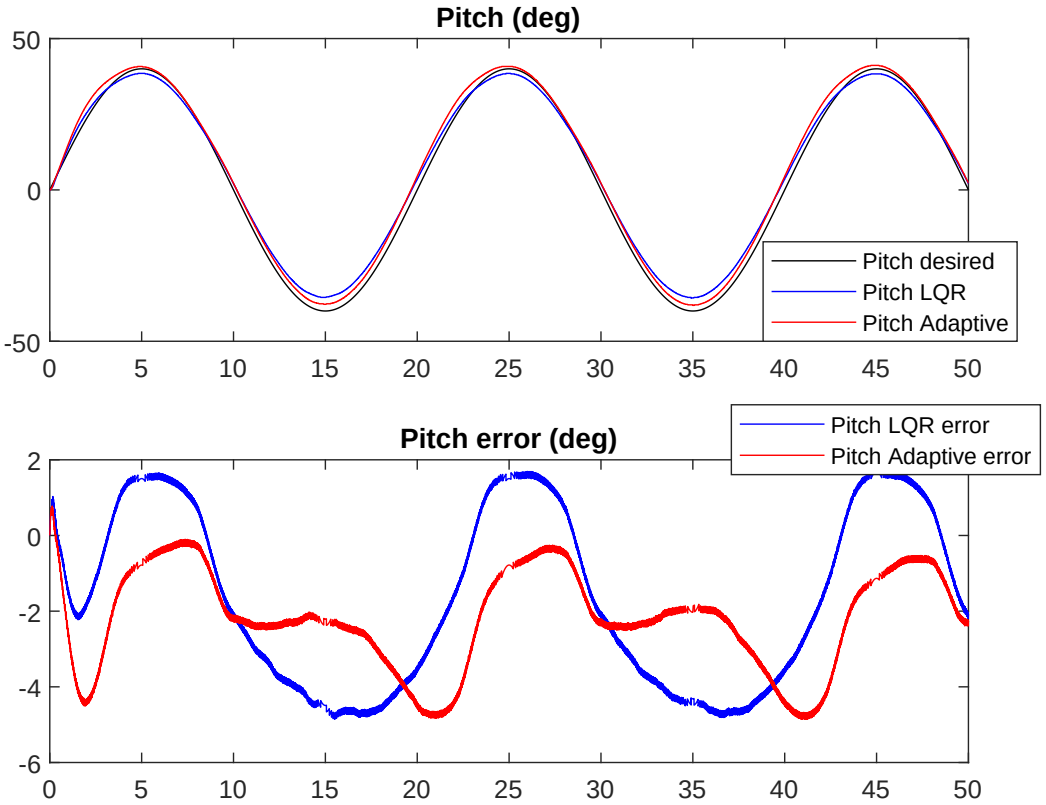

(a) Pitch angle and error for test 1 (sine wave) with disturbance of added mass, positive torque

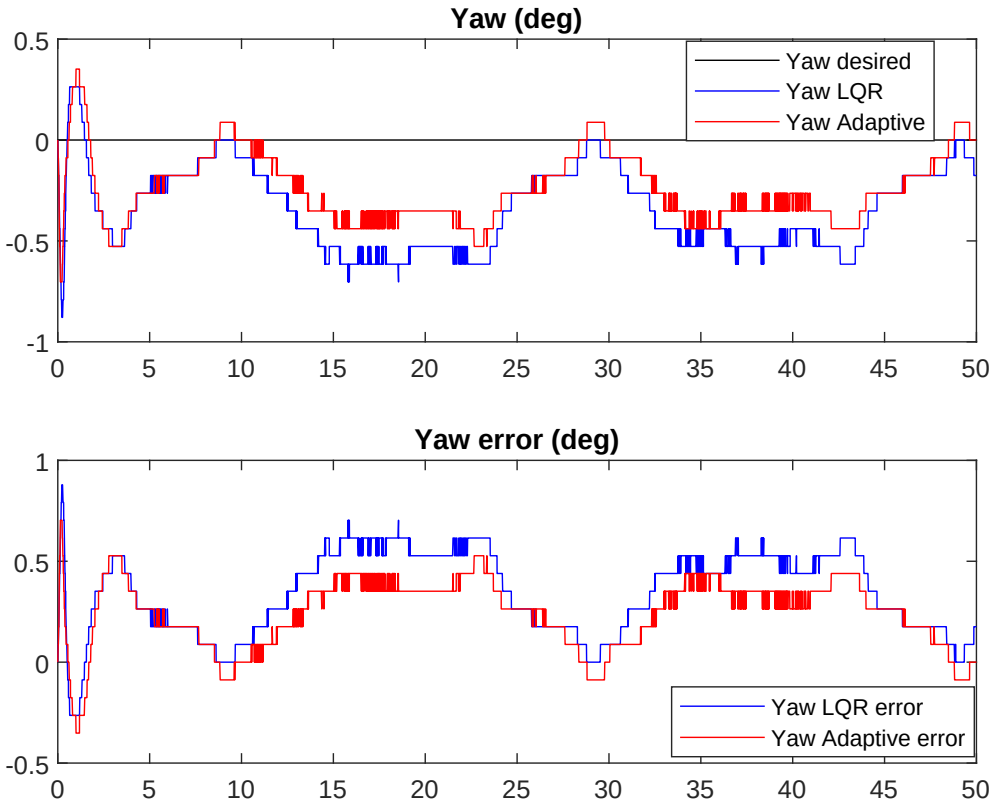

(b) Yaw angle and error for test 1 (sine wave) with disturbance of added mass,positive torque

Figure D.1: Angles and errors for test 1 (sine wave) with disturbance of added mass, positive torque

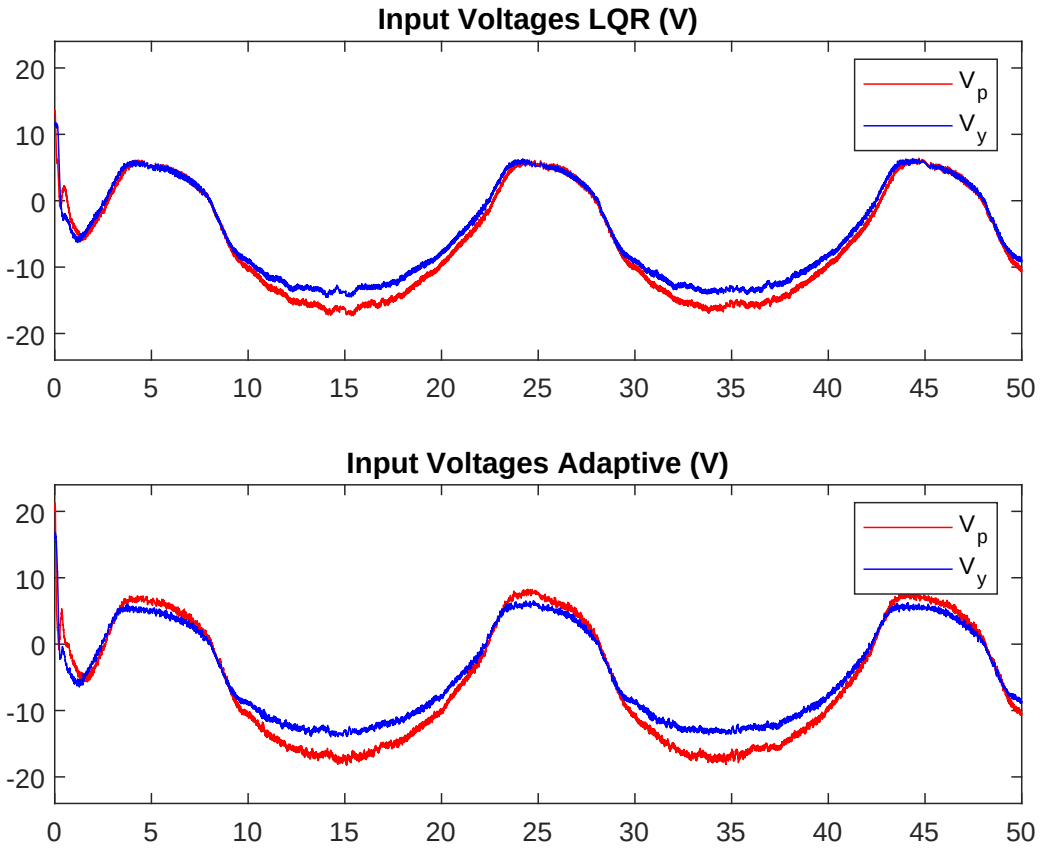

Figure D.2: Voltage for test 1 (sine wave) with disturbance of added mass, positive torque

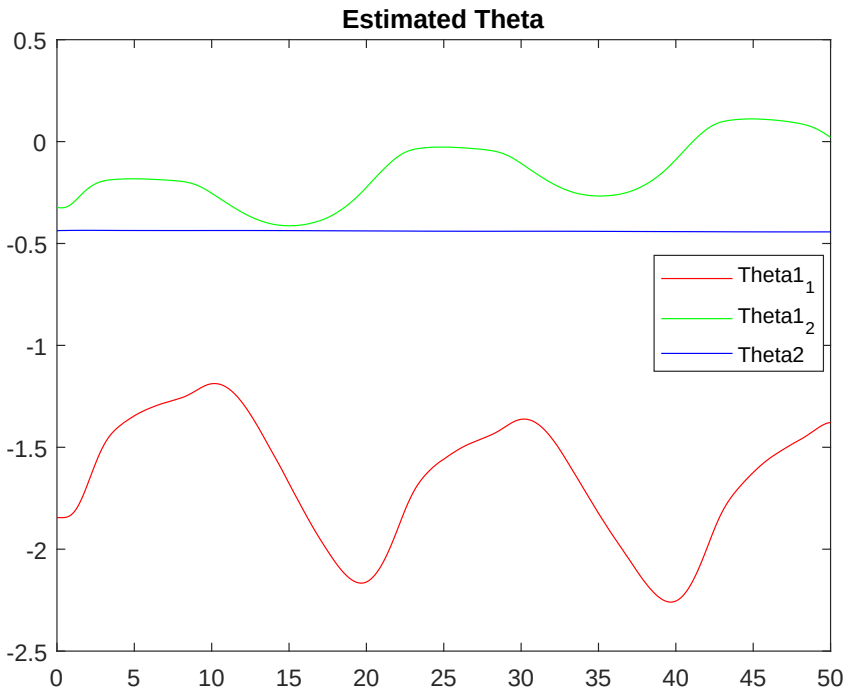

Figure D.3: Estimated theta for test 1 (sine wave) with disturbance of added mass, positive torque

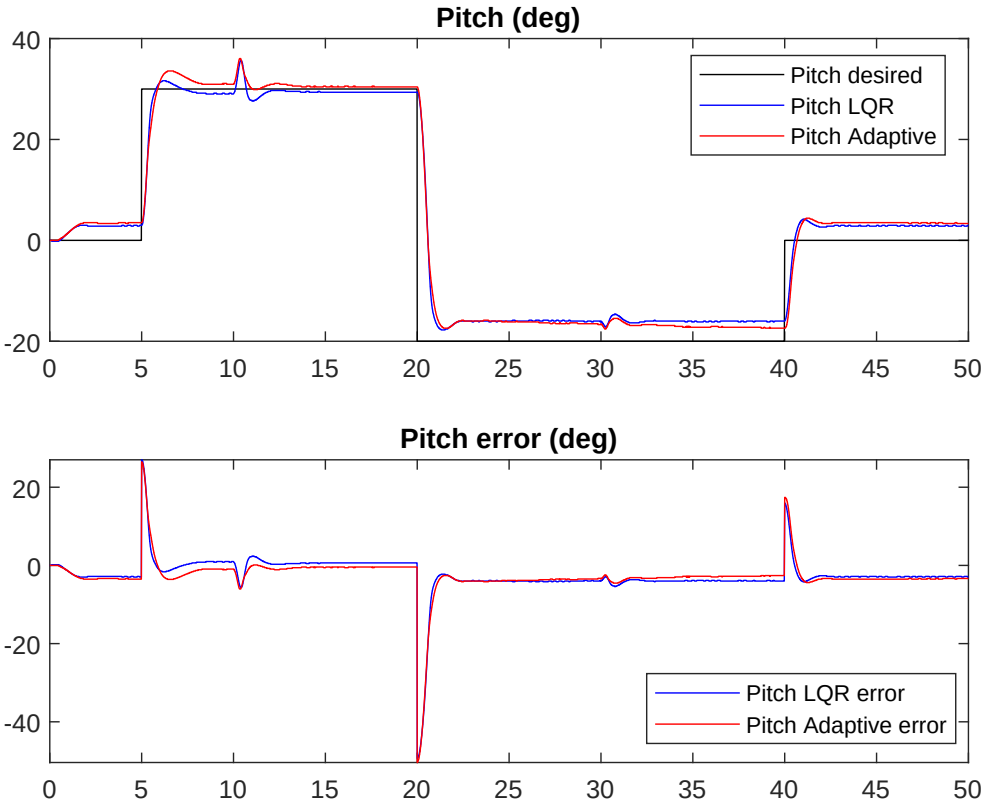

(a) Pitch angle and error for test 2 (step) with disturbance of added mass, positive torque

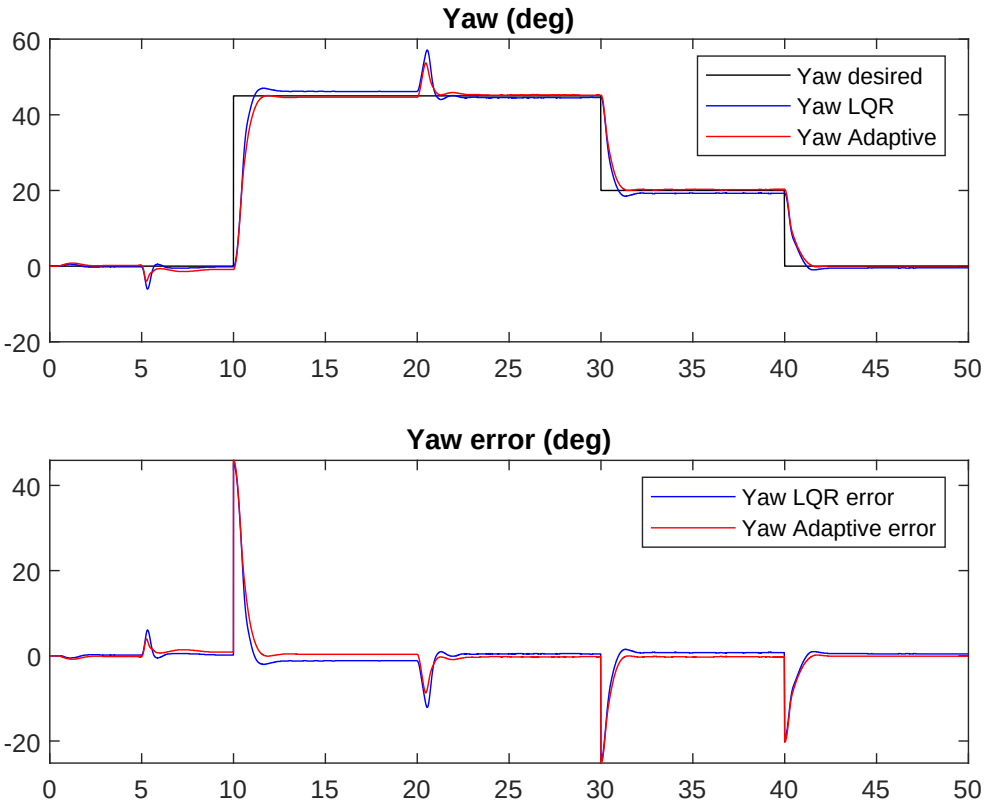

(b) Yaw angle and error for test 2 (step) with disturbance of added mass, positive torque

Figure D.4: Angles and errors for test 2 (step) with disturbance of added mass, positive torque

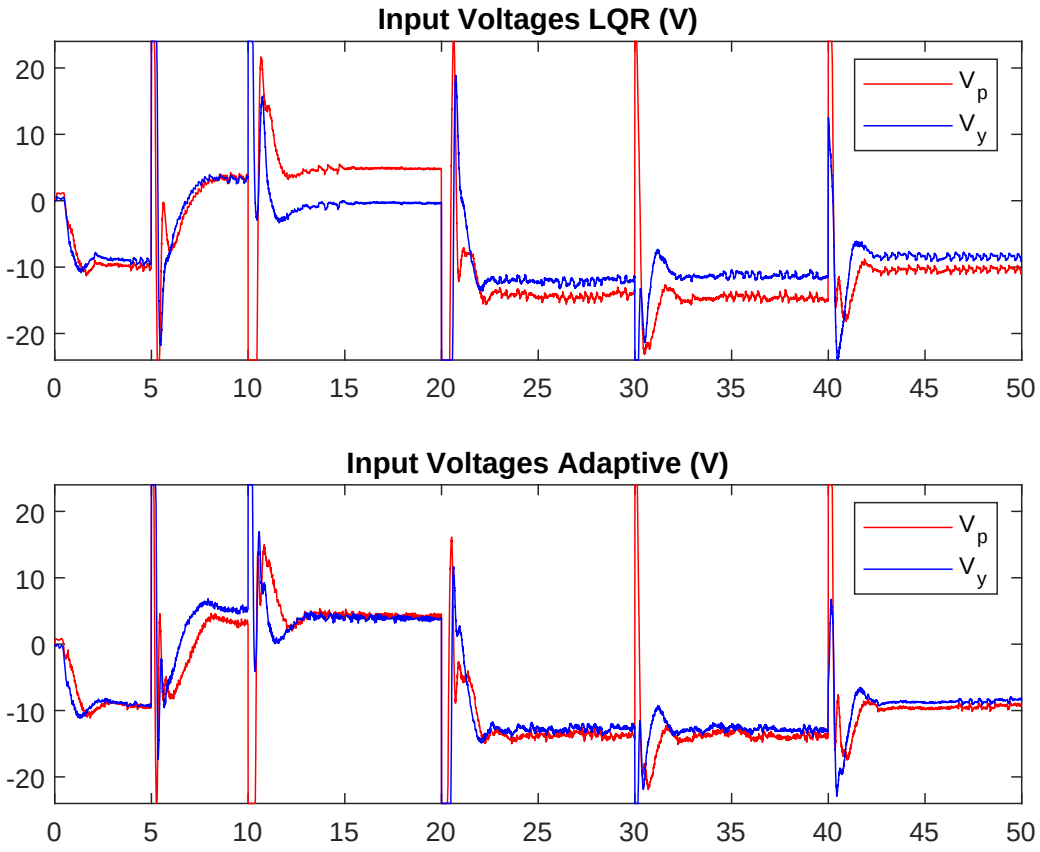

Figure D.5: Voltage for test 2 (step) with disturbance of added mass, positive torque

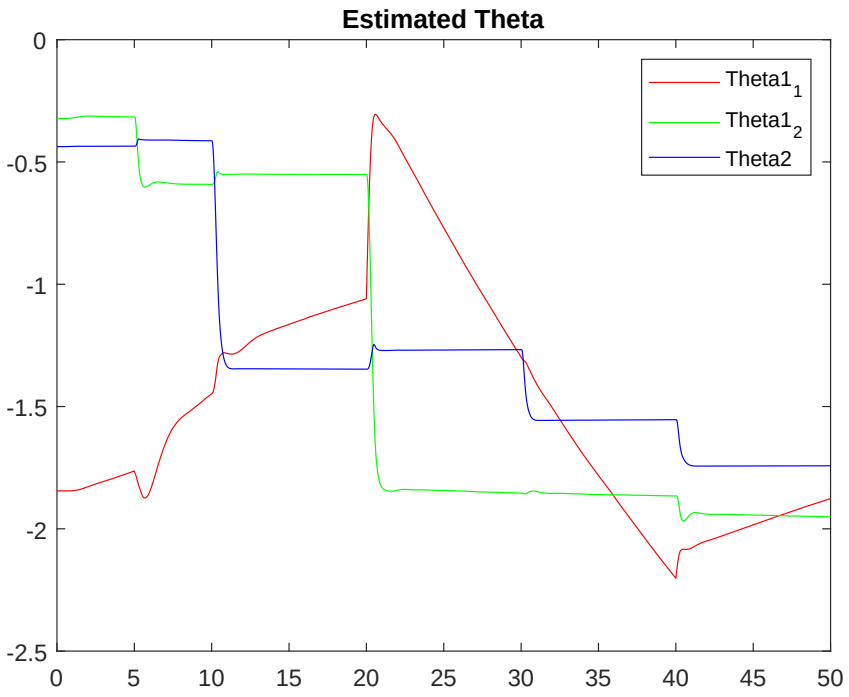

Figure D.6: Estimated theta for test 2 (step) with disturbance of added mass, positive torque

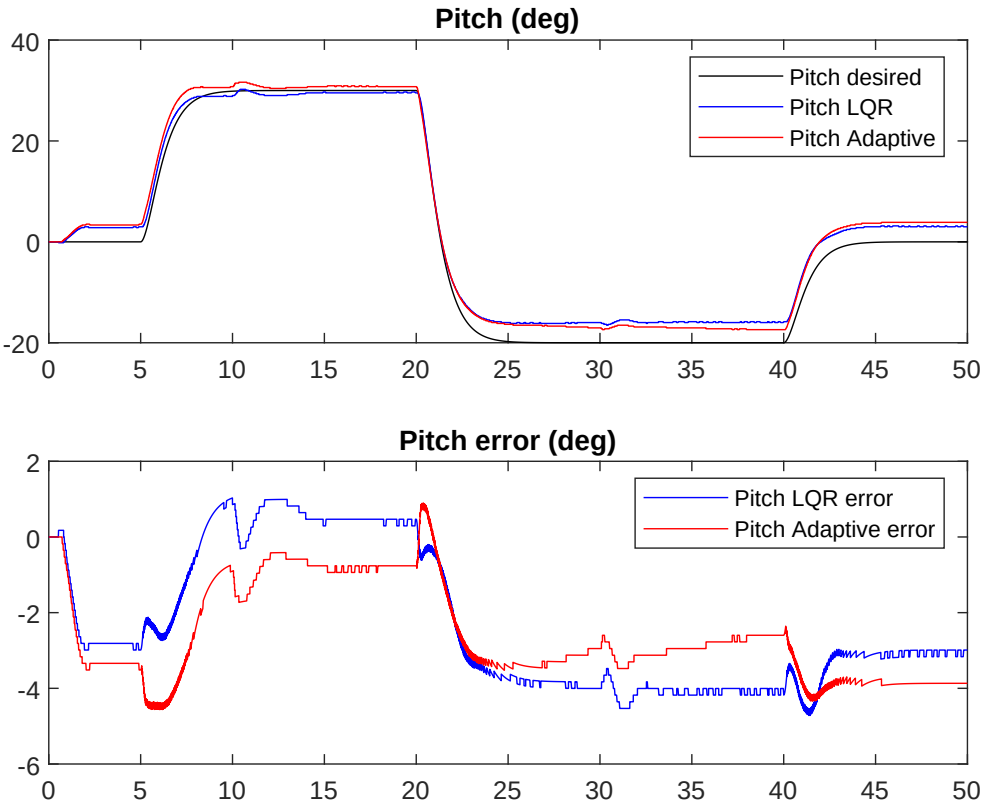

(a) Pitch angle and error for test 3 (smooth step) with disturbance of added mass, positive torque

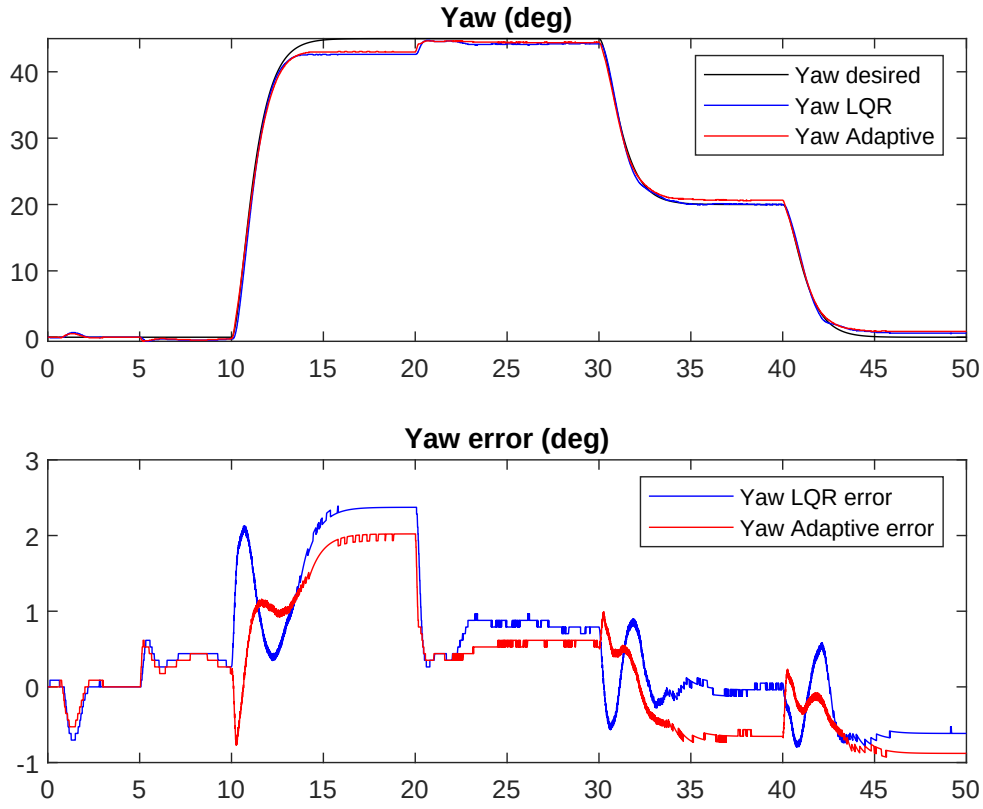

(b) Yaw angle and error for test 3 (smooth step) with disturbance of added mass, positive torque

Figure D.7: Angles and errors for test 3 (smooth step) with disturbance of added mass, positive torque

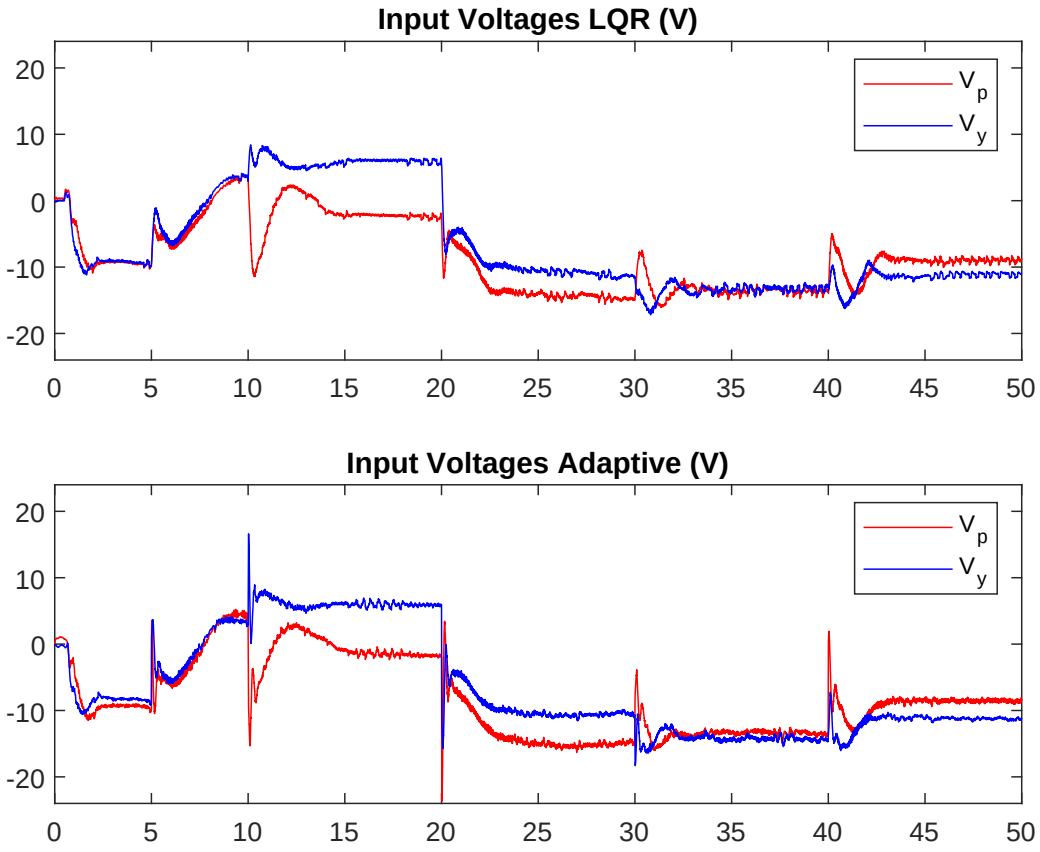

Figure D.8: Voltage for test 3 (smooth step) with disturbance of added mass, positive torque

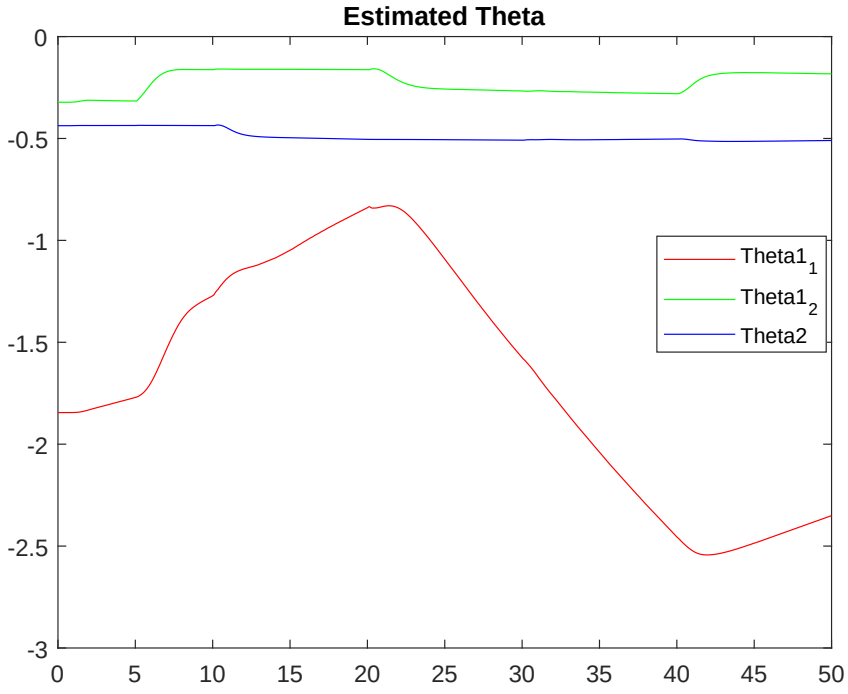

Figure D.9: Estimated theta for test 3 (smooth step) with disturbance of added mass, positive torque

Appendix E

Test with Disturbance of Changed Tail Propeller

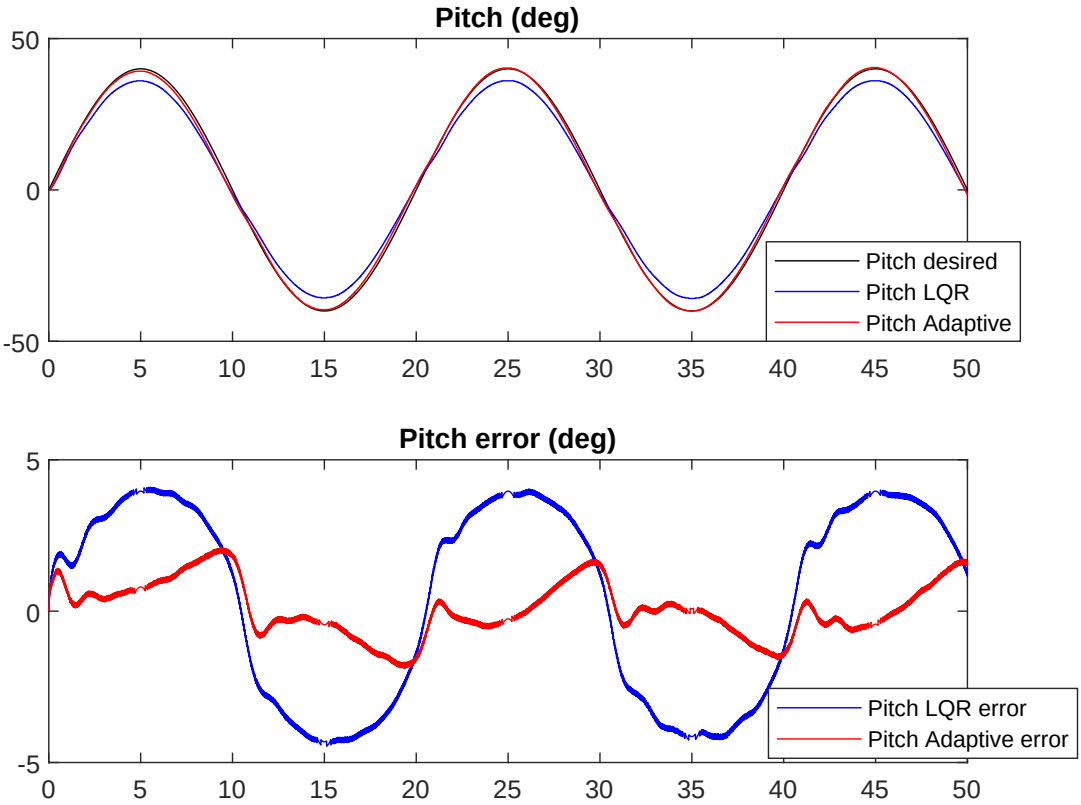

(a) Pitch angle and error for test 1 (sine wave) with disturbance of changing tail propeller

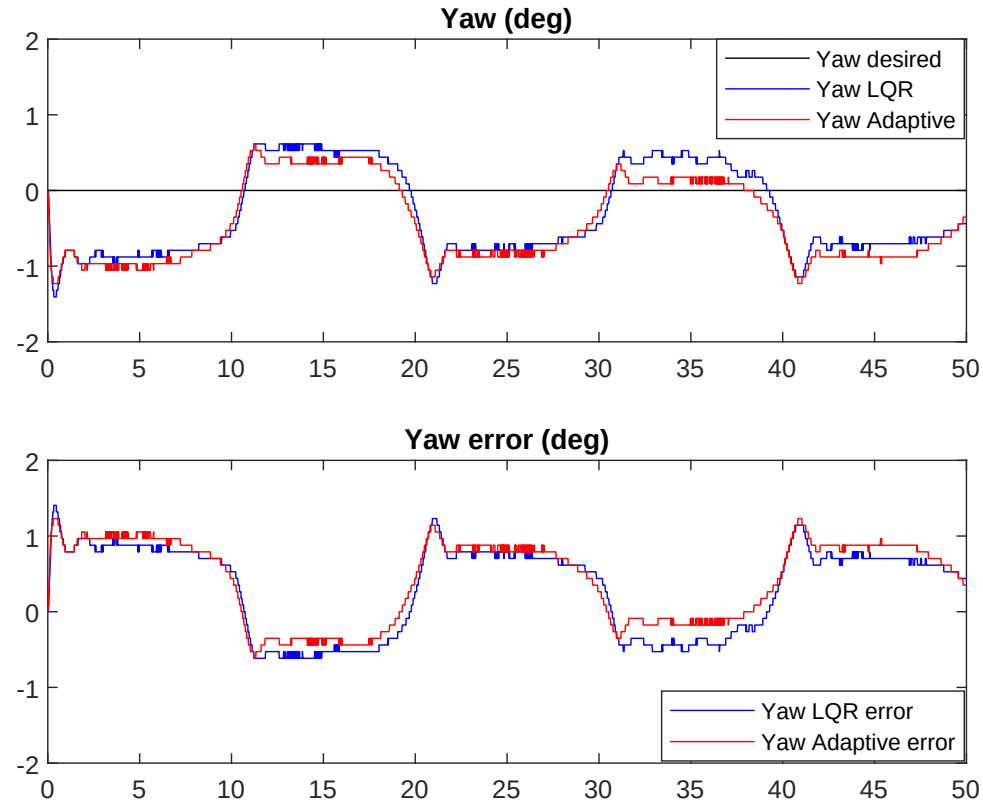

(b) Yaw angle and error for test 1 (sine wave) with disturbance of added mass,positive torque

Figure E.1: Angles and errors for test 1 (sine wave) with disturbance of changing tail propeller

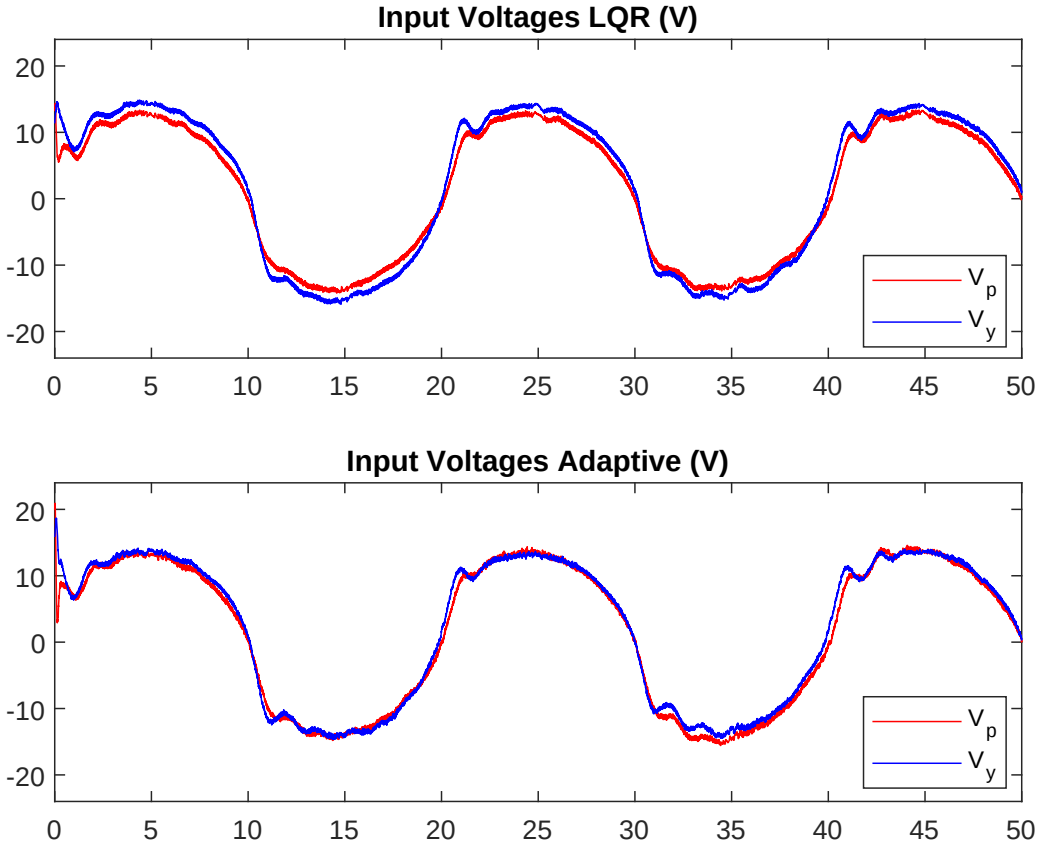

Figure E.2: Voltage for test 1 (sine wave) with disturbance of changing tail propeller

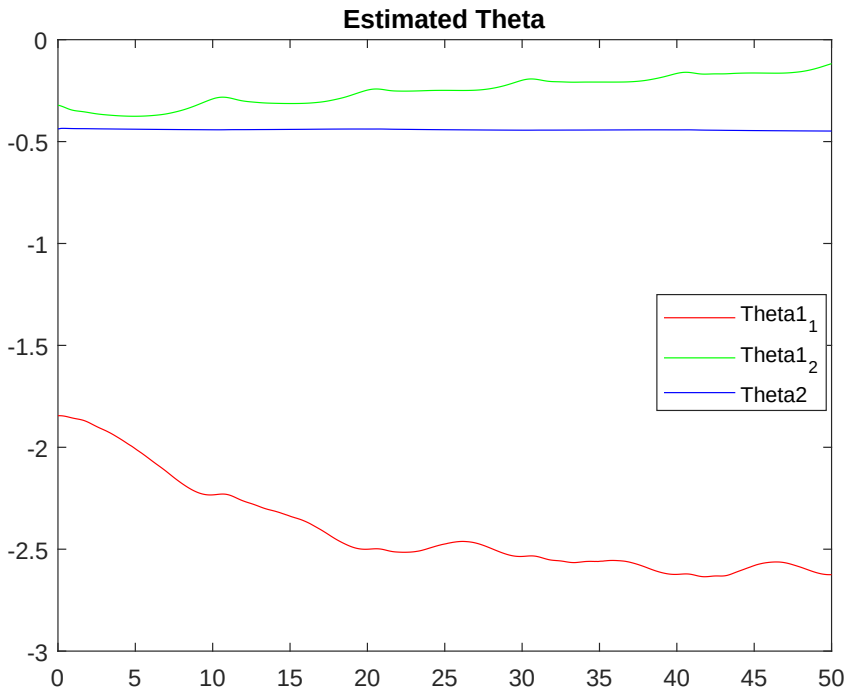

Figure E.3: Estimated theta for test 1 (sine wave) with disturbance of changing tail propeller

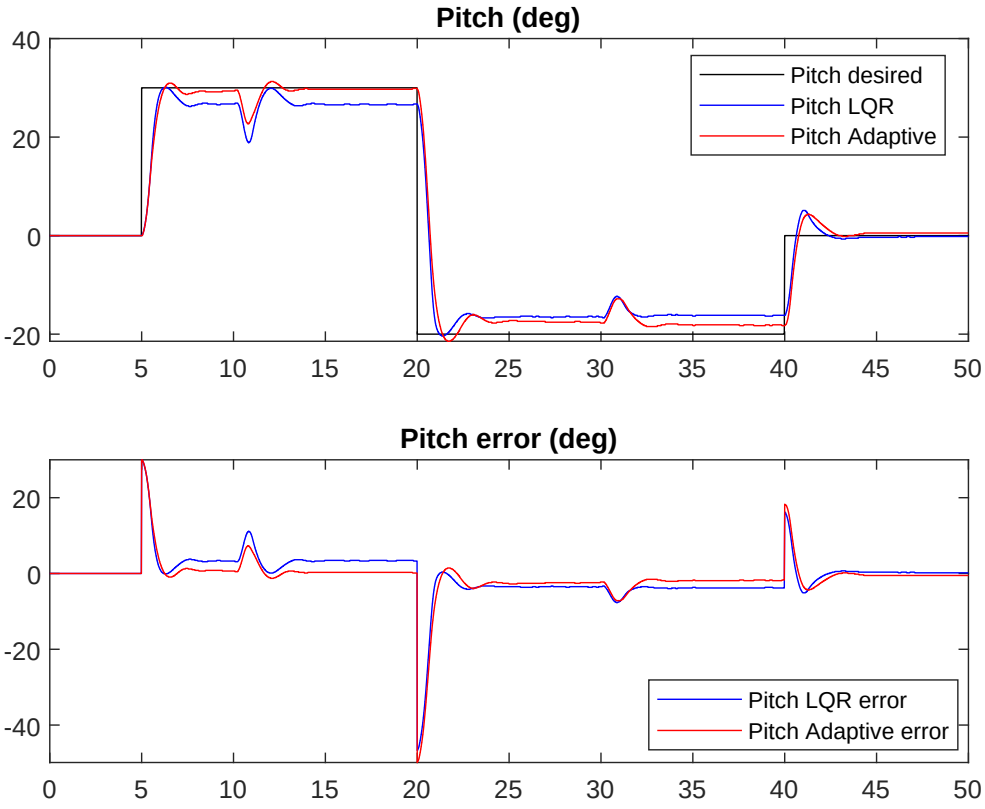

(a) Pitch angle and error for test 2 (step) with disturbance of changing tail propeller

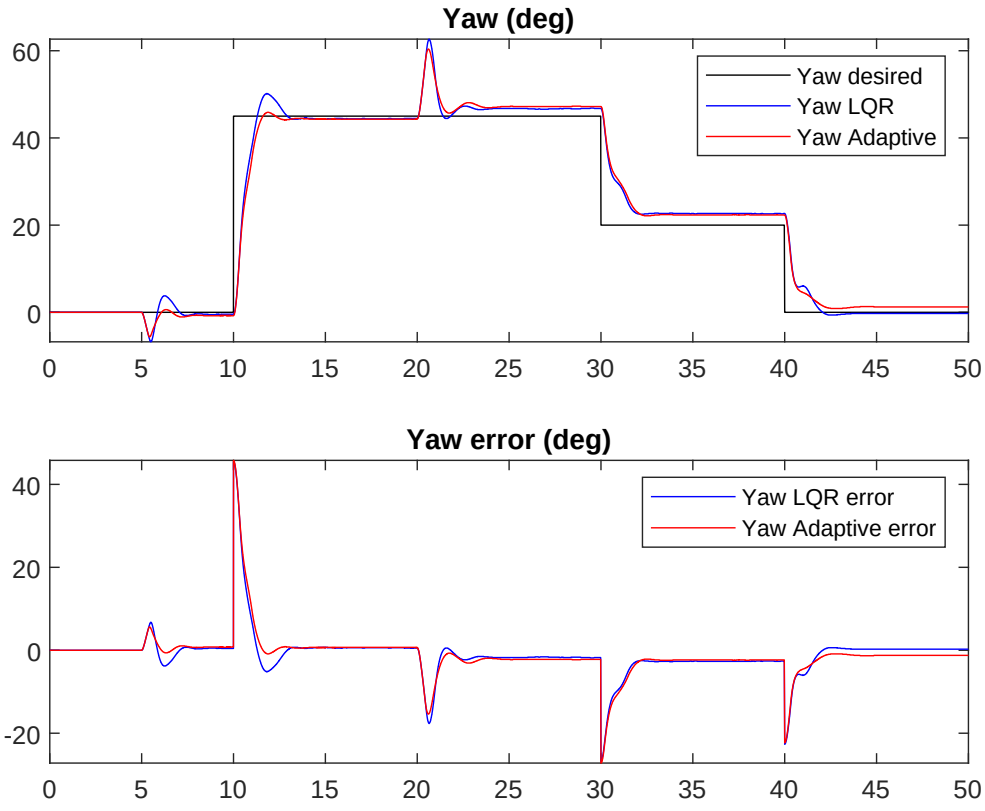

(b) Yaw angle and error for test 2 (step) with disturbance of changing tail propeller

Figure E.4: Angles and errors for test 2 (step) with disturbance of changing tail propeller

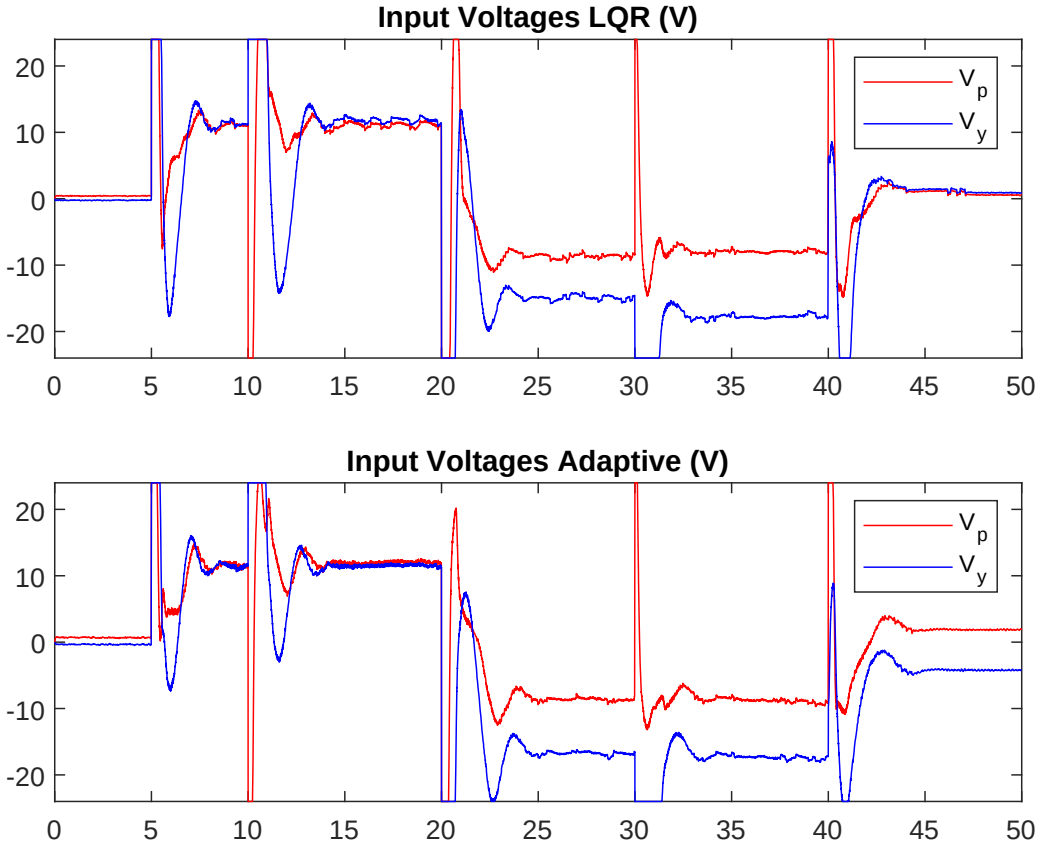

Figure E.5: Voltage for test 2 (step) with disturbance of changing tail propeller

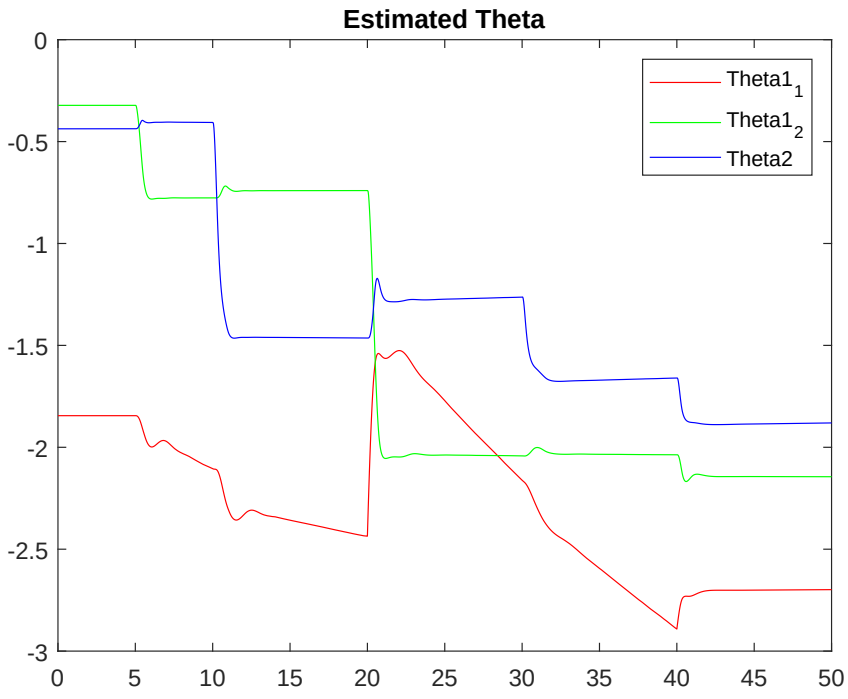

Figure E.6: Estimated theta for test 2 (step) with disturbance of changing tail propeller

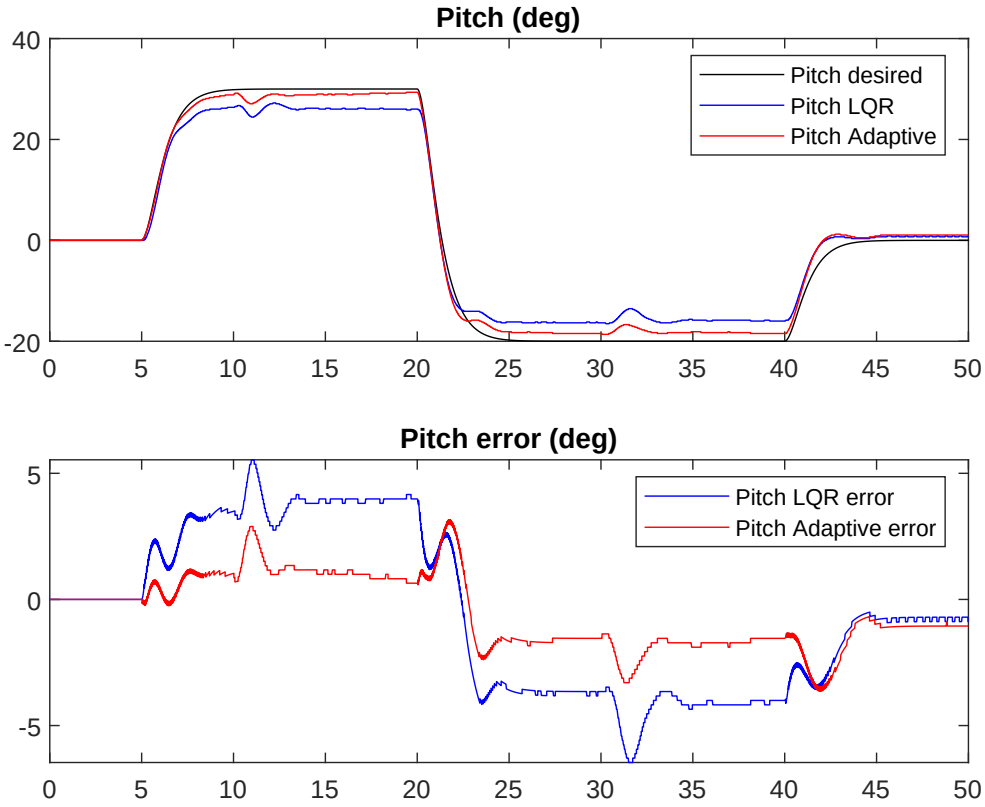

(a) Pitch angle and error for test 3 (smooth step) with disturbance of changing tail propeller

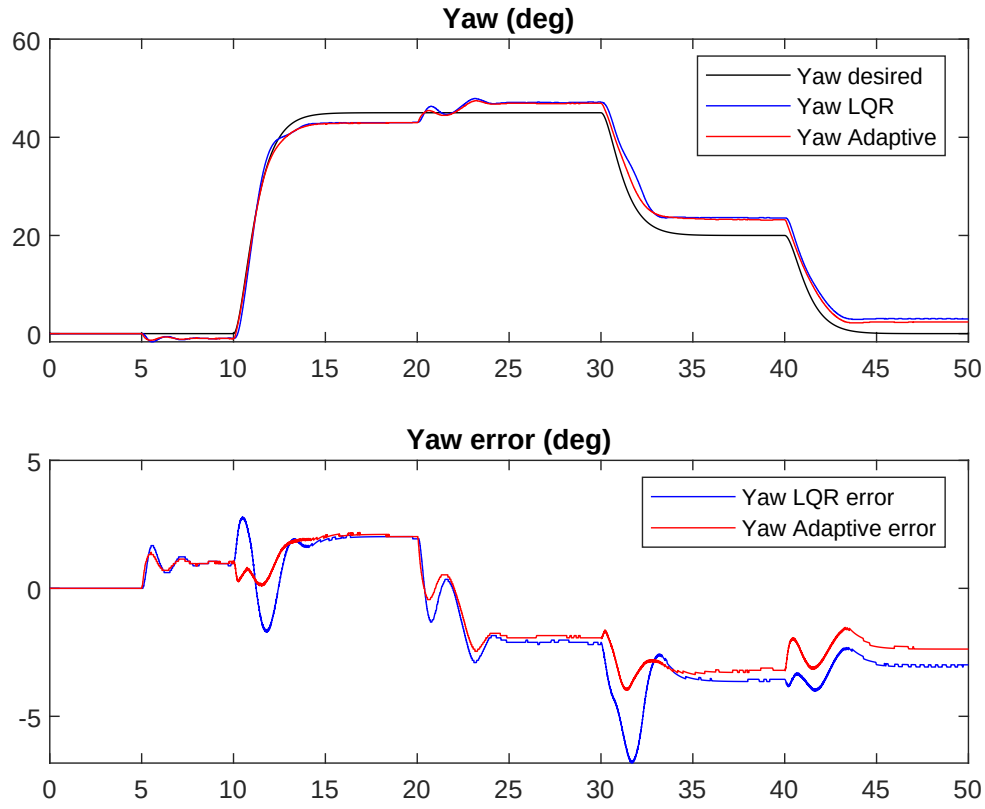

(b) Yaw angle and error for test 3 (smooth step) with disturbance of changing tail propeller

Figure E.7: Angles and errors for test 3 (smooth step) with disturbance of changing tail propeller

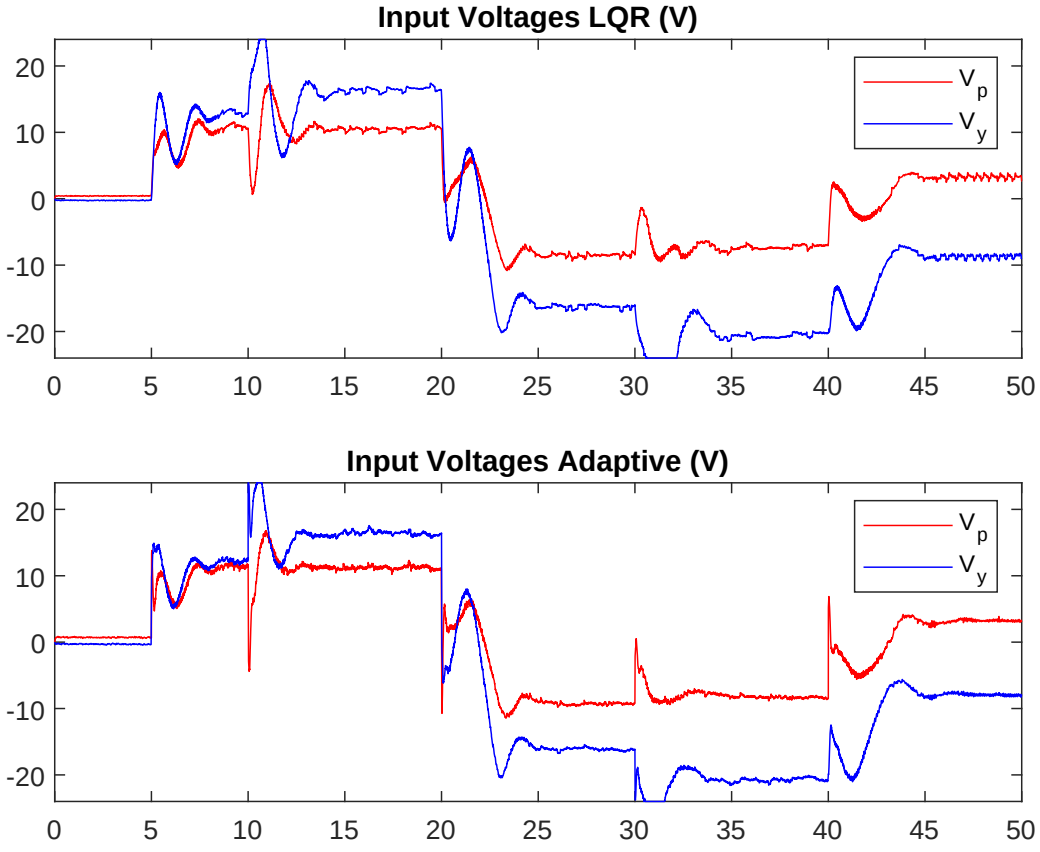

Figure E.8: Voltage for test 3 (smooth step) with disturbance of changing tail propeller

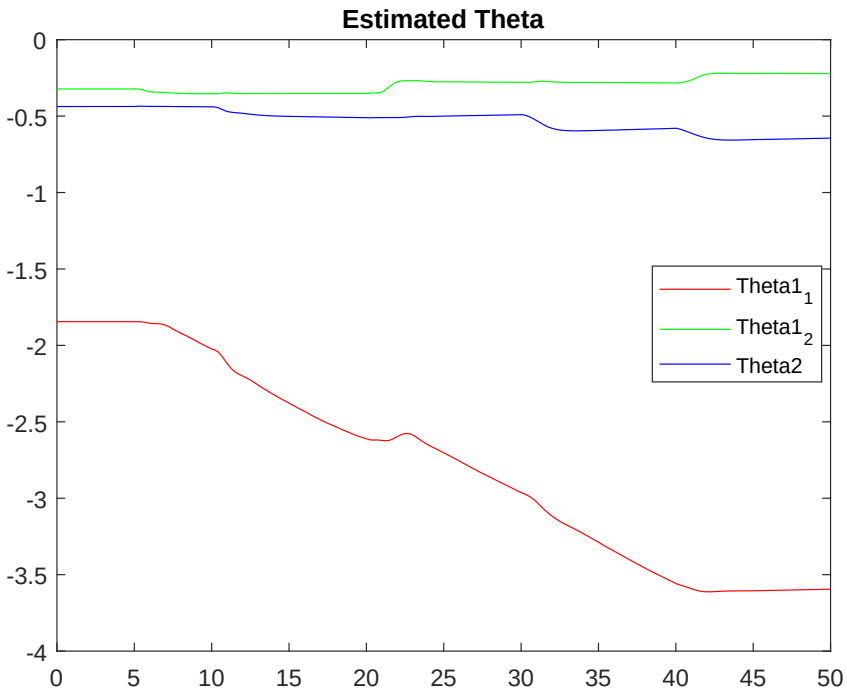

Figure E.9: Estimated theta for test 3 (smooth step) with disturbance of changing tail propeller

Appendix F

Test with Disturbance of Changing both Propellers

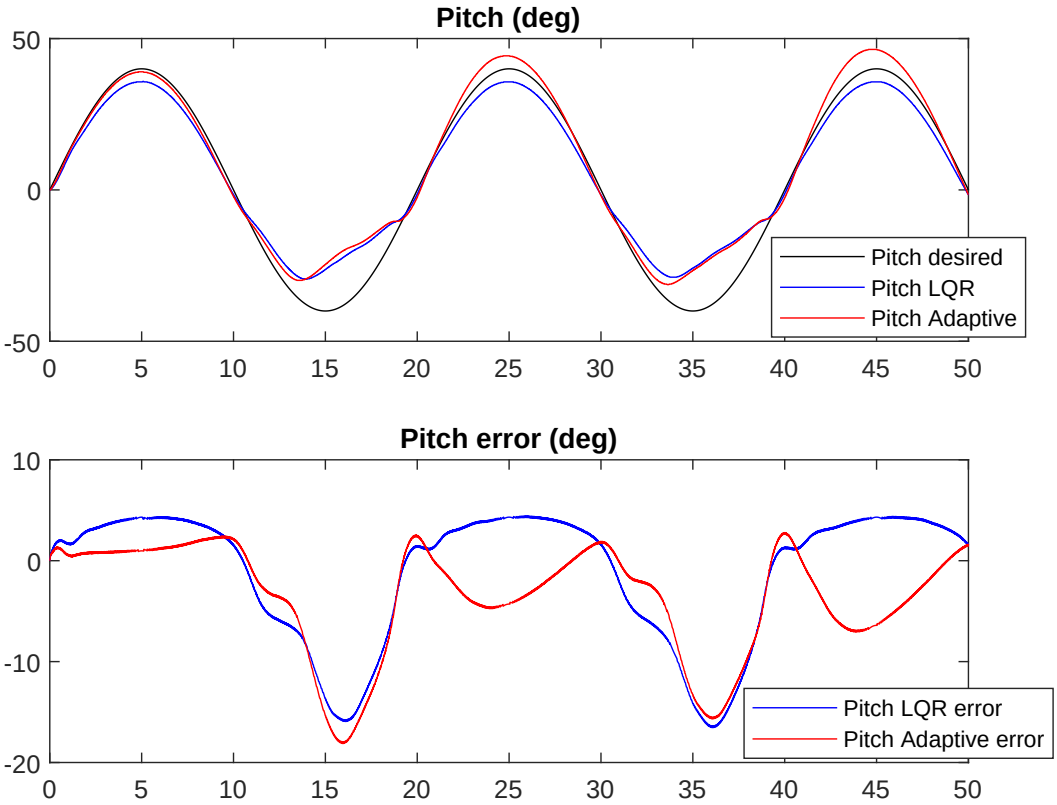

(a) Pitch angle and error for test 1 (sine wave) with disturbance of changing both propellers

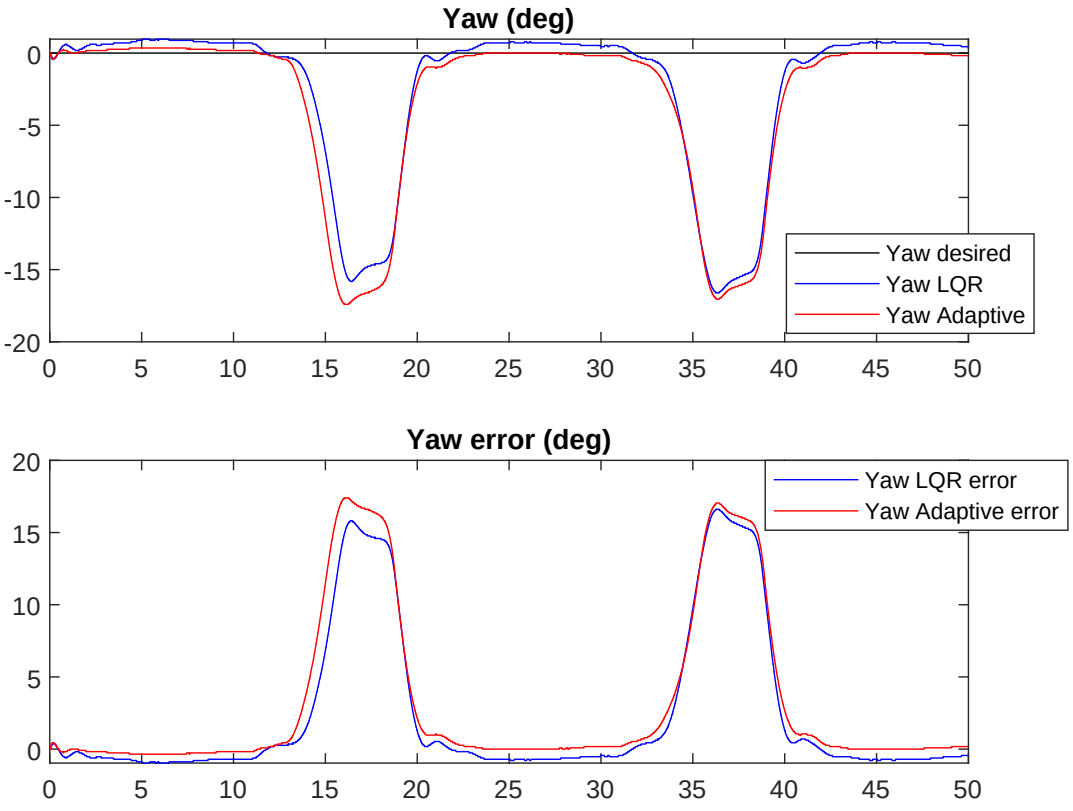

(b) Yaw angle and error for test 1 (sine wave) with disturbance of changing both propellers

Figure F.1: Angles and errors for test 1 (sine wave) with disturbance of changing both propellers

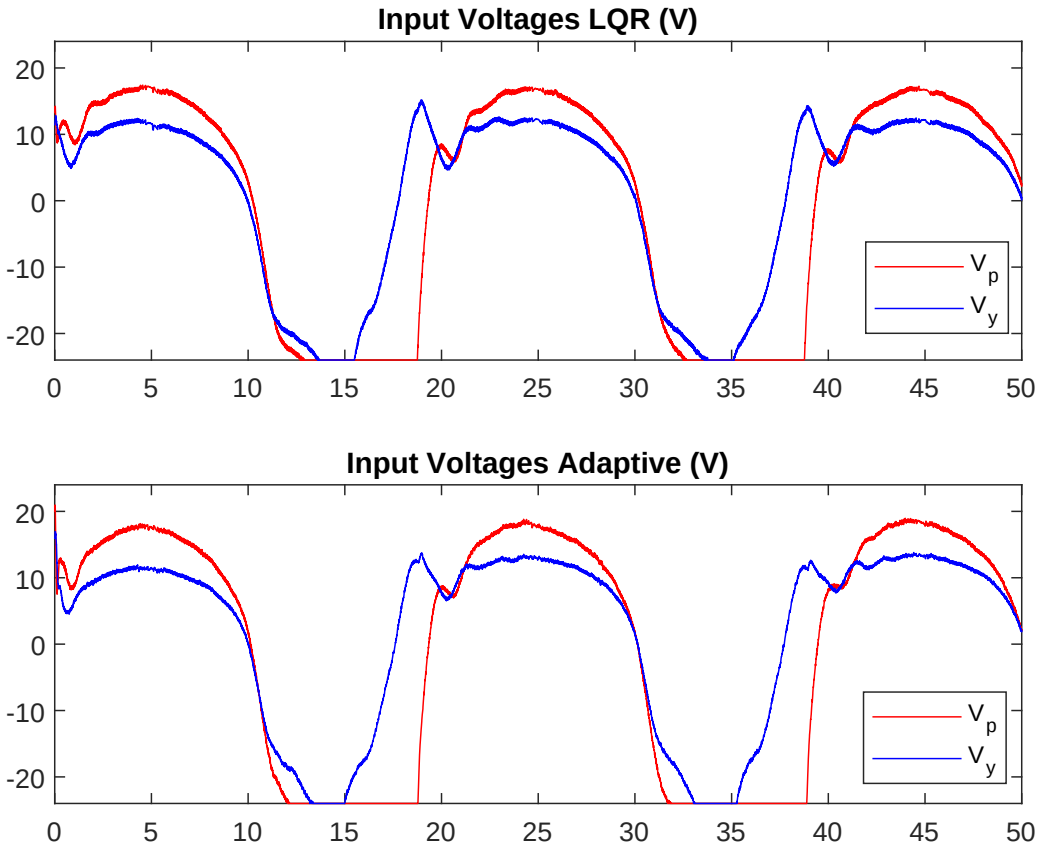

Figure F.2: Voltage for test 1 (sine wave) with disturbance of changing both propellers

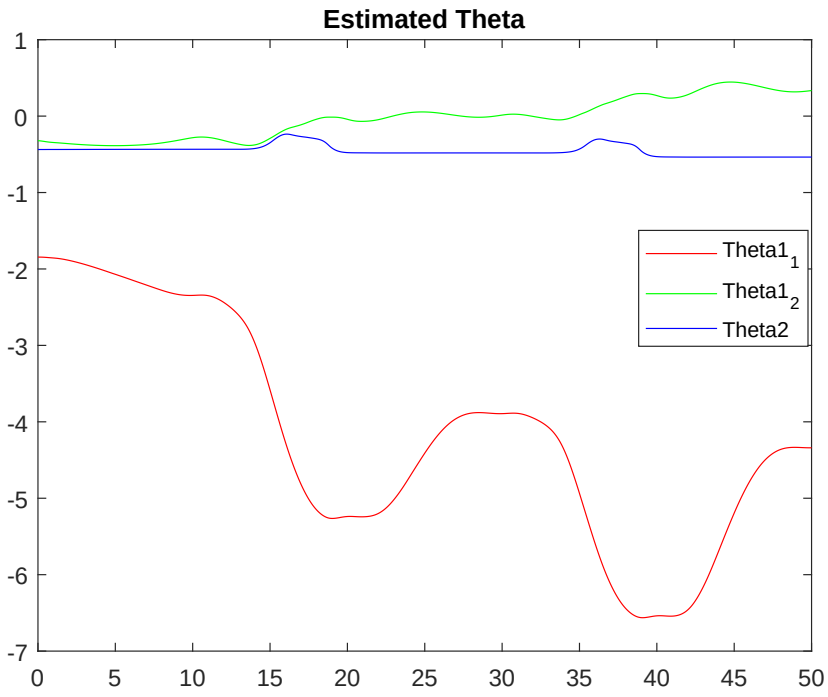

Figure F.3: Estimated theta for test 1 (sine wave) with disturbance of changing both propellers

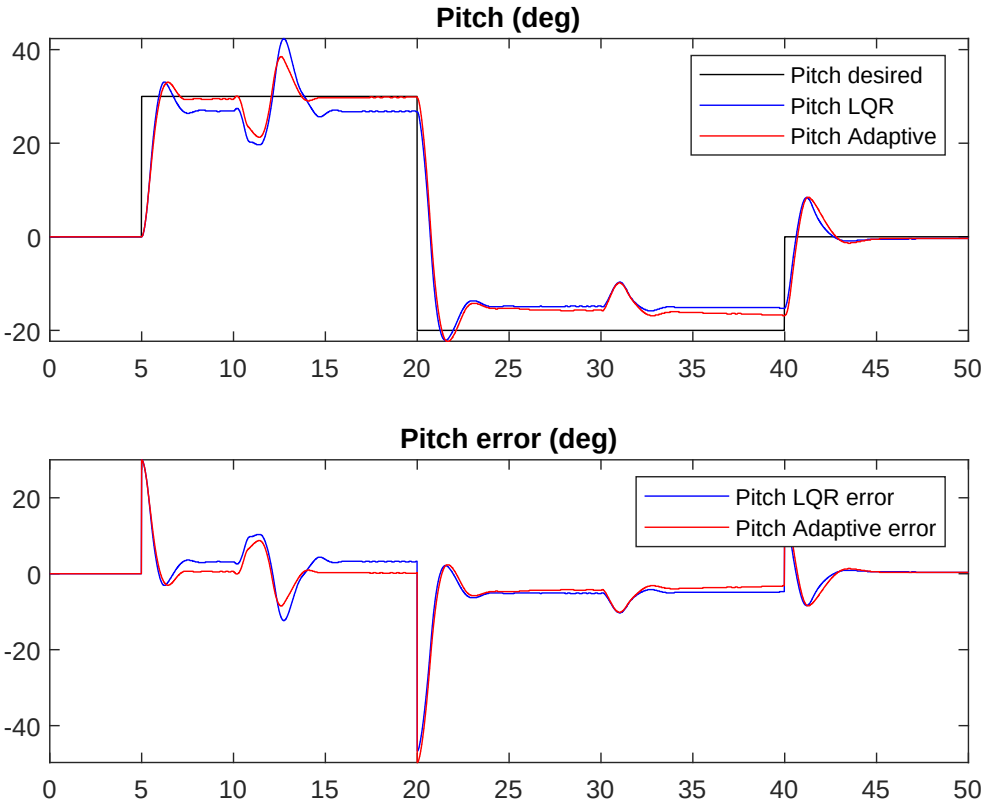

(a) Pitch angle and error for test 2 (step) with disturbance of changing both propellers

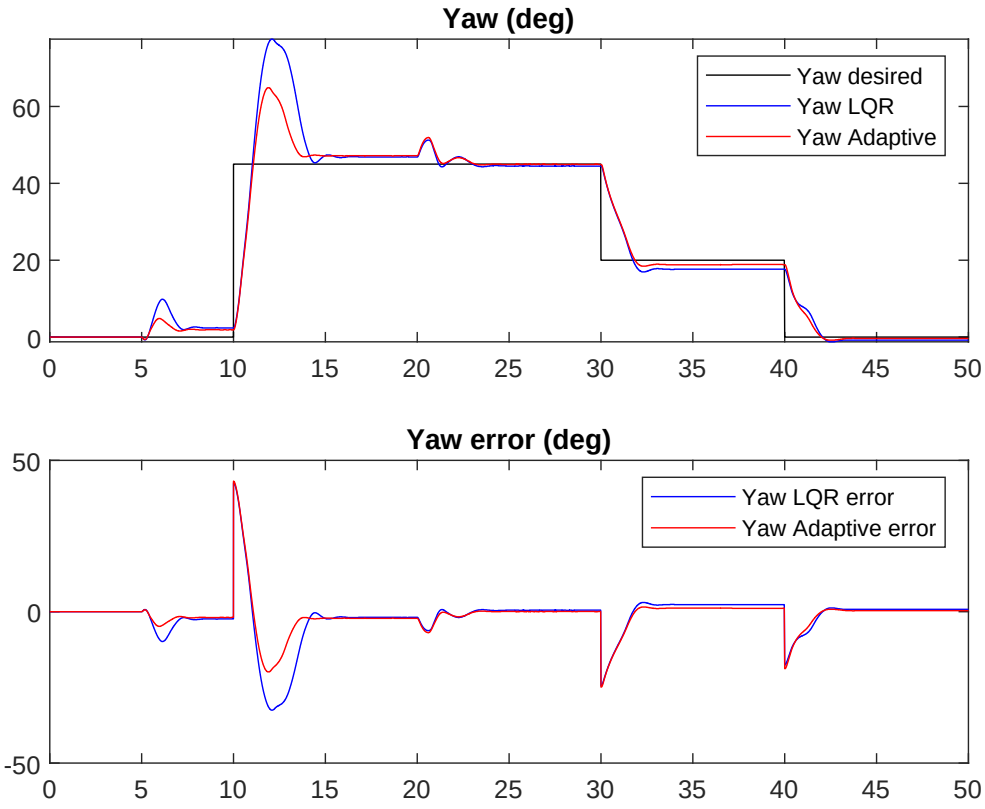

(b) Yaw angle and error for test 2 (step) with disturbance of changing both propellers

Figure F.4: Angles and errors for test 2 (step) with disturbance of changing both propellers

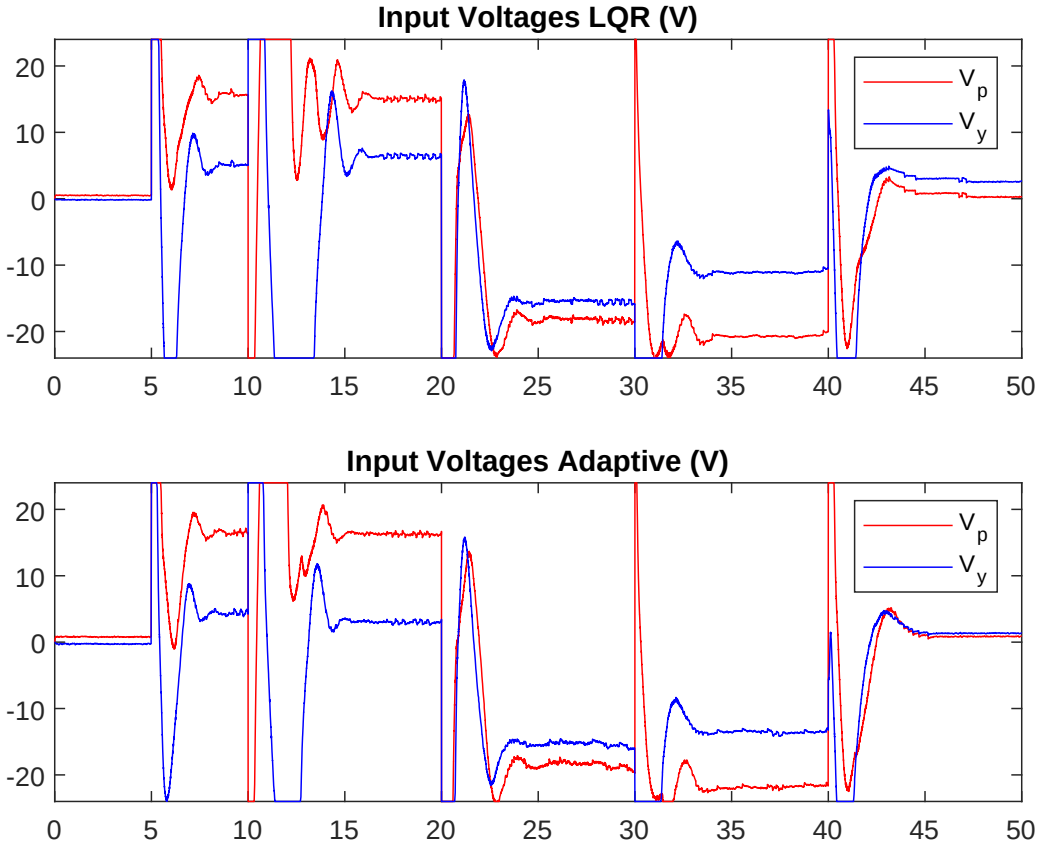

Figure F.5: Voltage for test 2 (step) with disturbance of changing both propellers

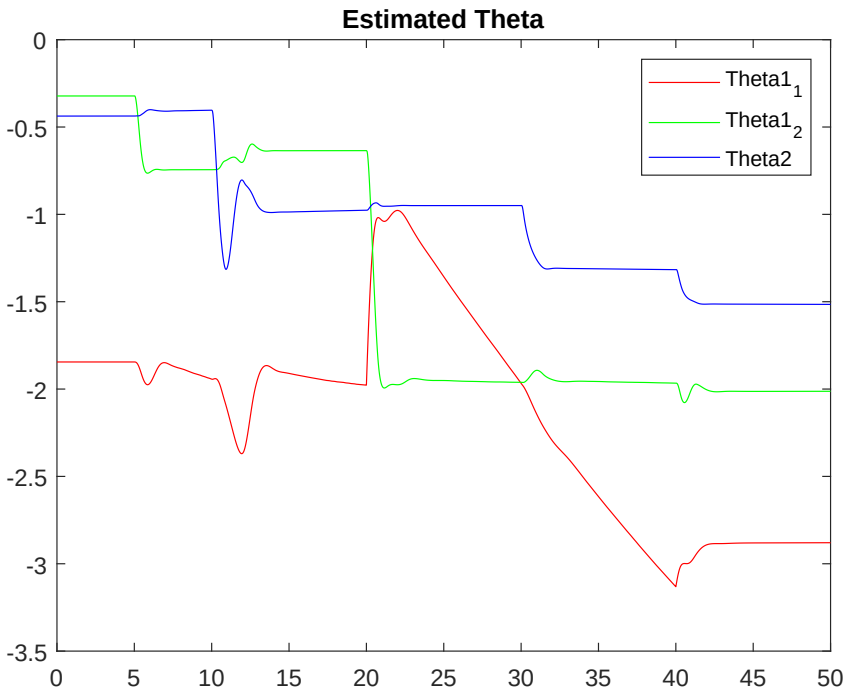

Figure F.6: Estimated theta for test 2 (step) with disturbance of changing both propellers

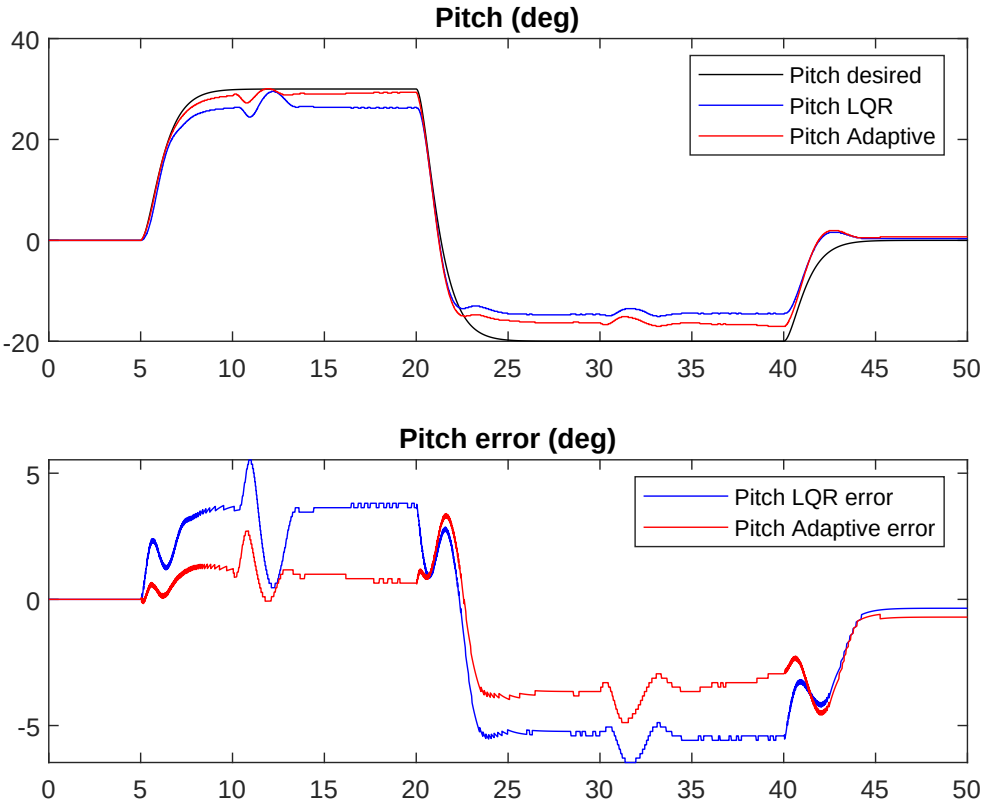

(a) Pitch angle and error for test 3 (smooth step) with disturbance of changing both propellers

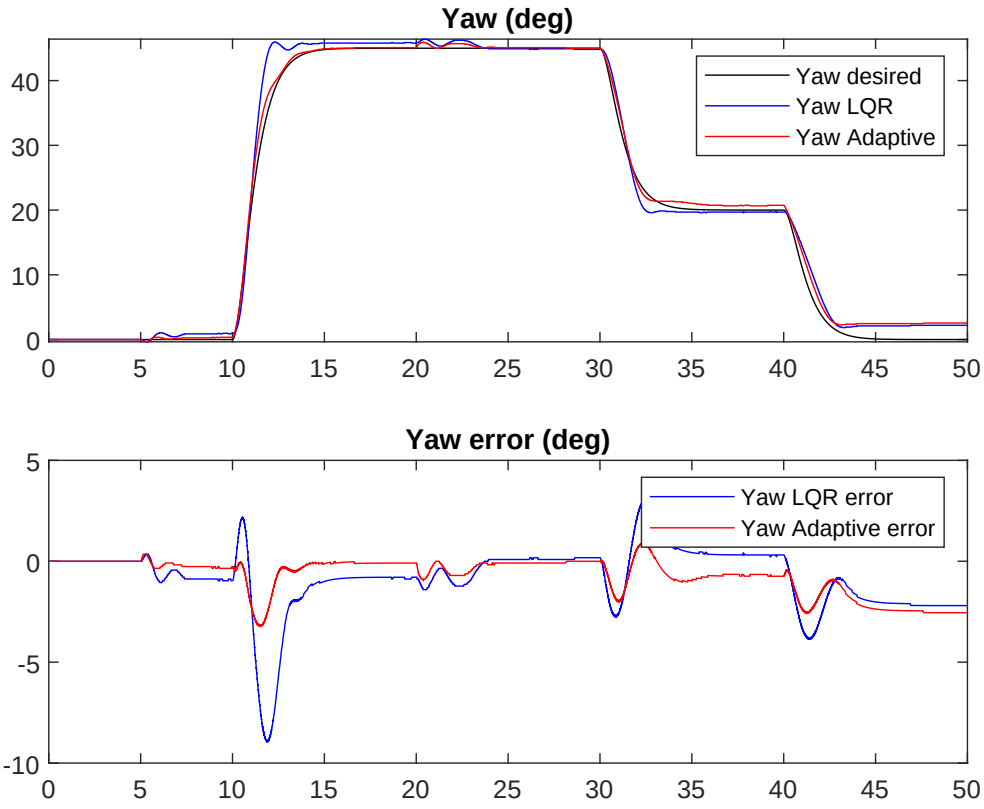

(b) Yaw angle and error for test 3 (smooth step) with disturbance of changing both propellers

Figure F.7: Angles and errors for test 3 (smooth step) with disturbance of changing both propellers

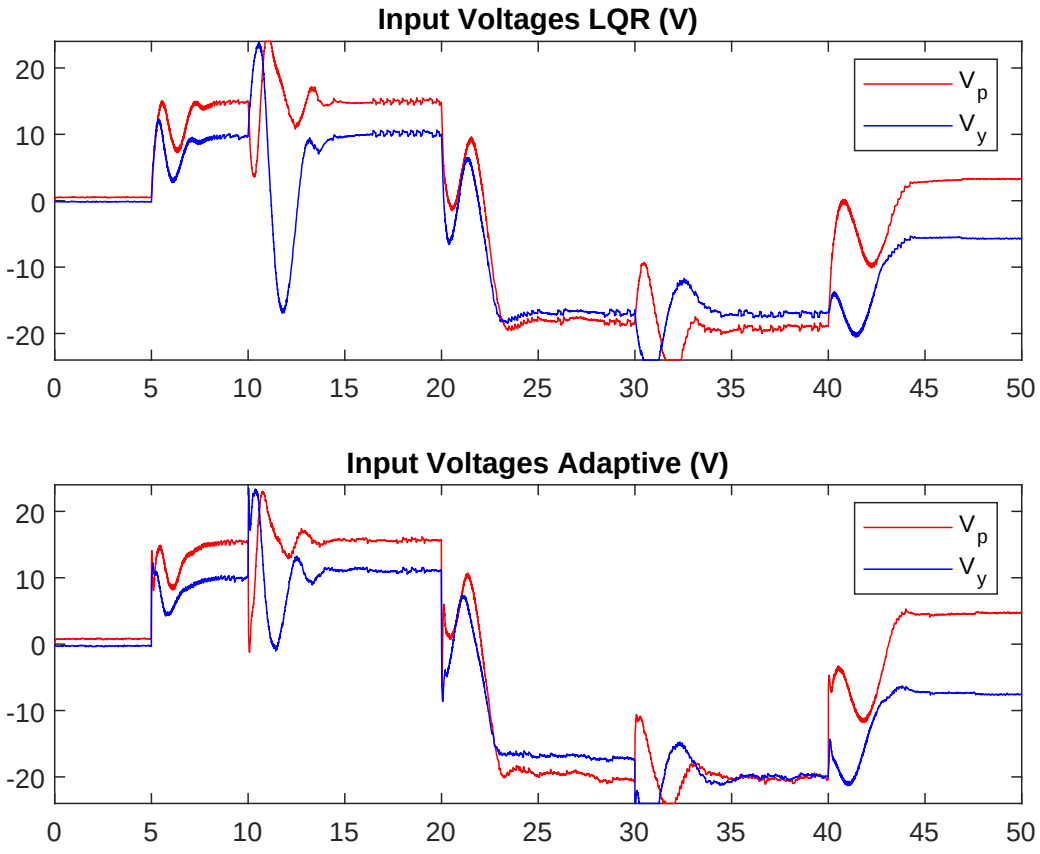

Figure F.8: Voltage for test 3 (smooth step) with disturbance of changing both propellers

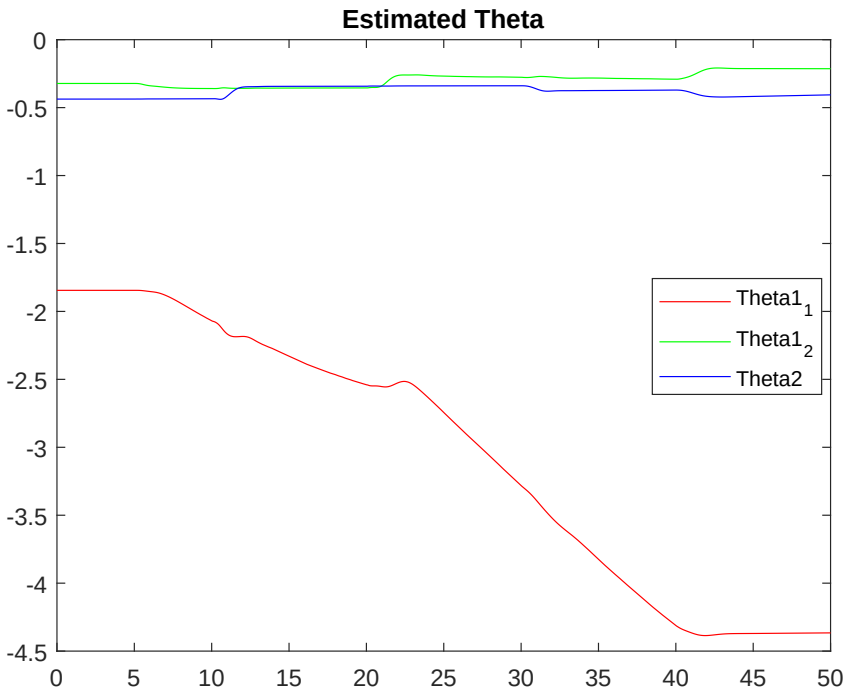

Figure F.9: Estimated theta for test 3 (smooth step) with disturbance of changing both propellers